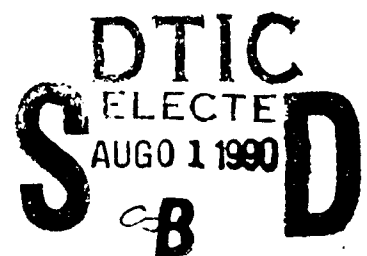


AD-A224 684

<b>REPORT DOCUMENTATION PAGE</b>			Form Approved OMB No. 0704-0188	
Public reporting burden for this collection of information is estimated to average 1 hour per response, including the time for reviewing instructions, searching existing data sources, gathering and maintaining the data needed, and completing and reviewing the collection of information. Send comments regarding this burden estimate or any other aspect of this collection of information, including suggestions for reducing this burden, to Washington Headquarters Services, Directorate for Information Operations and Reports, 1215 Jefferson Davis Highway, Suite 1204, Arlington, VA 22202-4302, and to the Office of Management and Budget, Paperwork Reduction Project (0704-0188), Washington, DC 20503.				
1. AGENCY USE ONLY (Leave blank)	2. REPORT DATE 1990	3. REPORT TYPE AND DATES COVERED Thesis/Dissertation		
4. TITLE AND SUBTITLE USE OF POWER BALANCE TO MODEL CONVERGING FLOWS IN BILATERAL JUNCTIONS FOR VENTILATION SYSTEMS			5. FUNDING NUMBERS	
6. AUTHOR(S)  JAMES PATRICK CURRAN				
7. PERFORMING ORGANIZATION NAME(S) AND ADDRESS(ES) AFIT Student at: University of Washington		8. PERFORMING ORGANIZATION REPORT NUMBER AFIT/CI/CIA - 90-043		
9. SPONSORING/MONITORING AGENCY NAME(S) AND ADDRESS(ES) AFIT/CI Wright-Patterson AFB OH 45433		10. SPONSORING/MONITORING AGENCY REPORT NUMBER		
11. SUPPLEMENTARY NOTES				
12a. DISTRIBUTION/AVAILABILITY STATEMENT Approved for Public Release IAW AFR 190-1 Distribution Unlimited ERNEST A. HAYGOOD, 1st Lt, USAF Executive Officer, Civilian Institution Programs			12b. DISTRIBUTION CODE	
13. ABSTRACT (Maximum 200 words)				
				
14. SUBJECT TERMS			15. NUMBER OF PAGES 136	
			16. PRICE CODE	
17. SECURITY CLASSIFICATION OF REPORT UNCLASSIFIED	18. SECURITY CLASSIFICATION OF THIS PAGE	19. SECURITY CLASSIFICATION OF ABSTRACT	20. LIMITATION OF ABSTRACT	

Use of Power Balance to Model Converging Flows in Bilateral  
Junctions for Ventilation Systems

by

James Patrick Curran

A thesis submitted in partial fulfillment of  
the requirements for the degree of

Master of Science

University of Washington

1990

Approved by

*Thomas Eugene Jeffrey*  
(Chairperson of Supervisory Committee)  
*Donald A. Covert*  
*William S. Jones*

Program Authorized  
to Offer Degree

School of Public Health and Community Medicine -

Environmental Health

Date

8 June '90

Master's Thesis

In presenting this thesis in partial fulfillment of the requirements for a Master's degree at the University of Washington, I agree that the Library shall make its copies freely available for inspection. I further agree that extensive copying of this thesis is allowable only for scholarly purposes consistent with "fair use" as prescribed in the U.S. Copyright Law. Any other reproduction for any purposes or by any means shall not be allowed without my written permission.

Signature James J. Curran  
Date 8 June 90

<b>Accession For</b>	
NTIS GRA&I	<input checked="" type="checkbox"/>
DTIC TAB	<input type="checkbox"/>
Unannounced	<input type="checkbox"/>
Justification	
By	
Distribution/	
Availability Codes	
Dist Special	
A-1	



University of Washington

Abstract

Use of Power Balance to Model Converging Flows in Bilateral Junctions for Ventilation Systems

by James P. Curran

Chairperson of the Supervisory Committee: Professor Steven E. Guffey  
Department of Environmental Health

Little information is available on the nature of flow in bilateral junctions for industrial ventilation systems. The American Conference of Governmental Industrial Hygienists recommends against bilateral junctions without providing any justification. The American Society of Heating, Refrigeration and Air-conditioning Engineers provides a table of coefficients for one type of bilateral junction; this table was found to be in error.

The main objective of this study was to determine if the power balance method and the linear kinetic power model could be used to characterize and predict the flows in bilateral junctions. A secondary goal was to determine the relative energy efficiency of bilateral junctions compared to two single lateral junctions in series.

Power losses in one bilateral junction were experimentally determined for 35 conditions where the velocity ratios of the converging ducts were varied from 0-3.7. The linear kinetic power model provided a good fit to the empirical data (Adjusted  $R^2 = 90.9\%$ ). An adjusted  $R^2$  of 97.7% was obtained for an important subset of data (velocity ratios ranging from 0.75 to 1.25). As expected, power losses were lowest when velocity ratios were near one. The power losses in the bilateral junction tested were 45-92% higher than the predicted power losses for two single lateral junctions in series. This increase in power loss will have an insignificant impact on the overall pressure requirements for most ventilation systems. In this study, the maximum increase in total pressure due to the bilateral junction was estimated as 3.5% higher than the predicted total pressure in a hypothetical setup containing two single-lateral junctions.

## TABLE OF CONTENTS

	Page
List of Figures.....	iv
List of Tables.....	vi
CHAPTER I: Introduction.....	1
Background.....	1
Research Objectives.....	2
Current Design Methods.....	3
ACGIH Method.....	3
ASHRAE Method.....	3
Power Balance Method.....	5
The Case for Bilateral Junctions.....	9
CHAPTER II: Materials and Methods.....	12
Laboratory Setup.....	12
Fan, Motor and Transmission.....	12
Duct System.....	12
Pressure Measurement Stations.....	15
Leak Tests.....	15
Computer Data Acquisition and Data Reduction.....	17
Measuring Equipment and Calibration.....	21
Pressure Measuring Equipment.....	21
Other Measuring Devices.....	28
Friction Loss Determination.....	29
Junction Power Loss and Modelling.....	33
Power Loss Determination.....	33
Junction Modelling.....	44
CHAPTER III: Discussion of Results.....	45
Friction and Flow Estimation.....	45
Friction Estimation.....	45
Flow Estimation.....	51
Junction Modelling.....	54
Goodness of Fit.....	54
Predicted Value at Zero Flow.....	54

Regression Diagnostics.....	56
Influence of Branch Velocity Ratios on Junction Lost Powers.....	58
Velocity in Side Branches with Respect to the Center Branch.....	58
Velocity of Side Branches with Respect to Each Other.....	62
Estimation of "True" Coefficients for the Junction Tested.....	64
Comparison of Power Losses Between a Bilateral Junction and an Equivalent Two Single-lateral Junction Setup.....	66
Significance of the Higher Power Losses for Bilateral Junctions Compared Compared to Single-lateral Junctions.....	71
 CHAPTER IV: Conclusions.....	 76
 V: References.....	 78
 Appendix A: ACGIH Bilateral Junction Recommendations.....	 80
Appendix B: ASHRAE Coefficients for Bilateral Junctions.....	82
Appendix C: Idelchik's Coefficients for Bilateral Junctions.....	84
Appendix D: Corrected ASHRAE Coefficients for Bilateral Junctions.....	92
Appendix E: Calibration Data Worksheet.....	96
Appendix F: Equipment Calibration Curves.....	97
Appendix G: Equipment List.....	103
Appendix H: Friction Data Collection Procedure.....	107
Appendix I: Friction Data Collection Worksheet.....	110
Appendix J: Junction Data Collection Procedure.....	112
Appendix K: Impedance Method.....	115
Appendix L: Junction Data Collection Worksheet.....	117
Appendix M: Friction Calculations.....	119
Appendix N: Selected Raw Data.....	131

## LIST OF FIGURES

<u>Number</u>	<u>Page</u>
1. Bilateral Junction.....	2
2. Single-lateral Junction.....	2
3. ACGIH "Preferred" Option to Bilateral Junctions.....	4
4. ACGIH "Acceptable" Option to Bilateral Junctions.....	4
5. Bilateral Junction with Nomenclature.....	7
6. Bilateral Junction Design Option.....	9
7. Parallel Systems Design Option.....	11
8. Offset Single-Lateral Junctions Design Option.....	11
9. Photograph of Plywood Vertical Spacers.....	13
10. Photograph of Branch Supports.....	14
11. Measuring Station Connector Compared with Standard Connector.....	14
12. Diagram of Pitot Tube Holding Device and Mounting.....	16
13. Photograph of Pitot Tube Holding Device.....	16
14. Velocity Pressure Measuring Station Setup.....	17
15. Transducer Wiring Diagram.....	18
16. Binary-Coded Thumbwheel Wiring Diagram.....	18
17. Velocity Contour Output from Digest Workbench Data Program.....	21
18. Photograph of the Pressure Transducers Used.....	23
19. Hook Gage Pressure Correction Factor For Indicating Fluid Density Changes.	25
20. Illustration of Transducer Zero Shift.....	27
21. Illustration of Transducer Zero and Gain Shift.....	28
22. Friction Measurement Setup.....	30
23. Photograph of Bilateral Junction Tested.....	34
24. Dimensions of Bilateral Junction Tested.....	35
25. Inside of Junction Before Grinding.....	36
26. Inside of Junction After Grinding.....	36
27. Top View of Bilateral Junction Setup.....	37
28. Bottom View of Bilateral Junction Setup.....	37
29. System Components and Layout.....	38
30. System Dimensions.....	38
31. Distances from Branch Measuring Stations to Junction.....	39

32. Figure 32: Power Law Regression Fit to Observed Friction Loss/100 feet (Section 1 ↔ 4 ).....	48
33. Effect of the Number of Connectors on Friction Loss.....	49
34. Percent of Total Power Loss Resulting from Friction .....	50
35. Contribution of Different Ducts to the Friction Power Losses.....	51
36. Percentage of Error Between Measured and "Mass" Flows In Duct M.....	52
37. Normal Probability Plot for the Percent Error Between Measured and Mass Flows.....	53
38. Influence of Velocity Ratio ( $V_b/V_s$ ) on Junction Lost Power.....	59
39. Influence of Lateral to Coaxial Duct Velocity Ratio ( $V_b/V_s$ ) on Junction Lost Power When $V_a = V_b$ .....	60
40. Influence of Velocity Ratio ( $V_a/V_s$ ) on Junction Lost Power.....	61
41. Influence of Velocity Ratio ( $V_a/V_s$ ) on Junction Lost Power When $V_a = V_b$ .....	62
42. Influence of Velocity Ratio ( $V_b/V_a$ ) on Junction Lost Power.....	63
43. Influence of Velocity Ratio ( $V_b/V_a$ ) on Junction Lost Power When $V_a = V_b$ .....	64
44. Comparison of Kinetic Power Coefficients Provided by Regression and an Average of $K_a$ and $K_b$ .....	65
45. Comparison of Measured and Predicted Lost Junction Powers (normalized)....	66
46. Hypothetical Setup with Two Single-Lateral Junctions Equivalent to the Bilateral Junction Tested.....	67
47. Comparison Measured Bilateral and Two Single-lateral Junction Power Losses for Velocity Ratio ( $V_b/V_s$ ) Where $V_a = V_b$ .....	69
48. Comparison of Measured Bilateral and Predicted Two Single-lateral Junction Power Losses for Velocity Ratio ( $V_b/V_a$ ) Where $V_a = V_s$ .....	70
49. Comparison of Excess Bilateral Junction Losses to a 90° Elbow and Equivalent Lengths of 10" Diameter Duct for Velocity Ratio( $V_b/V_s$ ) Where $V_a = V_b$ .....	73
50. Comparison of Excess Bilateral Junction Losses to Equivalent Lengths of 10" Diameter Duct for Velocity Ratio ( $V_b/V_a$ ) Where $V_a = V_s$ .....	74



## LIST OF TABLES

<u>Number</u>		<u>Page</u>
1.	Computer Acquired Data Coding System.....	19
2.	Calibration Summary.....	24
3.	Lengths of Test Sections for Friction Runs.....	31
4.	Number of Connectors per Test Section for Friction Runs.....	31
5.	Regression Diagnostics Summary.....	44
6.	Empirical Friction Loss Equations.....	47
7.	Regression Results for Junction Modelling.....	55
8.	Summary Analyses for Collinearity Between Independent Variables.....	56
9.	Summary of Regression Results from After Removing Possible Outlying Data.....	58
10.	Summary Statistics for the Percentage of Excess Power Losses in the Bilateral Junction as Compared with Predicted Power Losses for Two Single Lateral Junctions.....	68
11.	Excess Bilateral Junction Losses as Equivalent Lengths of 10 inch Diameter Duct and 90° elbows for Velocities in the Range of 1000-4000 feet per minute.....	72
12.	Percentage of System Total Pressure Increase Resulting from the Bilateral Junction as Compared with the Predicted Total Pressure for a Two Single-lateral Setup.....	75

## ACKNOWLEDGEMENTS

I would like to thank Dr. Mike Morgan and Dr. Dave Covert for their help and guidance during this research and for their assistance in preparing the final manuscript. I am greatly indebted to Dr. Steve Guffey for who's continuous guidance and computer programming ability made this project an order of magnitude less difficult than originally anticipated. Finally I would also like to extend my sincere appreciation to Hugh McCloone, a fellow graduate student, who provided much assistance in setting-up the laboratory and in collecting friction data.

## DEDICATION

This work would not have been possible without the love, support, and patience of my wife Jayne and my sons Brandon and Jonathan. In addition, this accomplishment would not have been realized had it not been for my parents, Jim and Carol, who instilled in me the drive and determination to achieve the goals I have set in life. Thanks, I love you!

## CHAPTER I INTRODUCTION

### Background

Currently most industrial exhaust ventilation systems are designed using one of two methods to estimate system pressure requirements. In the American Conference of Governmental Industrial Hygienist's (ACGIH) method, "static pressure losses" are calculated for system components.<sup>(1)</sup> "Total pressure losses" are calculated in the American Society of Heating and Air-conditioning Engineer's (ASHRAE) method.<sup>(2)</sup> These methods have much in common since total pressure (TP) can be calculated by adding the velocity pressure (VP) to the static pressure (SP) and since they both compute losses in terms of velocity pressure coefficients. On the other hand, these methods differ in the way they estimate the distribution of flows and assign "pressure losses" at junctions. The ACGIH method assumes that flows are determined by a "governing" static pressure in the junction (SP<sub>J</sub>), while the ASHRAE method assumes the total pressure downstream from a junction (TP<sub>m</sub>) must be the same for all paths through the junction. Both methods assume junction pressure losses are proportional to velocity pressures.

The power balance method and the linear kinetic power model provide a third method of estimating the distribution of flows and the losses in a junction.<sup>(3,4)</sup> The power balance model is an application of the law of conservation of energy to determine the energy change per unit time (i.e. power) for conditions typical in converging flow junctions.<sup>(3)</sup> The linear kinetic power model assumes that the power losses in any junction are related linearly with the kinetic powers of each branch entering the junction.

ACGIH currently does not provide information to predict flows and pressures in bilateral junctions (see Figure 1) and recommends against them without providing any justification. ASHRAE provides information on a very limited subset bilateral junction configurations. The kinetic power model should theoretically apply to bilateral junctions but only single-lateral junctions (see Figure 2) have been tested with this method.

There are many practical applications for bilateral junctions; but, in the absence of data for design their use is problematic. Bilateral junctions may provide economic benefits;

however, the potential costs of using these junctions (i.e. increased pressure requirements, increased settling, etc.) are not currently known.

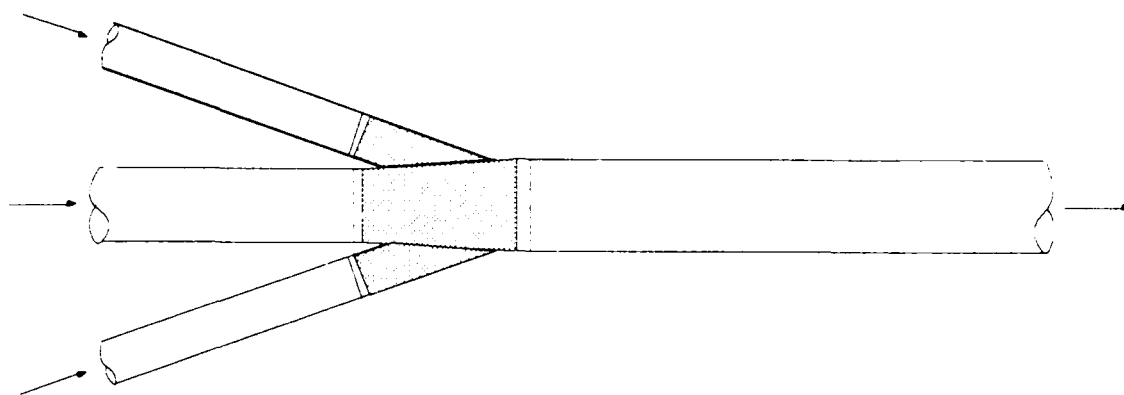


Figure 1: Bilateral Junction

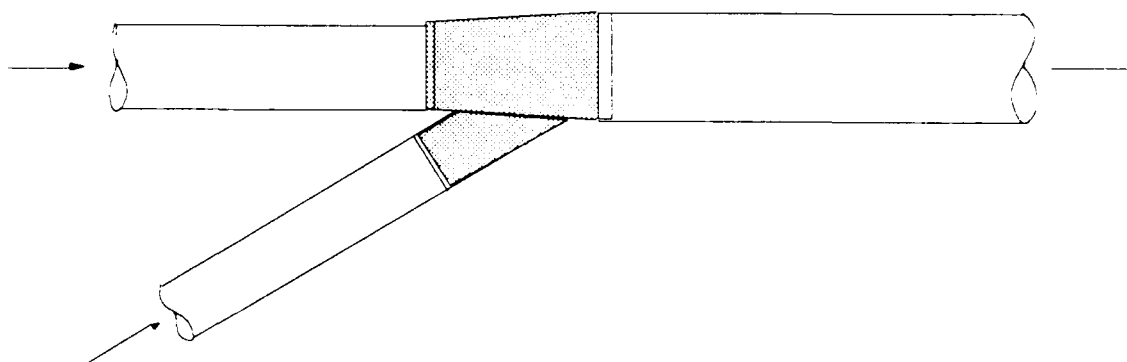


Figure 2: Single-lateral Junction

### Research Objectives

The primary goal of this research was to characterize the flow in a bilateral junction and to determine if the kinetic power model could be successfully applied to predict power losses. If successful, similar research could be completed on many bilateral junctions with various geometric variables to develop a general model applying to a wide range of bilateral

junctions as has been done with single-lateral junctions.<sup>(4)</sup> A secondary goal was to test the hypothesis that the power losses for three flows joined at a bilateral junction are not significantly different than the combined power losses of identical flows joined by two single-lateral junctions.

## Current Design Methods

### ACGIH Method

In Industrial Ventilation, the ACGIH provides a method for designing systems containing single lateral junctions.<sup>(1)</sup> ACGIH recommends against bilateral junctions, but provides no justification for this recommendation and does not provide a method of designing systems containing these junctions.<sup>(1)</sup> However, ACGIH does provide two alternatives to bilateral junctions. The "preferred option" is to place two single lateral junctions in series very close together as shown in Figure 3. The second "acceptable option" (Figure 4) is similar to a bilateral junction except that the side laterals are offset from each other. Appendix A contains the original figure from the ACGIH manual showing these recommendations.

### ASHRAE Method

ASHRAE provides loss coefficients for a single type of bilateral junction in its 1989 Fundamentals Handbook; Appendix B contains a copy of the table of coefficients.<sup>(2)</sup> In the ASHRAE bilateral junctions, the diameters of laterals are equal to each other and the coaxial ducts also have equal diameters. This type of junction may be useful for general room ventilation in a plenum type system; but its value is limited in industrial ventilation design particularly in systems carrying particulates. In these systems, maintaining minimum target velocities is critical to prevent settling. The bilateral junction cited by ASHRAE forces designers toward systems with excessive velocities in the duct downstream of the junction since the combined areas of the upstream ducts are greater than the downstream duct. These excessive velocities increase system operating and

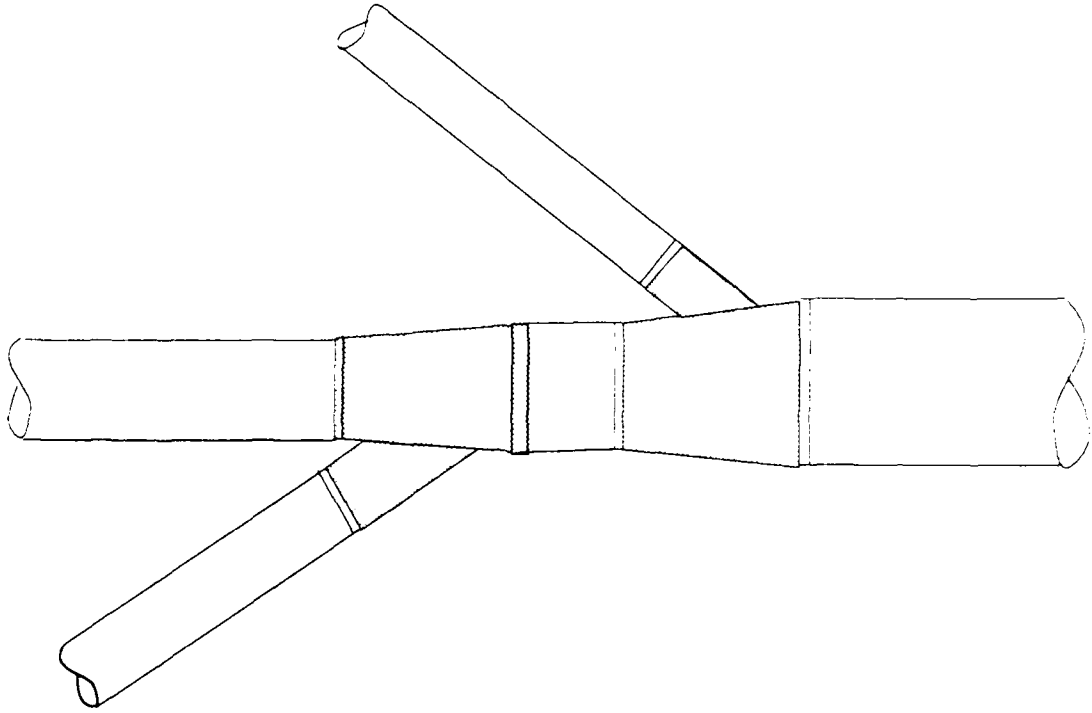


Figure 3: ACGIH "Preferred" Option to Bilateral Junctions

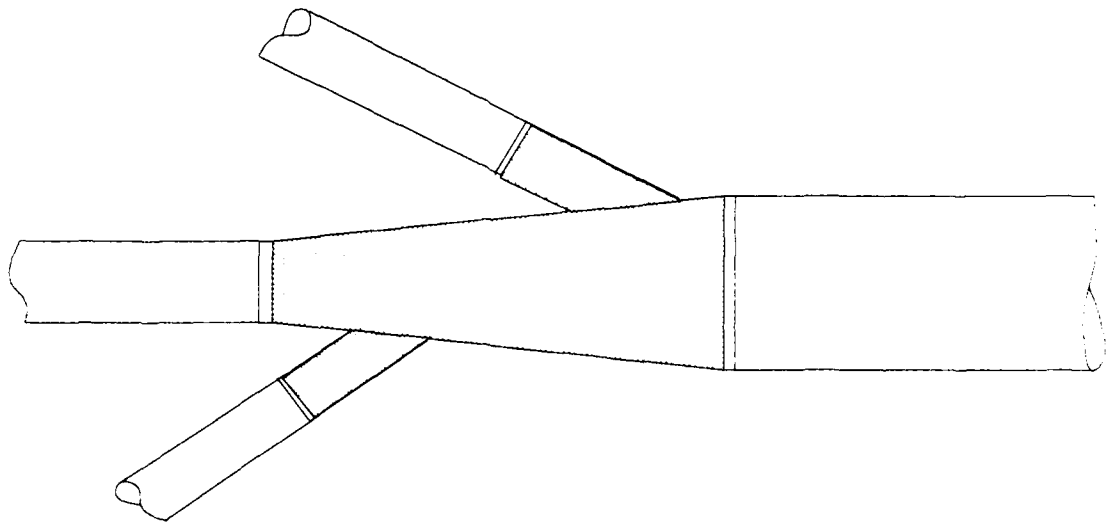


Figure 4: ACGIH "Acceptable" Option to Bilateral Junctions

maintenance costs because of higher power requirements and abrasion. In gas and vapor conveying systems, minimum target velocities are not critical; but similar tradeoffs occur between initial costs and long-term operating costs.

ASHRAE adapted their coefficients from Idelchik.<sup>(5)</sup> When transferring Idelchik's table of coefficients, ASHRAE made an error in the coefficients for the "main" portion of the table by printing the ratio of the areas for the side branches ( $A_{2b}/A_{1b}$ ) as an independent variable. Idelchik's original table lists the ratio of flows ( $Q_{2b}/Q_{1b}$ ) as the independent variable. Idelchik provides several tables of coefficients for similar junctions with different branch entry angles (see Appendix C).

The author verified Idelchik's table of coefficients that was adapted by ASHRAE by substituting the independent variables from the tables into the equations accompanying the tables. Several differences were found between the calculated loss coefficients and the table values. In most cases, the difference between the table and calculated values was only 0.01-0.03 (dimensionless coefficient); however, in several cases the difference was between 0.10 and 0.50. In one case the table value was 10 times the calculated value. Appendix D contains the tables of corrected coefficients. No effort was made to verify the coefficients for any of the other bilateral junctions provided by Idelchik.

### Power Balance Method

Air flowing through a ventilation system has three energy components: kinetic, potential and internal.<sup>(3)</sup> The static pressure between two points in a system provides the driving force for air and is thus the source of potential energy. The air moves from one point to another at a certain velocity and thus has kinetic energy. Finally, air has internal energy that changes because of heat transfer. At any cross-section, the air flows through a system at a certain rate. As a result, these energies can be expressed as an energy rate, or power.<sup>(3)</sup>

The general form of the total power of flow at a cross-section (Equation 1) is quite complicated; however, assumptions can be made which greatly simplify the general equation without significant loss in accuracy for typical ventilation systems.<sup>(3)</sup> Following is the general equation for the total power flow at a cross section:<sup>(6)</sup>



$$TFP = \int_A (v_x \rho) \left[ \frac{SP}{\rho} + e + \frac{1}{2} (v_x^2 + v_y^2 + v_z^2) + h_z g \right] dA \quad \dots(1)$$

where: TFP = total flow power at a cross section of duct

$v_x$  = velocity of air along the axis of the duct

$\rho$  = mass density of air

SP = static pressure at the cross section

$e$  = specific internal energy of the airstream

$v_y$  = air velocity toward the side of the duct along the y axis

$v_z$  = air velocity toward the side of the duct along the z axis

$h_z$  = elevation of the flow from a datum

$g$  = acceleration due to gravity

For any junction, where no external power is added, the power of the airflow exiting the junction must equal the sum of the powers of the incoming airflows minus the power lost (dissipated as heat). Power may also be lost from the system by the conduction of heat through the walls of the junction to the surrounding environment. Equation 1 may be simplified based on the following assumptions:<sup>(3)</sup>

1. One dimensional flow. Air flows axially along the duct; therefore,  $v_y$  and  $v_z$  are zero.
2. Incompressible flow. Negligible errors result from this assumption for velocities up to Mach 0.2 <sup>(7)</sup> Mach 0.2 is equivalent to 13,200 feet per minute. The maximum velocity used in this study was less than one half this value, yet represents an extreme value for practical ventilations.
3. Adiabatic conditions. Since the air in the duct comes from within the laboratory, there is very little difference ( $\pm 2^\circ\text{C}$ ) between the temperature of the air in the duct and the environment surrounding the duct. As a result, there is no large temperature gradient to effect a significant amount of conduction across the junction or across the ducts between the junction and the measuring stations. In addition, the lengths of duct are relatively short which minimized the opportunity for heat transfer.
4. Uniform flow. This assumption can be verified by observing the uniformity of the velocity profiles during data collection. If the velocity profiles are reasonably

uniform, then the air density and static pressure should also be uniform. In fact, it is not necessary for the velocity profiles to be uniform as long as the velocity contours are nearly the same upstream and downstream.<sup>(3)</sup>

5. No change in elevation. Since the density of air is low, negligible errors will result from small elevation changes within the laboratory. All measurement stations were within 1 inch of the same elevation in this experiment.

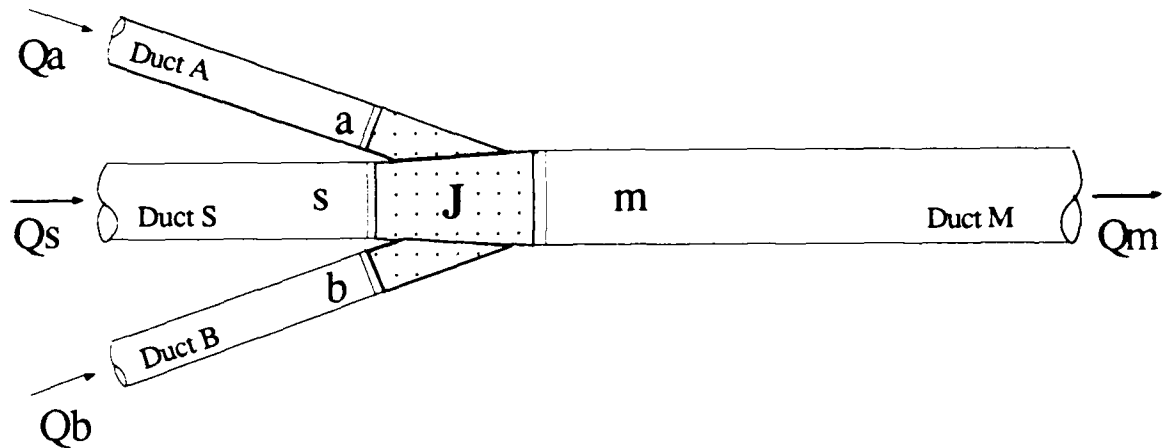


Figure 5: Bilateral Junction with Nomenclature

Following is the simplified Power Balance equation for a bilateral junction (see Figure 5):<sup>(3)</sup>

$$LP = Q_a(SP_a + VP_a) + Q_b(SP_b + VP_b) + Q_s(SP_s + VP_s) - Q_m(SP_m + VP_m) \quad \dots(2)$$

where: LP = total lost power

Q = flow in the duct

SP = static pressure in the duct

VP = average velocity pressure in the duct

Subscripts a, b, s, and m represent reference cross-sections in ducts A, B, S and M

Flows and pressures cannot be measured near the junction because of the disturbances induced by the colliding airstreams. As a result, these measurements must be taken at some distance from the junction. Measurements taken far upstream and downstream include the

losses attributable not only to the junction but to friction as well. To find the power loss attributable to the junction alone, the power lost due to friction between the points where pressure measurements are taken and the junction must be estimated and then subtracted from the total dissipated power. The expression for the power lost due to friction follows:

$$LPF = Q_m(\Delta SPF_{J-m}) + Q_a(\Delta SPF_{J-a}) + Q_b(\Delta SPF_{J-b}) + Q_s(\Delta SPF_{J-s}) \quad \dots(3)$$

where: LPF = power lost due to friction

$\Delta SPF_{J-i}$  = predicted change in static pressure (due to friction)  
between the junction and the duct measuring station

Q = airflow in the duct

Subscripts a, b, s, and m represent reference cross-sections in ducts A, B, S and M

Finally, the lost power attributable to a junction can be determined empirically from the following:

$$LPJ = LP - LPF \quad \dots(4)$$

where: LPJ = power lost due to the junction

LPF = power lost due to friction

LP = total lost power

By expansion, Equation 4 becomes:

$$LPJ = [Q_a(SP_a + VP_a) + Q_b(SP_b + VP_b) + Q_s(SP_s + VP_s) - Q_m(SP_m + VP_m)] \quad \dots(5) \\ - [Q_m(\Delta SPF_{J-m}) + Q_a(\Delta SPF_{J-a}) + Q_b(\Delta SPF_{J-b}) + Q_s(\Delta SPF_{J-s})]$$

where: LPJ = power lost due to the junction

$\Delta SPF_{J-i}$  = predicted change in static pressure (due to friction)  
between the junction and the duct measuring station

Q = airflow in the duct

SP = static pressure in the duct

VP = average velocity pressure in the duct

Subscripts a, b, s, and m represent reference cross-sections in ducts A, B, S and M

Guffey and Fraser determined that the power losses in a single lateral junction were a linear function of the kinetic powers of the incoming and outgoing ducts.<sup>(4)</sup> Applying the kinetic power model to a bilateral junction, the following model results:

$$LPJ = Q_a VP_a K_a + Q_b VP_b K_b + Q_s VP_s K_s \quad \dots(6)$$

where: LPJ = power dissipated across the junction

Q = air flow through the duct

VP = average velocity pressure in the duct

K is an empirical loss coefficient for the duct

Subscripts a, b and represent reference cross-sections in ducts A, B and S

### The Case for Bilateral Junctions

Bilateral junction systems have practical advantages over multiple single-lateral systems. Normally, plant equipment is located to provide the most efficient flow for the work process and to conserve floor space. As a result, equipment is often positioned on the plant floor symmetrically. If plant processes require local exhaust ventilation in this situation, a bilateral junction to merge system branches is an attractive alternative since it simplifies system design and installation (see Figure 6).

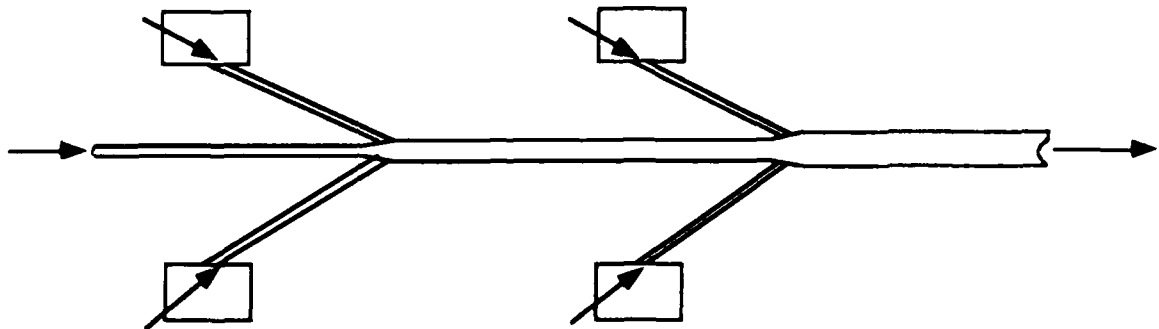


Figure 6: Bilateral Junction Design Option

In reality, the ACGIH alternatives to bilateral junctions (Figures 3 and 4) may be no more efficient than bilateral junctions. One might assume that the loss coefficients for single lateral junctions apply to these alternatives since ACGIH provides no correction factors or further explanations. However, this is a precarious assumption since locating system components too close together can cause calculated pressure losses to be in error by a factor of two or more because of interaction effects.<sup>(8)</sup> Miller suggests an interaction correction factor of unity can be used only when the junctions are three or more diameters apart.<sup>(8)</sup> The ACGIH "preferred" option does not appear to meet this guideline (see Appendix A).

Since the behavior of flow in bilateral junctions has not been well characterized, and since they are not recommended by the ACGIH, designers are forced into less economical alternate designs. Worse yet, designers may be forced into guessing what will happen if these junctions are used and then to adjusting the system after construction to compensate for pressure loss calculation errors. Figures 7 and 8 show two alternate system designs that avoid bilateral junctions. The parallel systems design in Figure 7 has the disadvantages of higher initial costs and additional space requirements that may lead to interferences with other plant equipment or utilities. The offset single-lateral junction design shown in Figure 8 is more economical and consumes less space than the parallel system design; however, it is still inferior to the bilateral junction design with regards to initial costs and space requirements. Long-term operating costs will also be slightly higher in the offset single-lateral system than the bilateral system if the longer laterals increase system pressure requirements. A final factor that must be considered with the offset single-lateral design is the unknown increase in pressure losses that may result because of interaction effects if the single-lateral junctions are located close together.<sup>(8)</sup>

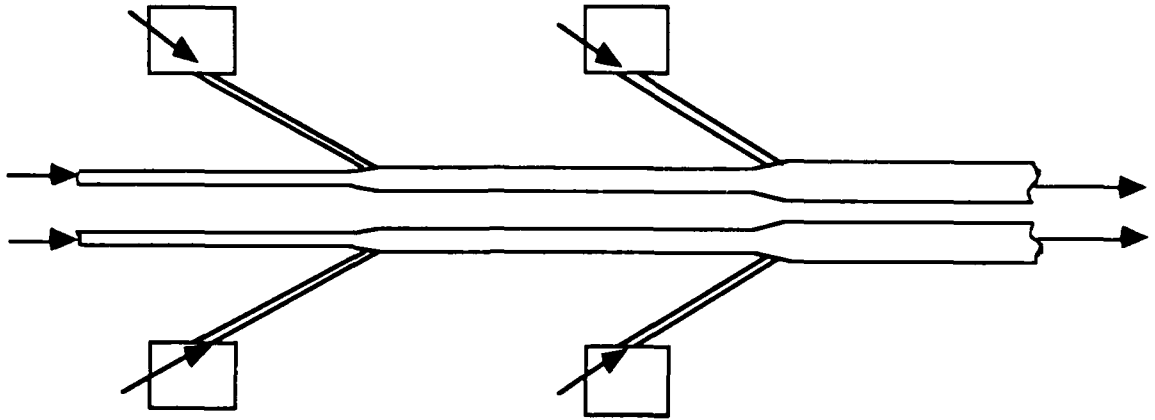


Figure 7: Parallel Systems Design Option

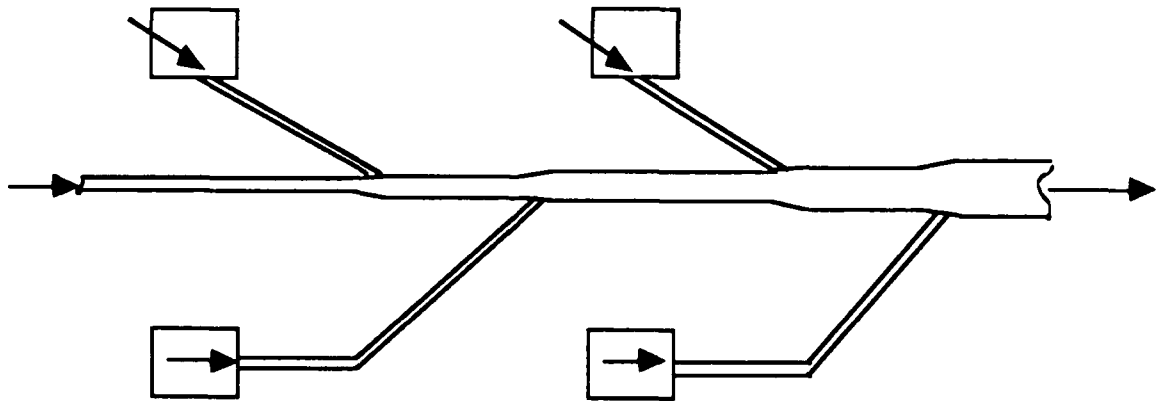


Figure 8: Offset Single-Lateral Junctions Design Option

## CHAPTER II MATERIALS AND METHODS

### Laboratory Setup

The apparatus included the fan; the ducts and their connectors; the supporting frame for the ducts; the velocity pressure measurement stations; Pitot tubes and associated tubing; pressure sensors; and the computer and its peripheral devices for data collection.

### Fan, Motor and Transmission

Airflow was provided by a centrifugal fan (Buffalo Forge, MW40, Buffalo NY) and was varied using an infinitely variable geared transmission device (Speed Control Industries Inc, Model 7-10A (E) 0:1-1 CCW, Richland WA) connected to a 20 horsepower motor. The drive shaft of the fan was connected to the transmission by belts and pulleys, and the shafts of the motor and transmission were connected shaft to shaft with a locking device. Fan rotation rates were varied from about 200 to 1600 revolutions per minute (rpm). Rotation rates drifted from a nominally fixed rate by an average of 7.5 rpm/hour (range 2-28 rpm/hr over a 30 minute period). In general, the run-time per observation period was approximately 30 minutes for friction and 2 hours for junctions. The drift tended to be highest at higher rotation rates.

### Duct System

The ducts used in this study were standard 20 and 24 gauge spiral wound galvanized steel duct that was purchased from a manufacturer of ventilation system components (United McGill, Stockton CA). All ducts were cleaned with hot water and dishwashing detergent to remove a vegetable oil coating applied during the manufacturing process.

Ten foot lengths ( $\pm 3$  inches) of spiral wound duct rested on 0.75 inch cabinet-grade plywood vertical spacers (Figure 9) that were mounted every 10 feet on an 80 foot long metal frame suspended 30 inches from the laboratory ceiling. The frame was supported every 6 feet with 0.375 inch steel threaded rod, and was leveled with a rotating laser. Each

vertical spacer was centered on the longitudinal axis of the support frame. Separate hangers spaced at 6-8 foot intervals were installed to support the system branches (see Figure 10).

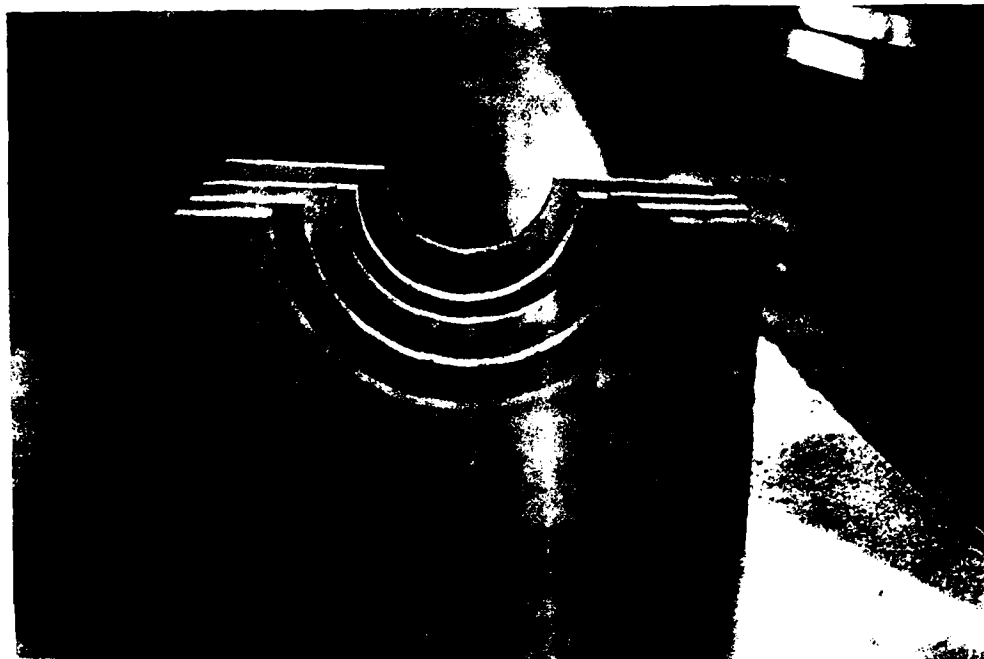


Figure 9: Photograph of Plywood Vertical Spacers

The ducts were connected to each other with 18 gauge galvanized steel insert couplers manufactured for that purpose. The couplers were 4 inches long, and were approximately equal to the nominal duct diameter at the midpoint and 0.18 inches less than the nominal duct diameter at each end to allow a tight-fitting insertion. The ends of the ducts connected to the measurement stations terminated in 2 inch iron flanges constructed from 0.14 inch thick angle iron. The upstream end of the each velocity pressure measurement station terminated with a plywood (0.75 inch thick) over-sized rectangular flange. The ducts were aligned to the measurement station by bolting each duct flange to a corresponding measurement station flange. No part of the flanged connectors projected into the airflow. These connectors provided very good alignment and minimized potential disturbances close to the measuring station. Figure 11 shows the standard connector on the left and the flanged connector on the right.





Figure 10: Photograph of Branch Supports

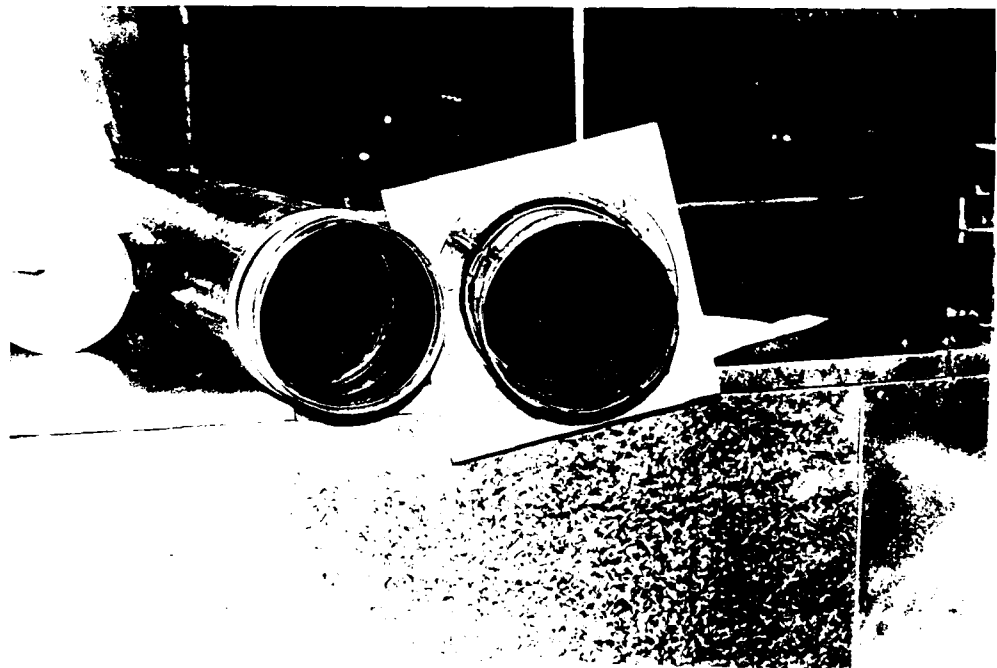


Figure 11: Measuring Station Connector Compared with Standard Connector

All duct-to-duct connections were sealed with duct tape to prevent leaks. The duct-to-measurement station connections were sealed with a combination of duct tape and silicone sealant. Ducts were aligned in the horizontal plane using a string line and their alignment in the vertical plane was verified with a construction-type level.

### Pressure Measurement Stations

A "drawn-over-mandrel" (DOM) 0.25 or 0.5 inch thick steel tube with an inner diameter matching the nominal inner diameters of the duct was used for all velocity pressure traverses. All static pressures and static pressure differentials were measured at the duct centerline.

All pressure measurements were taken using ANSI/ASHRAE Standard 41.2-1987 hemispherical head 0.125 inch Pitot tubes mounted in Pitot tube holders with log-linear insertion depths controlled to within 0.0005 inches (see Figures 12 and 13).<sup>(9,10,11,12)</sup> To minimize leaks around the Pitot tubes, a small (0.5 inch by 1.0 inch) galvanized steel sheet metal strip with a 0.15 inch diameter hole drilled in it was taped over the hole that had been drilled in the duct or DOM tubing before inserting the Pitot tube. All velocity pressure measuring stations contained three Pitot tubes for conducting 10-point traverses along 3 diameters off-set by 120 degrees but in the same plane (see Figure 14). Each of the Pitot tube holders was mounted to the DOM tubing as shown in Figure 12.

### Leak tests

Pressure was conducted from the Pitot tubes to the pressure sensors using 3/16 inch inside diameter (1/16 inch wall thickness) Tygon® tubing and low density polypropylene quick-disconnect fittings. The number of fittings was kept to a minimum to reduce the potential for leaks. Each pathway was tested in place for leaks with approximately 4 inches water gage (w.g.) pressure. Over a 5 minute span, none showed measurable pressure losses (<0.005 inches w.g.).

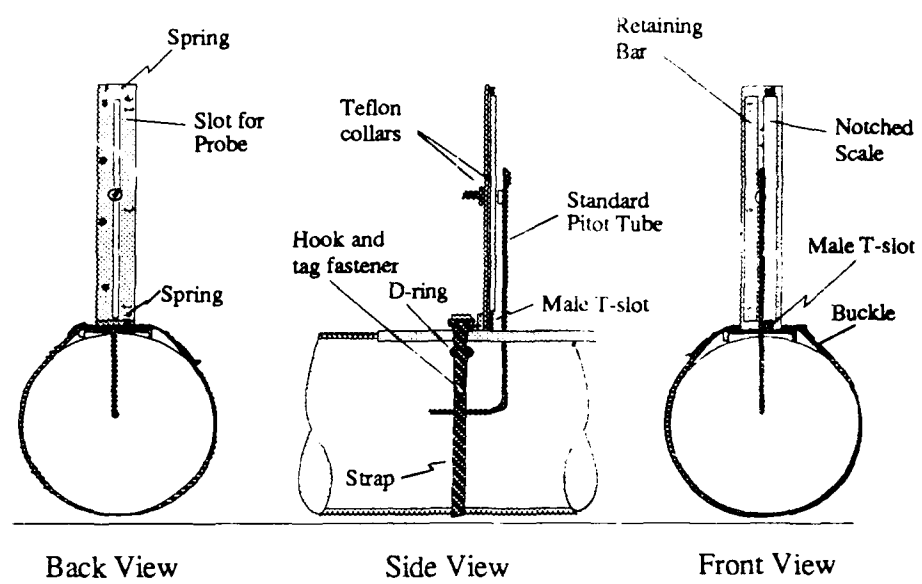


Figure 12: Diagram of Pitot Tube Holding Device and Mounting



Figure 13: Photograph of Pitot Tube Holding Device

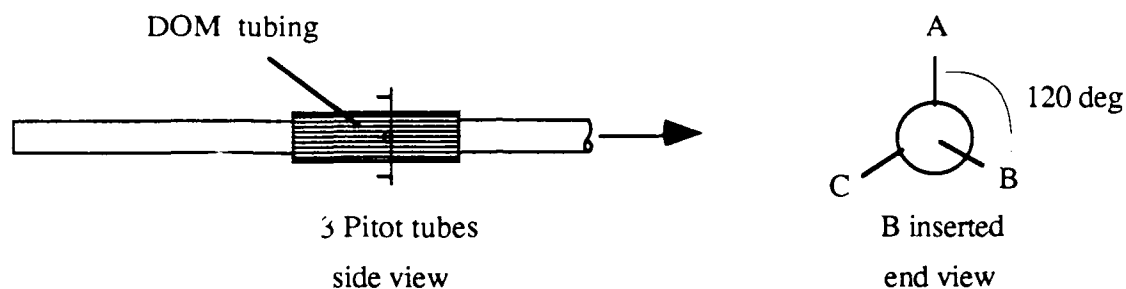


Figure 14: Velocity Pressure Measuring Station Setup

A leak test of ducts was completed on each setup before collecting data by sealing all duct inlets with duct tape and developing a static pressure of approximately 2.5 inches within the system. Leaks were sought and sealed until the differential static pressures across the experimental lengths were less than 0.005 inches and there was no measurable centerline velocity pressure. After completing the leak test, the duct tape was removed from the end of the ducts and a steel ring with open-celled honeycomb air-flow straightener was placed on the end of each duct not having this material already installed several diameters downstream of the opening.

#### Computer Data Acquisition System and Data Reduction

Pressure transducers were connected to a computer (Apple Macintosh™ SE) containing a data acquisition card via a terminal panel (Strawberry Tree, Sunnyvale CA). The acquisition card converted analog voltages to digital inputs that were recorded to a computer file using "Analog Connection Workbench™ 2.0" software (Strawberry Tree, Sunnyvale CA). A binary-coded thumb wheel (Cherry Electrical Products Corporation, Waukegan IL) was used to identify groups of data and individual data points. The Workbench™ computer program produced ASCII text files containing the date, time, identification code and transducer voltage output for each of eight channels. Figure 15 is a wiring diagram for the transducers and Figure 16 is a wiring diagram for the transducers.

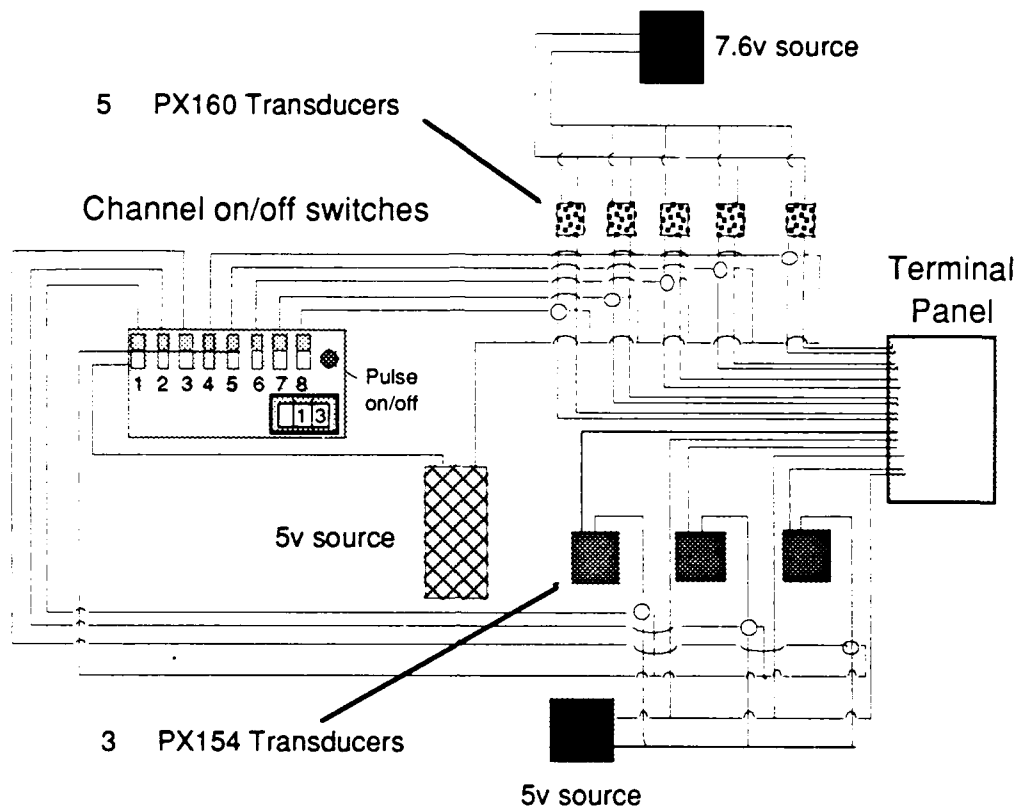


Figure 15: Transducer Wiring Diagram

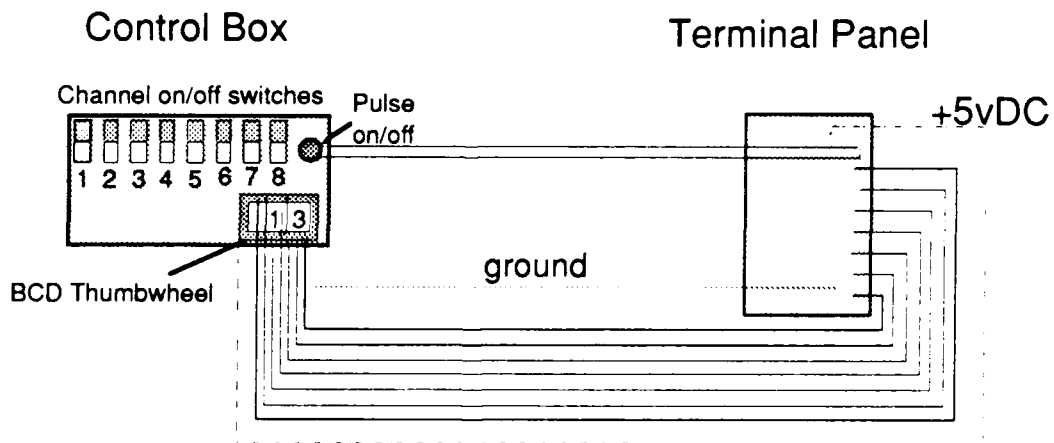


Figure 16: Binary-Coded Thumbwheel Wiring Diagram

During transducer calibration, individual calibration points were consecutively numbered with settings on the thumb wheel ranging from 0 through 79. Normally no more than 50 calibration points were accomplished in any one day.

During friction and junction data collection, groups of data were identified by setting the thumbwheel to a "run" number from 41 through 75 and pressing the "pulse on/off" switch while the switches for all transducers were in the off position. The thumbwheel was then set to a number (1-39) to identify an individual data point within a given run. Only one analog channel was switched on at a time. Table 1 contains the coding system used to identify data "runs" and individual data points. When all data for a "run" was collected the signal switches for all transducers were turned off and the next run number was logged.

Table 1: Computer Acquired Data Coding System

<u>Pressure Type</u>	<u>BCD Number</u>
Velocity pressure traverse points	1-30
Centerline velocity pressures	31-33
Static pressure at VP measuring location	34
Differential static pressures	35-39
Calibration pressures	76-79

Computer-generated ASCII text files were analyzed using one of two computer programs developed by Dr. Guffey. Calibration data was analyzed using the "Calibration Digestion" program. Friction and junction data were analyzed using the "Digest Workbench Data" program.

The "Digest Workbench Data Program" reduced data to the average velocity, average velocity pressure, and differential static pressures. The program opened and read the ASCII text file containing transducer voltages; converted all voltages to pressures based on calibration data; opened and read the text file containing the laboratory dry bulb and wet bulb temperatures, barometric pressure, and airstream temperature; calculated the corrected barometric pressure; calculated the airstream density factor from the duct temperature, water vapor concentration, duct static pressure and corrected barometric pressure; and calculated

the average velocity and average velocity pressure for each traverse. The average velocity pressure in this instance is not the average of the velocity pressures, but the average velocity pressure calculated from the average velocity in the duct.

While the "Digest Workbench Data" program was running, it graphed velocity contours for each traverse on the computer screen, allowing identification of possible data collection errors and poor flow conditions. Figure 17 is a photograph of the screen output during data analyses. The two traverses on the right side of Figure 17 have uniform velocity profiles while the left side shows a case where a leak developed at the tubing/Pitot tube interface.

The program produced three text files. One file contained information on each individual velocity pressure; this file could be used to reexamine velocity profiles. The second file contained the following information for each run:

- Date
- Time
- Run number
- Airstream temperature
- Corrected barometric pressure
- Room density factor
- Number of traverse points
- Duct density factor
- Average velocity pressure
- Average centerline velocity pressure
- Each centerline velocity pressure
- "True" velocity pressure
- Static pressure at the VP measuring station
- All differential static pressures measured

The third file was a self calibration file that contained recorded voltages and predicted pressures. This file was used to develop calibration curves for each data collection set using data points where both inclined manometer and a transducer measurements were taken. This procedure is discussed later in the equipment calibration portion of the methods.

The "Digest Workbench Data" program eliminated calculation errors that could be expected from reducing this large quantity of data by hand. The program also provided a better method of auditing calculations than is available with computer spreadsheet programs.

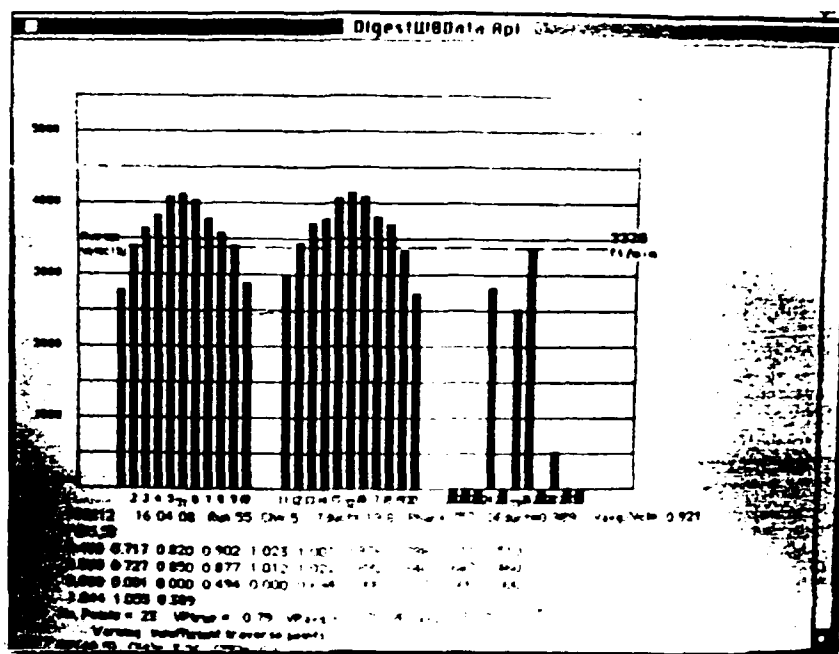


Figure 17: Velocity Contour Output from Digest Workbench Data Program

## Measuring Equipment and Calibration

### Pressure Measuring Equipment

Before pressure data were collected, pressure measuring devices were calibrated with a hook gage (Dwyer Instruments Inc, Series 1425, Michigan City IN) having a resolution of 0.001 inches w.g. The hook gage contained fluorescein green color concentrate that was mixed with distilled water according to the manufacturer's instructions.<sup>(13)</sup> Before each use, the hook gage was leveled using the built in bubble levels and the hooks were zeroed.

Two inclined manometers (Meriam Instrument, Model 40HE35WM, Cleveland OH) with resolutions of 0.005 inches w.g. were used as the predominant measuring devices for



static and differential pressures 4 inches w.g. or less. Each manometer contained Meriam 1000 Green Concentrate (No. 922WA) mixed with distilled water according to the manufacturer's instructions.<sup>(14)</sup> The inclined manometers were mounted on a wall and leveled using the built-in bubble level. The level and zero for each inclined manometer was checked and adjusted as necessary before each set of readings.

A Meriam Instruments Meri-cal® Model DP200I produced a digital readout with a display resolution of 0.01 inches w.g. It was electronically zeroed with the zero switch before each use and was used with internal damping toggled on. The Meri-cal® was very sensitive to pressure changes and occasionally displayed wide fluctuations in the digital readout even with the damping switch on. An attempt to provide physical damping by placing charcoal tubes in the Tygon® tubing leading from the Meri-cal® appeared to have little effect. Because of its low resolution and readout fluctuations, the Meri-cal® was used only to provide secondary measurements for pressures exceeding 4 inches w.g. When the Meri-cal® was used, the mean of the high and low readouts was recorded as the pressure.

Two models of pressure transducers (Omega Engineering Inc., PX160 and PX154 Series, Stamford CT) were used as the primary velocity pressure measuring devices in this study. The transducers were mounted on a plywood panel that was affixed to the laboratory wall (see Figure 18). The transducers produced voltages or currents proportional to applied pressures. The signal output was digitized and recorded to a computer file by the data acquisition system. Transducers were allowed to warm-up at least one-half hour before each use.

The hook gage, hand pump (Meriam Instruments, Model B34348), and all pressure sensing instruments, were connected to a glass manifold with Tygon® tubing for calibration. As a result, each instrument experienced the same pressure developed by the hand pump. All connections were sealed with a silicone sealant and the calibration setup was tested for leaks at the start of each run using approximately 3 to 4 inches w.g. of positive pressure. The setup was assumed to be free of significant leaks if the leakage rate was less than 0.0001 inches w.g. per minute. This assumption is based on the fact that all instruments were read for each calibration point in a period of 2 minutes or less.

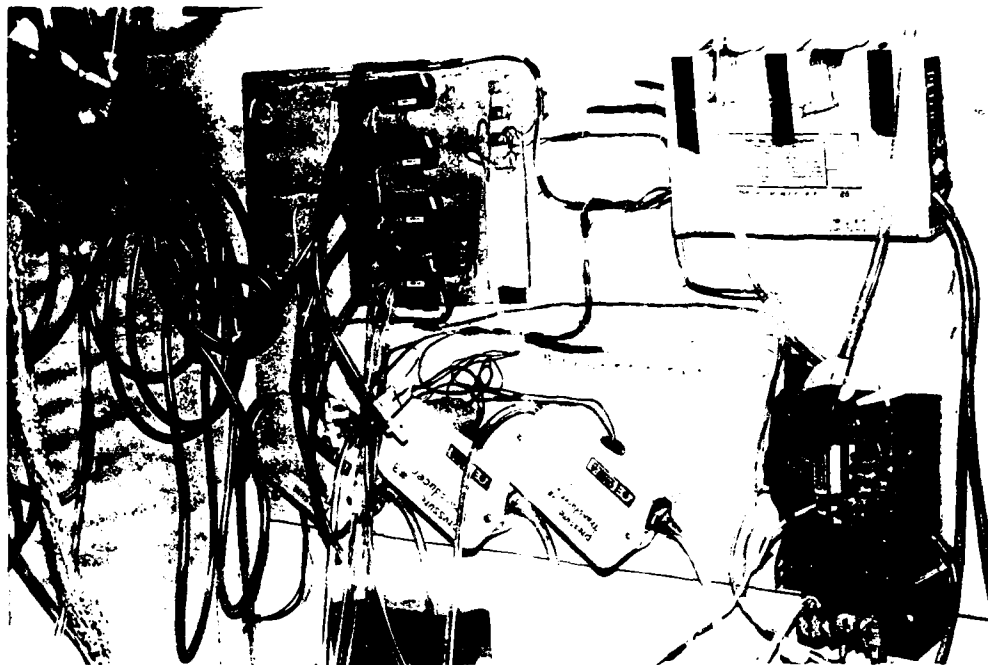


Figure 18: Photograph of the Pressure Transducers Used

The room temperature and barometric pressure were recorded at the start, the finish, and periodically during each calibration run. Generally, calibration runs started at the low end of the hook gage range and progressed to the high end of the range in one tenth of an inch w.g. increments. Once the high end of the range was reached, additional calibration points were obtained by successively releasing pressure from the system until the original pressure was achieved. The hook gage pressure and vacuum readings, inclined manometer readings, and the Meri-cal® readings were recorded on a data collection worksheet for each calibration point (see Appendix E). The hook gage range, which depended on the spacer rod selected, was also noted for each run. The voltage produced by each pressure transducer for each calibration point was recorded to a computer file using the computer data acquisition apparatus and software. To avoid the potential for electronic interference between transducers, the voltages resulting from the applied pressures were recorded for each transducer with the signal from all other transducers switched off.

Numerous calibration runs over a period of five months were completed before data collection began. Many calibration runs were conducted without the Meri-cal® because it

was out for repair. Table 2 provides a summary of the number of calibration points for each piece of equipment used in this study.

The hook gage pressure values were corrected for the slight changes in indicating fluid density due to temperature variation. Figure 19 shows the relationship between the hook gage correction factor and the laboratory temperature in degrees Celsius. The correction equation was developed from information provided by the manufacturer.<sup>(13)</sup>

$$\text{Corrected Hook Gage Pressure} = (\text{Observed Hook Gage Pressure})(\text{Correction Factor}) \dots(7)$$

Table 2. Calibration Summary

<u>Equipment</u>	<u>Number of Calibration Points</u>	
	<u>0-4 inch Range</u>	<u>4-6 inch Range</u>
Transducer No.8	290	0
Transducer No.5	305	16
Transducer No.4	295	0
Transducer No.3	252	0
Inclined Manometer No.1	305	N/A
Inclined Manometer No.2	305	N/A
Meri-cal®	138 points in the 0-12 inch range	

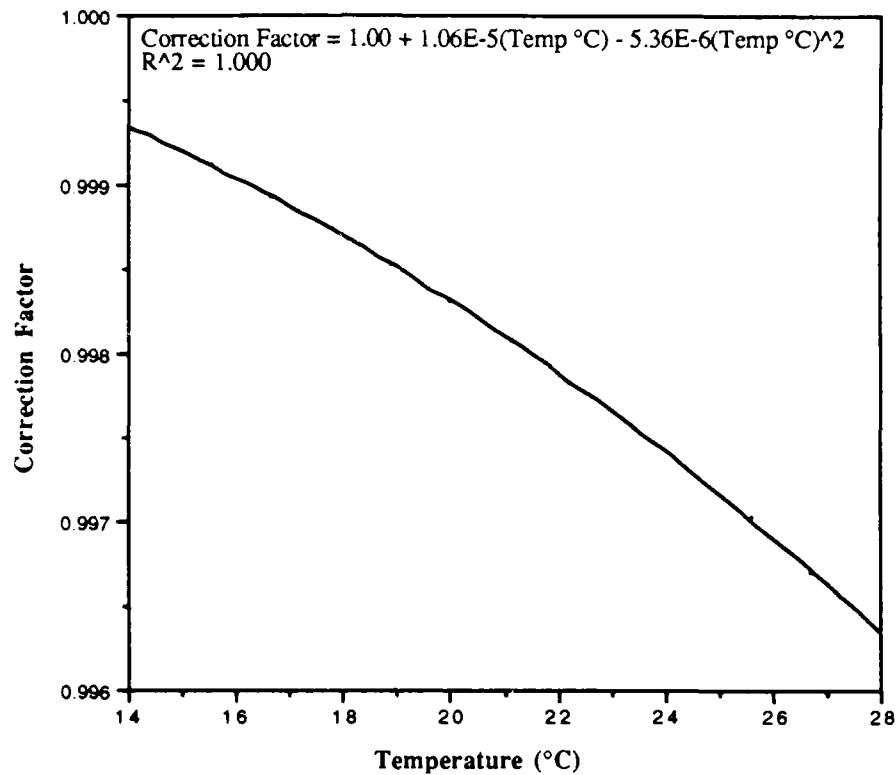


Figure 19: Hook Gage Pressure Correction Factor For Indicating Fluid Density Changes.

ASCII text files produced by the data acquisition software were opened and read by the "Calibration Digestion" computer program written by Dr. Guffey. This program determined which transducer was on and calculated the estimated pressure based on previously determined calibration coefficients. The resulting values were recorded to a "Digested Calibration Data" ASCII file containing the date, time, identification code, transducer number, measured voltage, and estimated pressure for each calibration point.

The contents of the calibration data file were imported into a computer spreadsheet program, and the observed pressure values from the hook gage and other instruments were entered adjacent to the proper identification code. Hook gage values were corrected for temperature using the relationship developed for indicating fluid density and temperature. Next, a text file of the resulting data was imported into a commercial statistics program

(Data Desk® Professional, Odesta Corporation, Northbrook IL). Scatter plots of corrected hook gage pressures versus transducer voltages and of the hook gage pressures versus the pressures observed with other instruments, identified errors resulting from miskeyed data, transposed numbers or spurious transducer voltages. The sources of errors were investigated by reviewing the original data collection sheets. When the source of error was found it was corrected; however, data points with unexplained error were removed from the data set for analysis since they would exert high leverage during regression analysis.

Transducer voltages were related to the pressures measured with the hook gage using the following regression equation:

$$\text{Hook Gage Pressure} = C_0 + C_1(\text{Voltage}) + C_2(\text{Voltage}^2) \quad \dots(8)$$

where:  $C_0$ ,  $C_1$ , and  $C_2$  = regression coefficients providing the best fit to the pressure range of interest

Linear regression was used to provide calibration curves for the inclined manometers and the Meri-cal®. Following is the general form of the model used:

$$\text{Hook Gage Pressure} = C_0 + C_1(\text{Pressure Reading}) \quad \dots(9)$$

where:  $C_0$ , and  $C_1$  = regression coefficients providing the best fit to the pressure range of interest

The pressure transducers apparently experienced small daily shifts in zero and gain. Figure 20 shows an apparent zero shift for one set of data, and Figure 21 shows an apparent gain shift coupled with a zero shift. As a result, transducers were calibrated for each set of measurements using experimental pressures measured with an inclined manometer.

Appendix F contains the calibration curves for the pressure measuring devices used in this study.

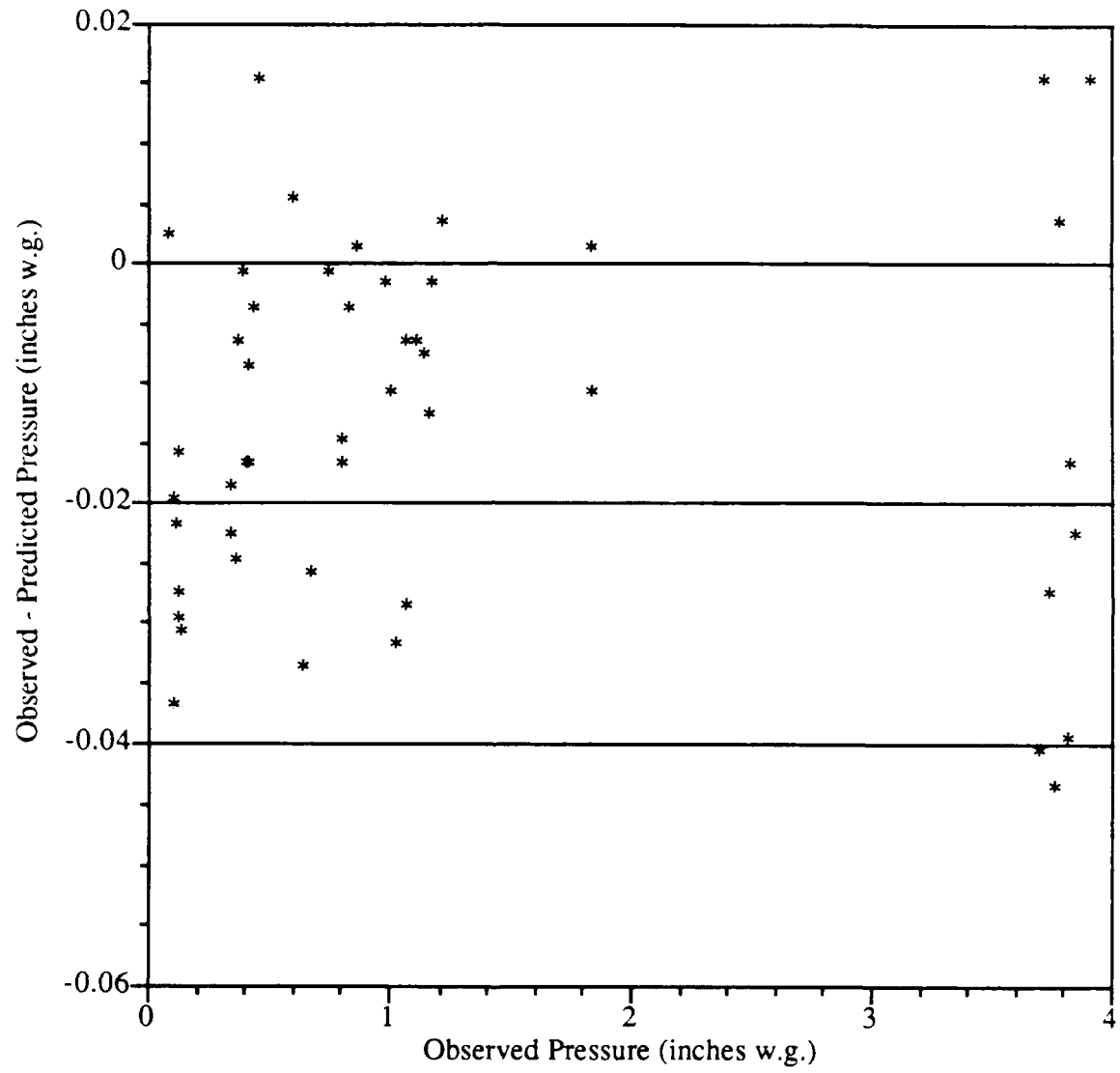


Figure 20: Illustration of Transducer Zero Shift

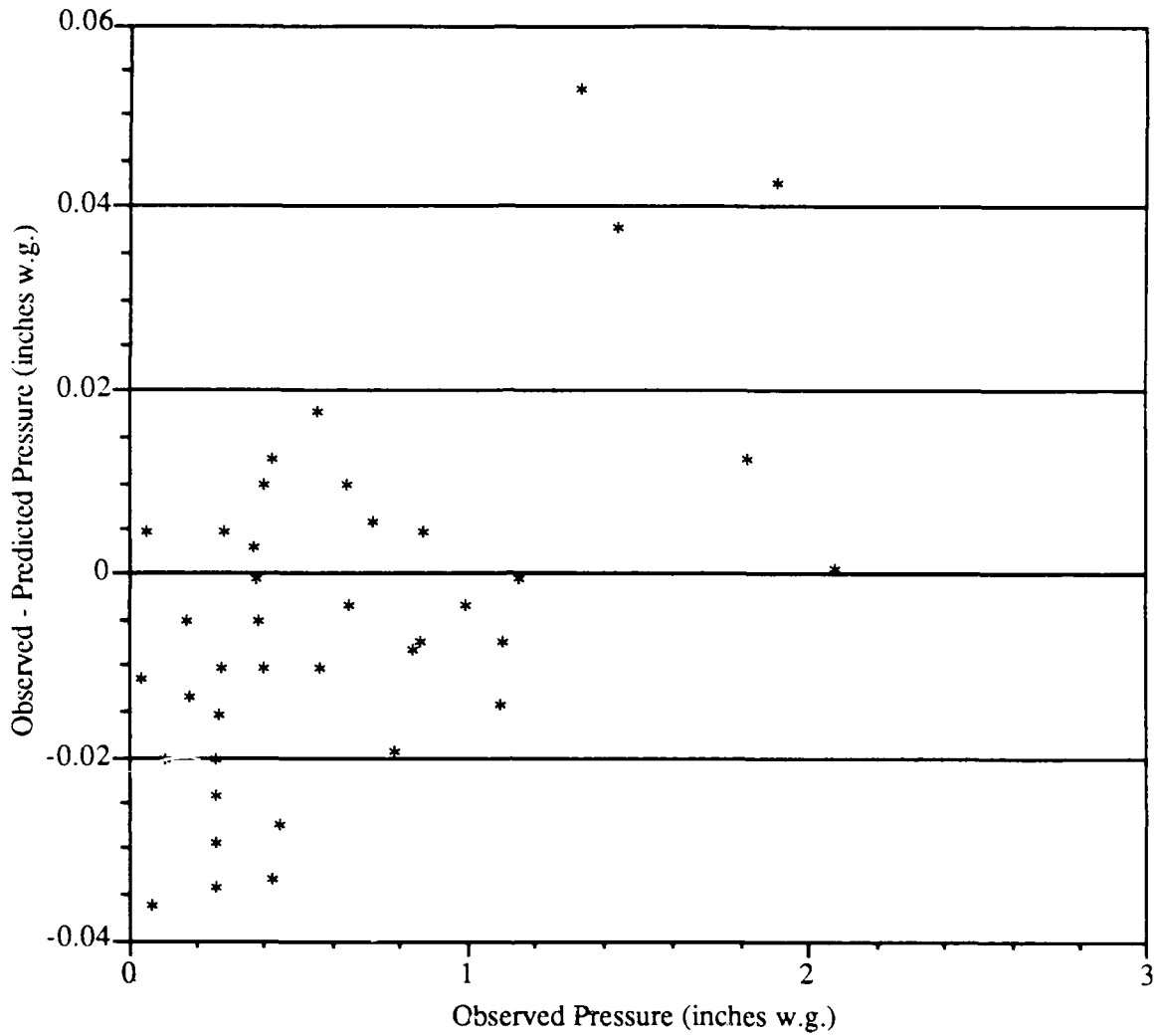


Figure 21: Illustration of Transducer Zero and Gain Shift

#### Other Measuring Devices

Barometric pressure was measured with a "National Weather Service type" barometer (Princo, Model 453, Southhampton PA). All readings were corrected for temperature and local gravity effects using equations provided by the manufacturer.<sup>(15)</sup> Corrected observed values from the laboratory were periodically checked against corrected values provided by the local U.S. Weather Bureau. Readings generally differed by less than 1 millimeter of mercury.

Duct temperatures were measured with a digital thermometer (Fluke, Model 52 K/J, Everett WA). After a 15 minute warm-up period, the digital readout on this thermocouple was compared to a mercury thermometer (Ever Ready Thermometer Co., NY) that was accurate to  $0.5^{\circ}\text{C}$  and traceable to the National Bureau of Standards. The offset for the digital thermometer was adjusted if necessary so that the digital readout was within  $0.2^{\circ}\text{C}$  of the thermometer.

Room dry bulb and wet bulb temperatures were measured with a battery powered psychrometer (Cole-Parmer Instrument Company, "Psychro-Dyne", Model 3312-40, Chicago IL). The dry bulb reading for both thermometers was compared to the mercury thermometer mentioned above. A discrepancy of less than  $2^{\circ}\text{C}$  was considered insignificant since the measurements were used only to determine the contribution of water vapor to the airstream density factor. In general, measurements were within  $0.5^{\circ}\text{C}$ .

Three different types of steel measuring tapes were used to measure lengths along the ducts. A caliper (manufactured in China, manufacture unknown) with a range up to 9 inches (readable to 0.001 inch) was used to measure the diameters of the ducts, connectors, and DOM measuring stations. The caliper was also used to measure the gage of the ducts and connectors.

An electronic tachometer (Red Lion Controls, "DITAK 5", Model DT-5, York PA) was used to measure the fan rotation rate. The tachometer determined the fan rotation rate by counting the teeth on a gear mounted directly on the fan drive shaft. It was readable to one rotation per minute.

### **Friction Loss Determination**

Friction loss equations were determined for 4, 5, 6, 7, and 10 inch diameter ducts for velocities ranging from 1000-6000 feet per minute. The friction loss equations for 5, 7 and 10 inch diameter ducts were used in this study.

To determine friction losses, 10 foot lengths ( $\pm 3$  inches) of spiral wound duct were placed on the ceiling mounted frame described earlier. Appendix H contains a detailed



outline of the procedure used to collect friction data. Figure 22 shows a generalized setup for all friction tests.

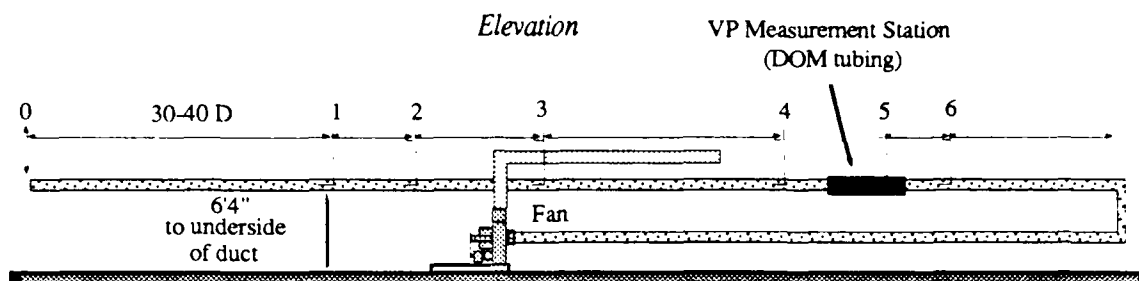


Figure 22: Friction Measurement Setup

After assembly, 0.16 inch (approximate) diameter holes were drilled at different locations along the duct (see Figure 22 and Table 3) to allow centerline static pressure measurements. The first measuring location was placed approximately 30-40 duct diameters downstream from the duct inlet to allow the friction loss per foot of duct to become a constant value. All measurement holes were placed at least 2 duct diameters downstream and at least 1 duct diameter upstream from duct connectors.

Short sections of 5 inch diameter duct were used to provide the desired distance between the lateral velocity pressure measurement stations and the junction fitting. As a result, two connectors were required between the DOM tubing and the junction. Since the friction loss per foot for this section was expected to differ significantly from tests conducted on 10 foot sections, this short section of duct was placed after the DOM tubing to model the friction losses that would occur during junction data collection. Table 4 shows the number of connectors per test section for each setup.

Table 3: Lengths of Test Sections for Friction Runs

<u>Diameter</u>	<u>Length of Test Section in inches</u>						
	<u>0-1</u>	<u>1-2</u>	<u>2-3</u>	<u>1-3</u>	<u>1-4</u>	<u>3-4</u>	<u>5-6</u>
4	177	321.5	101.4	422.9	544.0	121.1	40.5
5	208.5	302.5	99.8	402.3	513.3	111.0	48.3
6	272.3	98.5	121.6	220.1	447.5	227.5	50.5
7	258.5	280.4	101.6	382.0	497.3	115.3	46.5
10	334.6	x	x	x	497.3	257.5	x

Table 4: Number of Connectors per Test Section for Friction Runs

<u>Diameter</u>	<u>Number of Connectors per Test Section</u>					
	<u>1-2</u>	<u>2-3</u>	<u>1-3</u>	<u>1-4</u>	<u>3-4</u>	<u>5-6</u>
4	3	0	3	4	1	2
5	3	0	3	4	1	2
6	0	1	1	3	2	2
7	3	0	3	4	1	1
10	x	x	2	4?	2?	x

A duct leak test was accomplished and the duct alignment was verified before each set of data was collected. The fan rotation rate was adjusted to provide velocities in the range of 1000-6000 ft/min. Velocity pressures from the three 10-point traverses were measured with a pressure transducer and the resulting voltages were recorded to a computer file. Centerline velocity pressures were also measured with a transducer and an inclined manometer. All data not acquired with the computer were recorded to a friction data collection worksheet (see Appendix I).

The static pressure at duct centerline, the airstream temperature, and the laboratory environmental conditions (wet and dry bulb temperatures and barometric pressures) were

recorded and used to calculate the airstream density factors. The centerline static pressure was measured with the transducer and a redundant measurement was taken with an inclined manometer (if the pressure was less than 4 inches w.g.) or with the Meri-cal® (if the pressure was greater than 4 inches w.g.). Airstream temperatures were measured near the DOM tubing with the digital thermometer.

All static pressure differentials were measured with a pressure transducer and an inclined manometer using Pitot tubes inserted to centerline depths. If other Pitot tubes were between the two measuring points, they were raised to the sidewall of the duct to minimize any effect on the static pressure differential.

The "Digest Workbench Data" computer program was used to determine the average velocity and density factor. Occasionally, static pressures exceeded the capacity of the transducer or were in error. In these cases, the density factor and predicted average velocity were corrected using the static pressure measured with the inclined manometer or the Meri-cal.®

The relationship between friction loss and the average velocity for each duct was determined by conducting linear regression analysis on the log of the differential static pressures measured along a length of duct and the log of the corresponding average airstream velocity:

$$\log (\text{SPF}/L) = C_0 + C_1 \log V \quad \dots(10)$$

where:    SPF = differential static pressure measured  
               L = length of duct between measuring location  
               V = average velocity of air in duct  
               C<sub>0</sub> and C<sub>1</sub> are regression coefficients

The differential static pressures measured with the inclined manometer were used in these analyses except in the few cases where the manometer value was clearly incorrectly recorded. When inclined manometer readings were deemed incorrect, the differential static pressures predicted by the transducers were used instead. The predicted friction per length was calculated by rearranging Equation 10 as:

$$SPF = L ( 10^{C_0} V^{C_1} ) \quad \dots(11)$$

where:    SPF = differential static pressure measured  
           L = length of duct between measuring location  
           V = velocity of air in duct  
           C<sub>0</sub> and C<sub>1</sub> are regression coefficients

## **Junction Power Loss and Modeling**

### Power Loss Determination

Many of the methods used to collect junction data were identical to methods used in collecting friction data which were discussed in detail earlier. Only the methods that differ from friction are discussed in detail in this section. Appendix J contains a complete outline of the junction data collection procedure.

The bilateral junction used in this study was purchased from a manufacturer of ventilation system components (United McGill, Stockton CA). The junction was constructed from 18 gauge galvanized steel that was rolled into separated pieces and welded together to form the junction (see Figures 23 and 24). The laterals were welded approximately midway on the expansion and had sharp edges at the point of connection. The junction was designed so each connection was slightly smaller than the nominal diameter of the connecting duct; this allowed the ducts to slide onto the junction without requiring a separate fitting. The inside diameter values shown in Figure 24 are the average of 5 inside diameter readings taken with the caliper.

Before the junction was used, the inside surfaces at the lateral connections were ground with a grinding wheel attached to a hand drill to remove all metal projections in the path of the airstream. Figure 25 is a photograph of the inside of a junction before grinding; Figure 26 shows the inside of a junction after grinding.

The system was assembled on the ceiling mounted frame (see Figures 27 and 28). All ducts and measuring stations were aligned and the joints were sealed. Figure 29 shows the

system components and the general layout of the system and Figure 30 shows all dimensions for the system. Figure 31 is an enlargement of the junction showing the distance from the measuring station to the junction for each of the upstream branches. The dimensions shown in Figure 31 and the distance between the junction and the measuring station in the main shown in Figure 30 were used to calculate the lost power due to friction. Two inches were added to the distance between the branch measuring stations and the junction to account for the length of the Pitot probe along the axis of the duct. Similarly, two inches were subtracted from the distance between the junction and the measuring station in the main.

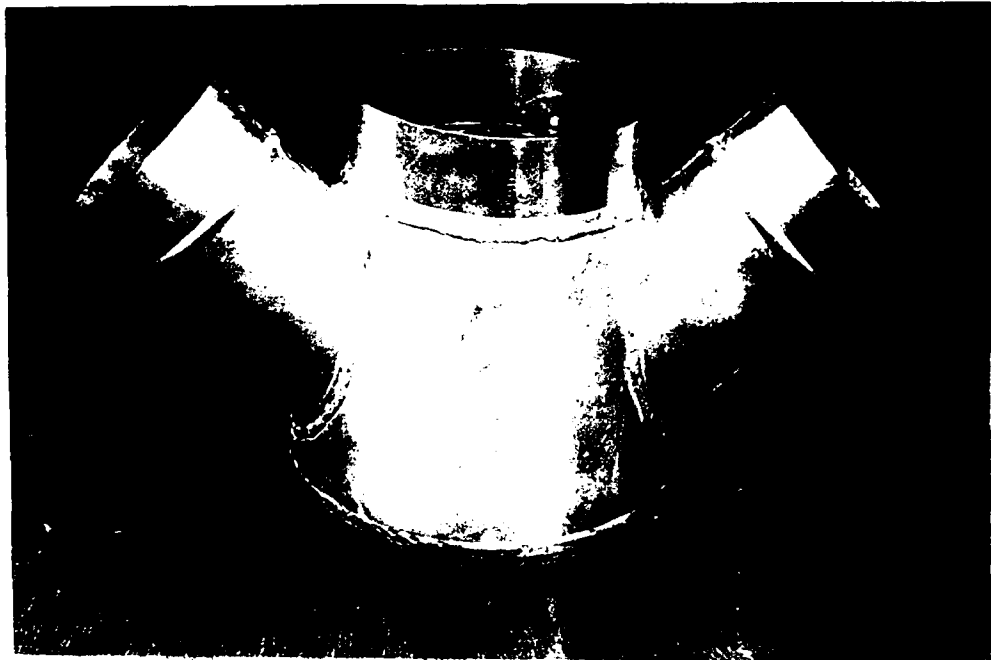


Figure 23: Photograph of Bilateral Junction Tested

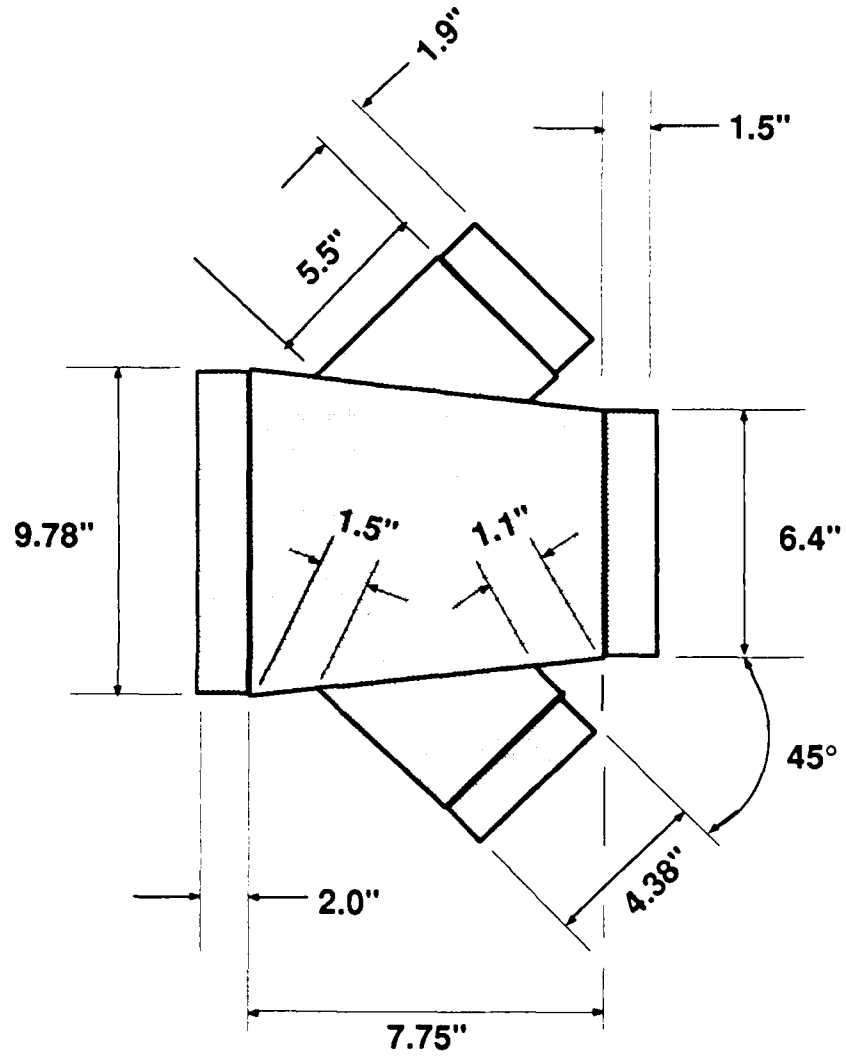


Figure not to scale

Figure 24: Dimensions of Bilateral Junction Tested



Figure 25: Inside of Junction Before Grinding



Figure 26: Inside of Junction After Grinding



Figure 27: Top View of Bilateral Junction Setup

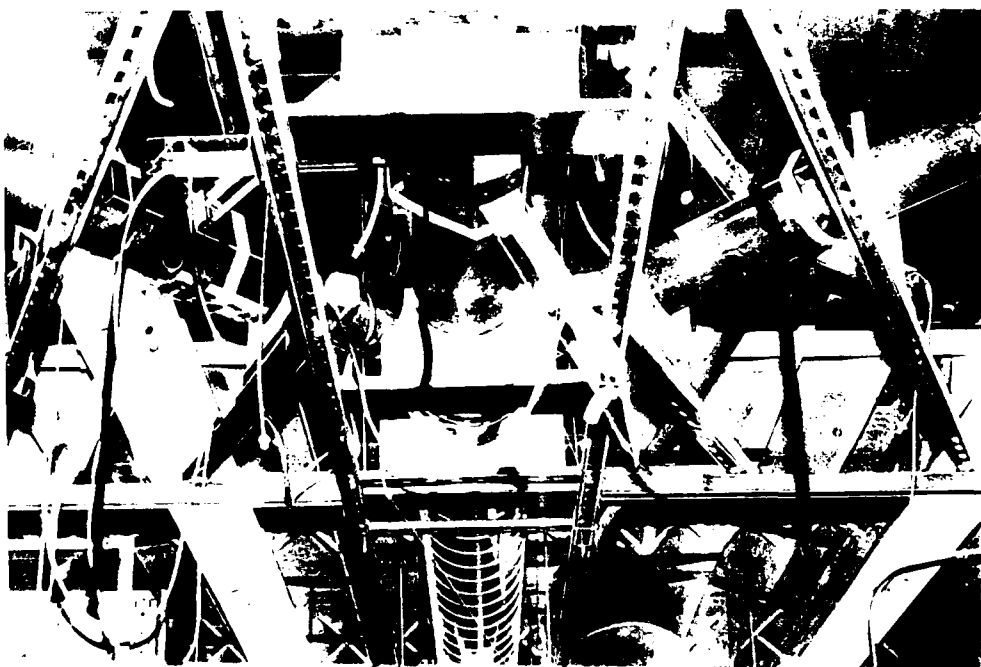


Figure 28: Bottom View of Bilateral Junction Setup



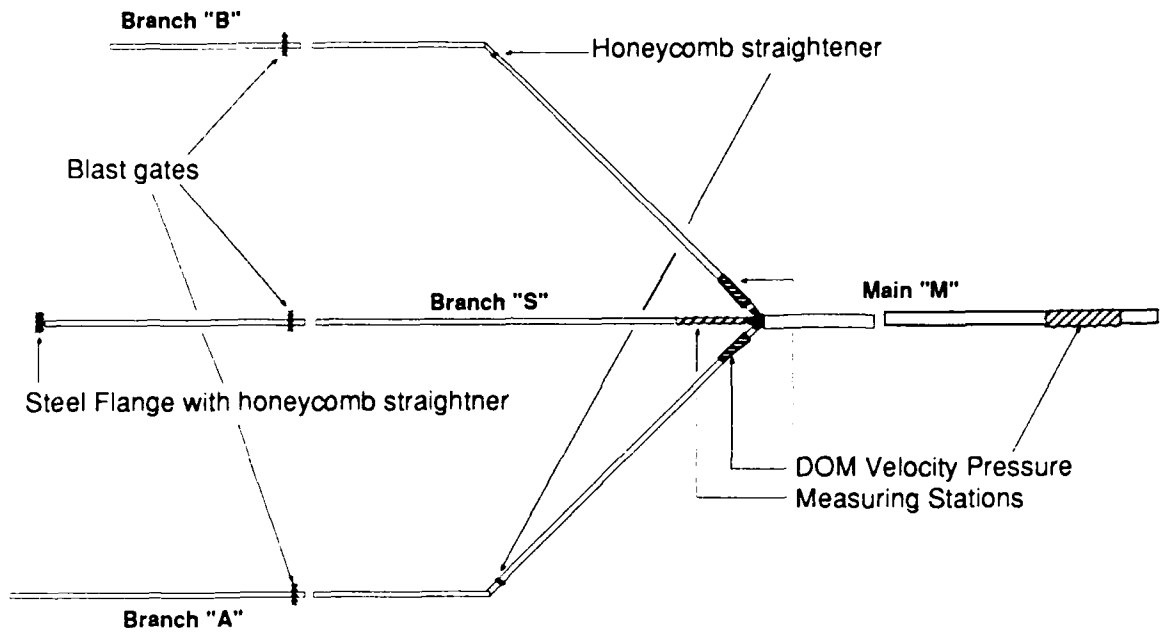


Figure 29: System Components and Layout

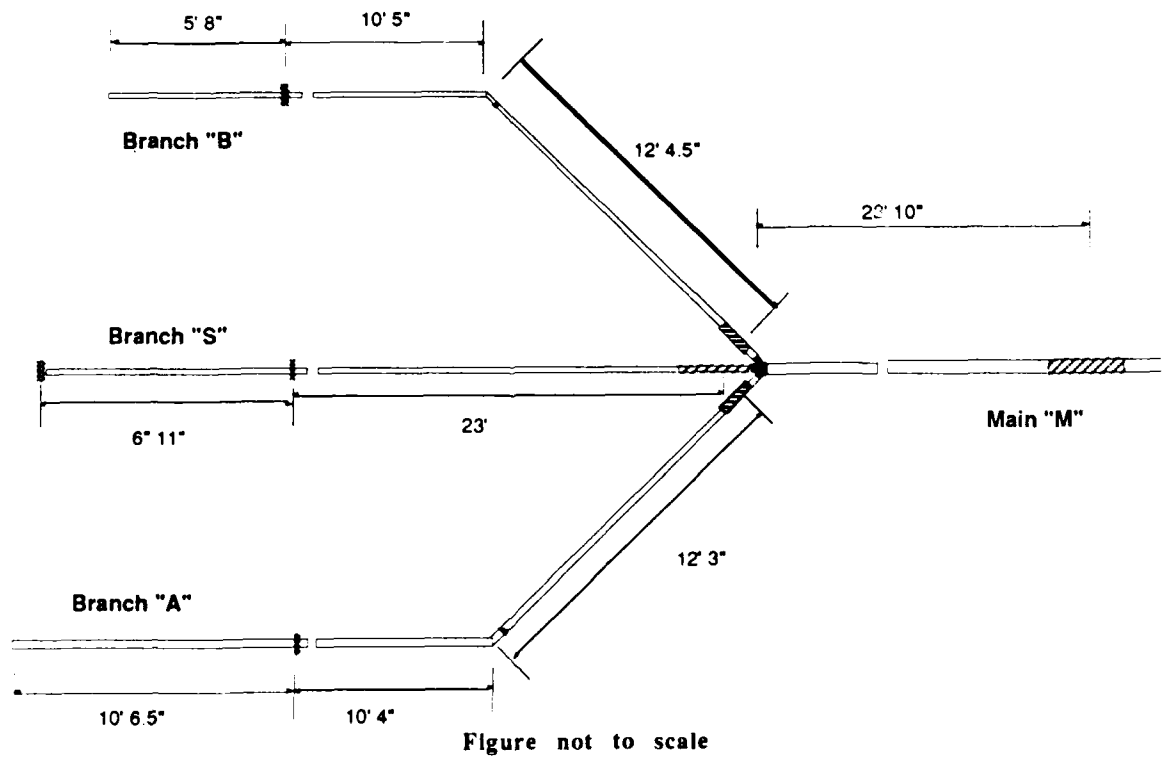


Figure 30: System Dimensions

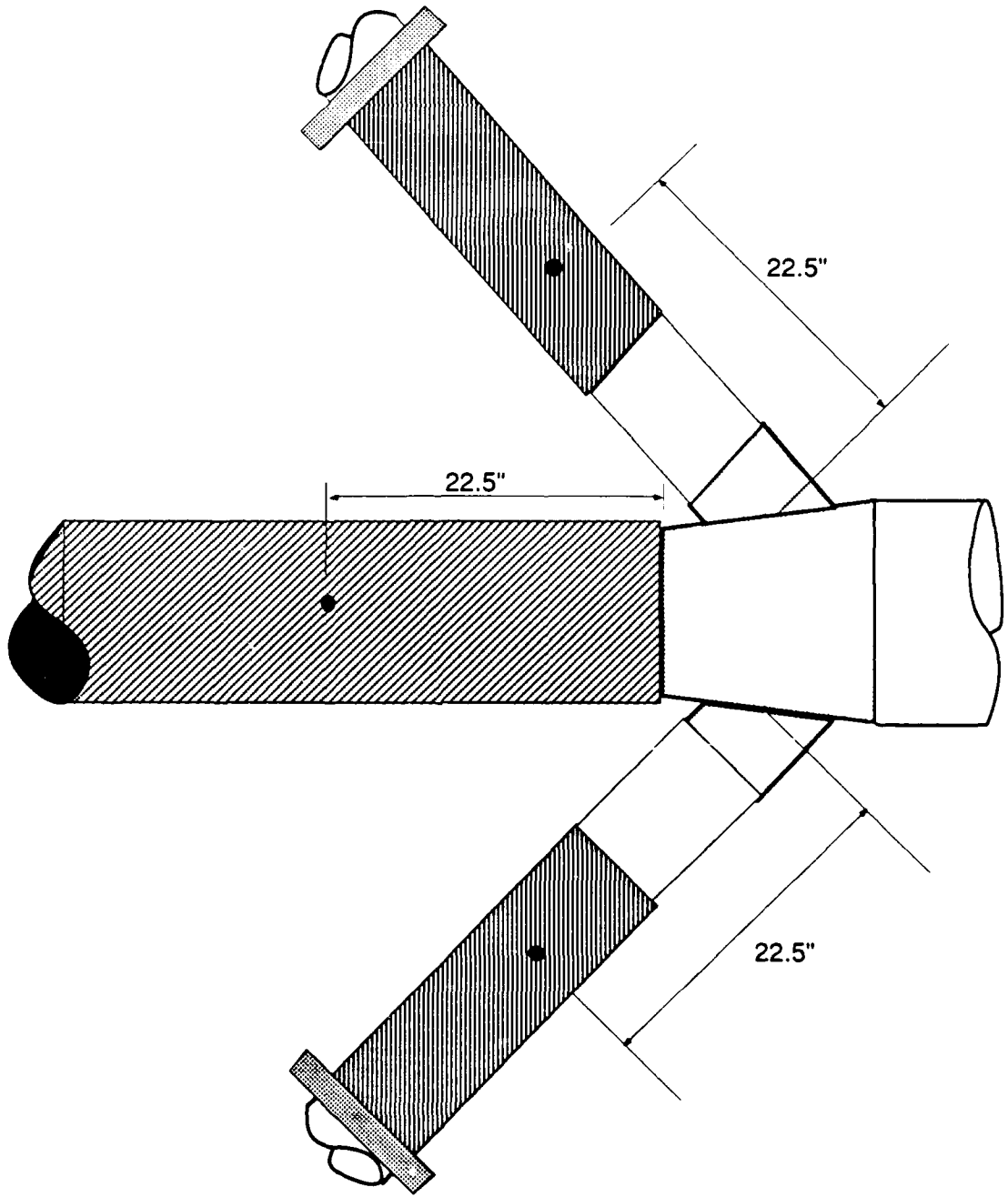


Figure not to scale

Figure 31: Distances from Branch Measuring Stations to Junction

Data were collected for 35 separate runs where the velocity ratios of the branches entering the junction were varied from 0-3.7. The airflows in the upstream ducts were set using the impedance method<sup>(16)</sup> to achieve the desired velocity ratios. Appendix K explains this method in detail.

Data collection and reduction procedures for each branch (and main) were nearly identical to those completed for friction analyses. The only difference was the number of differential static pressures collected. Detailed methods for computer data acquisition were discussed earlier in the "Computer and Data Acquisition and Reduction" section. Appendix L contains a copy of the junction data collection worksheet used to record data not collected with the data acquisition program.

Final data reduction was performed using the calibration equations for the transducers based on redundant measurements collected with the inclined manometer. This method was used because of transducer zero and gain shift that was discussed earlier. The priorities used to determine which static pressure measurements should be used in data analyses were as follows:

1. First priority - inclined manometer measurements, unless clearly wrong
2. Second priority - transducer values.
3. Meri-cal® readings

Once the data was reduced to its final form all relevant data was merged into one computer file. Most of the final calculations were accomplished on a computer spreadsheet program. Following is a list of the major calculations performed on the spreadsheet for each junction setup:

1. Density factor correction
2. Branch velocity ratios
3. Average velocity for each branch
4. Airflow for each branch
5. Static pressure at each measuring station (based on the static pressure differential from the cross section in duct S)
6. "Mass" airflow in the main
7. Velocity in the main based on the "mass" flow

8. Average velocity pressure in the main based on the "mass" flow
9. Total pressure for each duct based on the "mass" flow
10. Power in each branch
11. Total lost power
12. Lost power due to friction
13. Lost power of the junction

The static pressure measured by the transducer at the measuring station was used to calculate the airstream density factor. The density factor was corrected for each branch since the transducer values were given a lower priority than the inclined manometer values. The following equation was used:

$$cDF_{duct} = DF_{duct} \left( \frac{P_{bar} + 1.876 SP_{used}}{P_{bar} + 1.876 SP_{Tran}} \right) \quad \dots(12)$$

- where:  $DF_{duct}$  = density factor computed by data reduction program  
 $cDF_{duct}$  = corrected density factor  
 $P_{bar}$  = barometric pressure  
 $SP_{used}$  = static pressure at the measuring station used (usually the manometer reading)  
 $SP_{Tran}$  = static pressure at the measuring station sensed by the transducer

The factor of 1.876 in the Equation 12 is an equivalence factor between inches of water and millimeters of mercury (1 inch water = 1.876 mm of mercury). This conversion factor from the ACGIH Ventilation Manual<sup>(1)</sup> was later found to be incorrect (1.865 is the correct value;<sup>(2)</sup> fortunately this error had a trivial impact on the data analyses since the difference produced in the pressure was less than the resolution of the barometer (0.1 mm of mercury).

The corrected average velocity for each duct was calculated using the following formula:

$$cV_{avg} = 4005 \sqrt{\frac{tVP_{avg}}{cDF_{duct}}} \quad \dots(13)$$

where:  $cV_{avg}$  = corrected average duct velocity

$tVP_{avg}$  = transducer derived, average velocity pressure  
calculated by the data reduction program

$cDF_{duct}$  = corrected duct density factor

The static pressure differentials measured between the measuring station in duct S and the other ducts were used to calculate the static pressure at each measuring station. This was done to reduce the potential errors induced by slight variations in the fan rotation rate over time. The differential pressures were used in the following equations to give the static pressure for each cross-section:

$$calSP_s = SP_s \quad \dots(14)$$

$$calSP_m = calSP_s + \Delta SP_{s-m} \quad \dots(15)$$

$$calSP_a = calSP_s - \Delta SP_{s-a} \quad \dots(16)$$

$$calSP_b = calSP_s - \Delta SP_{s-b} \quad \dots(17)$$

where:  $calSP$  = calculated static pressure at the measuring station

$\Delta SP_{s-i}$  = static pressure differential measured between duct S  
and duct  $i$

Subscripts a, b, s, and m represent reference cross-sections in  
ducts A, B, S and M

Similarly, the sum of the flows in the branches was used as the "mass" flow in the main. Power loss calculations were based on the "mass" flow rates. The measured values of the flow in the main were compared with the "mass" flows to identify any errors.

The total lost power was calculated from the sum of the powers of the upstream branches and the power in the main using Equation 2. Using the nomenclature in Equations 14-16 above, Equation 2 becomes:

$$LP = Q_a(\text{calSP}_a + tVP_{\text{avg } a}) + Q_b(\text{calSP}_b + tVP_{\text{avg } b}) + Q_s(\text{calSP}_s + VP_{\text{avg } s}) - Q_m(\text{calSP}_m + tVP_{\text{avg } m}) \quad \dots(18)$$

where:      LP = total lost power  
                  Q = flow in the duct  
                  calSP = calculated static pressure in the duct  
                  tVP<sub>avg</sub> = average velocity pressure calculated by the data reduction program

Subscripts a, b, s, and m represent reference cross-sections in ducts A, B, S and M

As discussed in the Introduction, the total lost power has two components, the power dissipated due to the airflows mixing and the power dissipated because of friction between the measuring stations and the junction. The estimated static pressure loss due to friction was calculated using the loss equations developed in the friction study, the average velocity in the duct, and the distance from the measuring station to the junction. The lost power resulting from friction in all of the ducts was estimated using Equation 3.

Finally the lost power due to the junction was found by subtracting the lost power attributable to friction from the total lost power using Equation 5. Using the nomenclature from Equations 14-18 above, Equation 5 transforms to the following:

$$LPJ = \left[ Q_a(\text{calSP}_a + tVP_{\text{avg } a}) + Q_b(\text{calSP}_b + tVP_{\text{avg } b}) + Q_s(\text{calSP}_s + VP_{\text{avg } s}) - Q_m(\text{calSP}_m + tVP_{\text{avg } m}) \right] - \left[ Q_m(\Delta\text{SPF}_{J-m}) + Q_a(\Delta\text{SPF}_{J-a}) + Q_b(\Delta\text{SPF}_{J-b}) + Q_s(\Delta\text{SPF}_{J-s}) \right] \quad \dots(19)$$

where:      LPJ = power lost due to the junction  
                  ΔSPF<sub>J-i</sub> = predicted change in static pressure (due to friction) between the junction and the duct measuring station  
                  Q = airflow in the duct  
                  calSP = calculated static pressure in the duct  
                  tVP<sub>avg</sub> = average velocity pressure calculated by the "Digest Workbench Data program"

Subscripts a, b, s, and m represent reference cross-sections in ducts A, B, S and M

### Junction Modelling

Multiple regression analysis was accomplished using the kinetic powers in the upstream branches as the independent variables and the lost power due to the junction (LPJ) as the dependent variable (see Equation 6).<sup>(4)</sup> Unlike the approach used by Guffey and Fraser, the kinetic power of the main was not used as an independent variable since it is not independent of the kinetic powers in the upstream ducts.

The wide range of velocity ratios tested was important in evaluating the robustness of the kinetic power model. Some ratios were extreme enough that a poor fit to the kinetic power model was expected. Under extreme conditions the flow decelerates from a high velocity to a sharply lower velocity in the main. In these cases, the power losses may be more a response to a sudden expansion than a function of mixing phenomena. To evaluate model performance under more realistic conditions, subsets of data were analyzed using narrower velocity ratio ranges.

Regression diagnostics were executed to check multiple regression assumptions and to identify potential outliers in the data. Table 5 provides a summary of the regression diagnostics used and their purposes.

Table 5: Regression Diagnostics Summary

<u>Diagnostic Tool</u>	<u>Tests for</u>
Partial Regression Plot	Linearity between each independent variable and the dependent variable.
Leverage Histogram	How extreme the independent variables are in the individual test cases .
Externally Studentized Residuals	How extreme the dependent variable is in the individual test cases.
Cook's Distance and DFFITS	The overall influence of the individual test cases on the regression.

## CHAPTER III DISCUSSION OF RESULTS

### Friction and Flow Estimation

Pressure differentials measured across ventilation system components generally include substantial contributions due to friction losses since experimental measurements must be taken far downstream of the component to avoid disturbances induced by the component being evaluated. This is particularly true for junctions. To determine the contribution due to a junction alone, it was necessary to subtract the estimated contribution of friction. Similarly, the methodologies most widely used to design new ventilation systems (ASHRAE and ACGIH) compute dynamic and friction losses separately.

An accurate estimation of airflow in each duct is critical for the total power loss calculations and for estimating the power lost due to friction. In addition, deviations between the measured downstream flow and the sum of the measured upstream flows would produce a spurious change in power losses calculated using Equation 2. For that reason, the sum of flows in the ducts upstream of the junction (the "mass" flow) was used as the flow in duct M (the downstream duct) for all analyses.

#### Friction Estimation

Estimating the contribution from friction would seem straight forward: experimentally determine the friction loss per length, then use that value to predict the static pressure loss in the experimental setup resulting from friction. Unfortunately, the friction loss per length varies with the distance downstream of a disturbance. For example, in a duct containing a bellmouth hood opening, the loss per foot of duct does not become a constant value until a distance approximately 15 duct diameters downstream of where the hood connects to the duct.<sup>(17)</sup> Therefore, the dynamic loss of a system component is confounded with the effects of disturbed flow on friction losses.

Error is introduced by applying empirical friction loss equations based on measurements far downstream of a disturbance to a section of duct immediately downstream of a disturbance. However, there is no model currently available to estimate



friction losses in these circumstances. As a result, the friction losses in the ducts upstream and downstream of the junction were estimated from empirical equations that were based on data collected far downstream from the inlet of a long, straight duct (see Table 6 and Figure 32). Appendix M contains the results from the regression analyses conducted to determine these relationships.

Since differential pressures were measured at several cross-sections along the length of a single duct, it was possible to compare the friction loss per foot in the most upstream test section (section 1↔2 in Figure 22) with the most downstream test section (section 3↔4). This helped establish that the friction per unit length was the same in both sections. As a result, the data from the entire length (section 1↔4) was used to calculate the friction loss equations, thus minimizing the effects of measurement error.

Duct connectors are responsible for a portion of the overall friction loss along any length of duct and their loss per unit length is expected to be higher than that of the duct. In this study, the portion of total friction losses attributable to the connectors was estimated by comparing friction losses (on a per foot basis) between a section with no connectors and a section containing one or more connectors. Figure 33 shows the effect of varying the number of connectors in a 100 foot run of 7 inch diameter duct. The effect of connectors was similar for other duct diameters.

The short section of duct that was required between the measuring stations and the junction for the 5 inch diameter laterals was placed after the DOM measuring station during friction data collection (test section 5↔6 in Figure 22) to model the increase in friction loss per unit length due to the connector effect discussed above. Likewise, the DOM connection to the junction for the 7 inch diameter duct was also modeled to determine any increase in friction loss per unit length for this arrangement. For the 5 inch diameter duct the friction losses, when normalized for length, were approximately 1.7 times higher in test section 5↔6 than the longest test section (1↔4). For the 7 inch diameter, the friction losses were only 1.3 times higher for in test section 5↔6 than section 1↔4..

Table 6: Empirical Friction Loss Equations

<u>Diameter</u>	<u>Test Section</u>	<u>Equation</u>
4"	1↔4	$\Delta SP/100 \text{ ft} = 0.4081 \left( \frac{V_{\text{avg}}}{1000} \right)^{1.85}$
5"	1↔4	" $= 0.3268 \left( \frac{V_{\text{avg}}}{1000} \right)^{1.86}$
5"	5↔6	" $= 0.5484 \left( \frac{V_{\text{avg}}}{1000} \right)^{1.86}$
6"	1↔4	" $= 0.2854 \left( \frac{V_{\text{avg}}}{1000} \right)^{1.83}$
7"	1↔4	" $= 0.2156 \left( \frac{V_{\text{avg}}}{1000} \right)^{1.84}$
7"	5↔6	" $= 0.2753 \left( \frac{V_{\text{avg}}}{1000} \right)^{1.84}$
10"	1↔4	" $= 0.145 \left( \frac{V_{\text{avg}}}{1000} \right)^{1.89}$

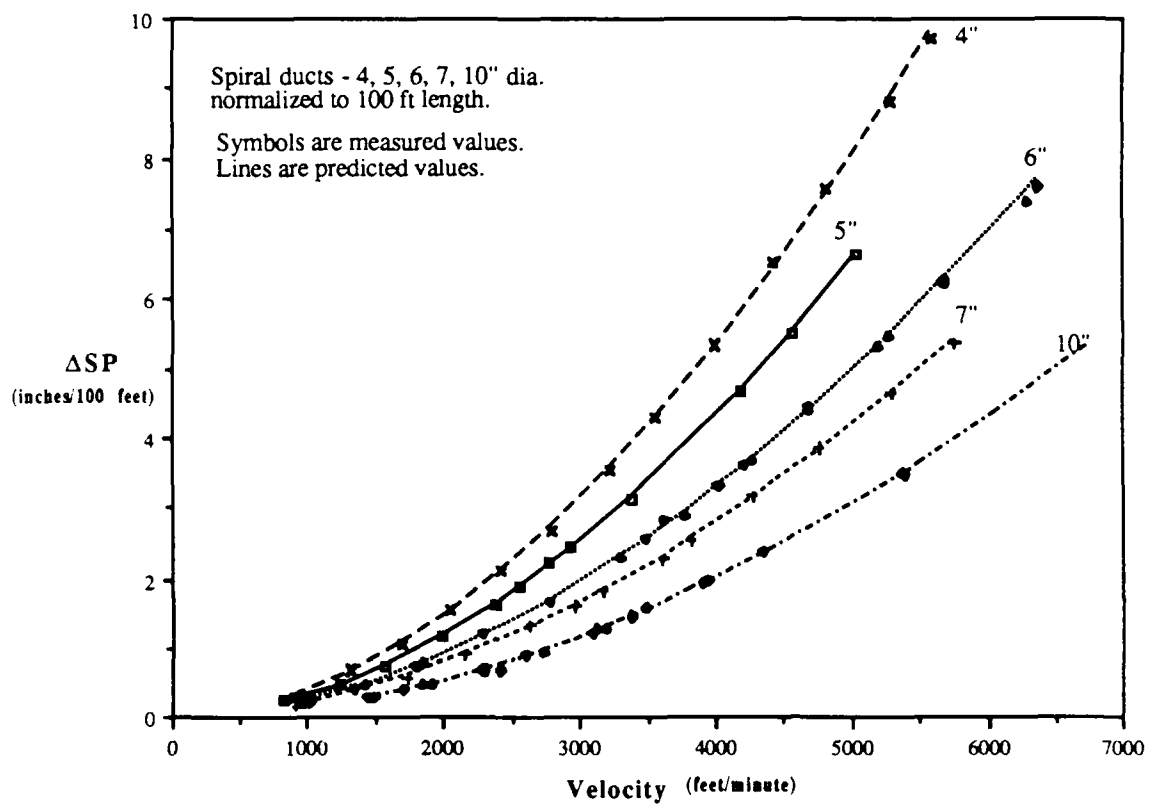


Figure 32: Power Law Regression  $F \propto V^n$  Observed Friction Loss/100 feet (Section 1↔4)

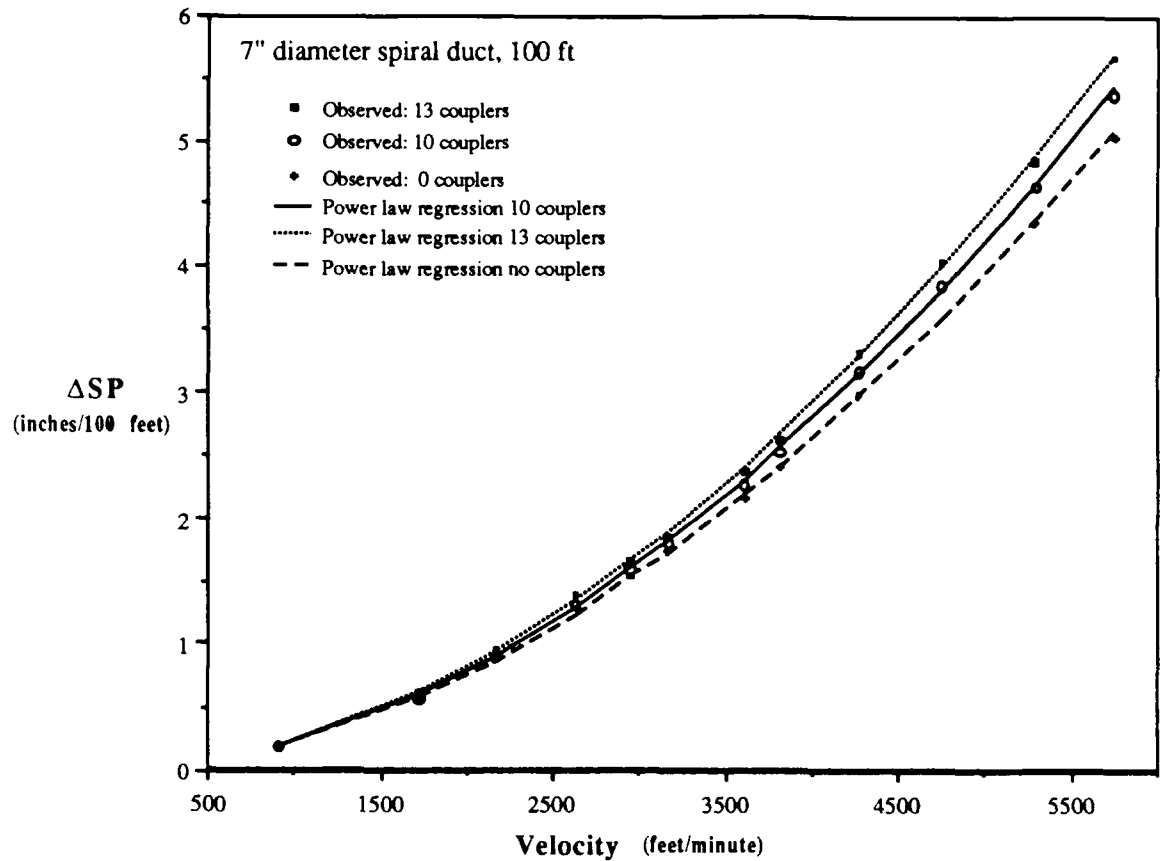


Figure 33: Effect of the Number of Connectors on Friction Loss

Accurate empirical models for friction losses were very important since the lost power due to the junction was estimated by subtracting the lost power due to friction from the total lost power. Analyses revealed the power lost due to friction accounted for a significant portion (an average of 58 percent) of the total power lost (see Figure 34). The proportion of power losses due to friction were highest when the duct airstream velocities were similar. This was true because the losses due to the junction were lowest for these conditions. Most of the power losses due to friction occurred in the relatively long section of duct downstream of the junction fitting, Duct M (see Figures 29 and 35). The contributions due to the upstream ducts varied as a function of the velocities through them, and were relatively small in all cases.

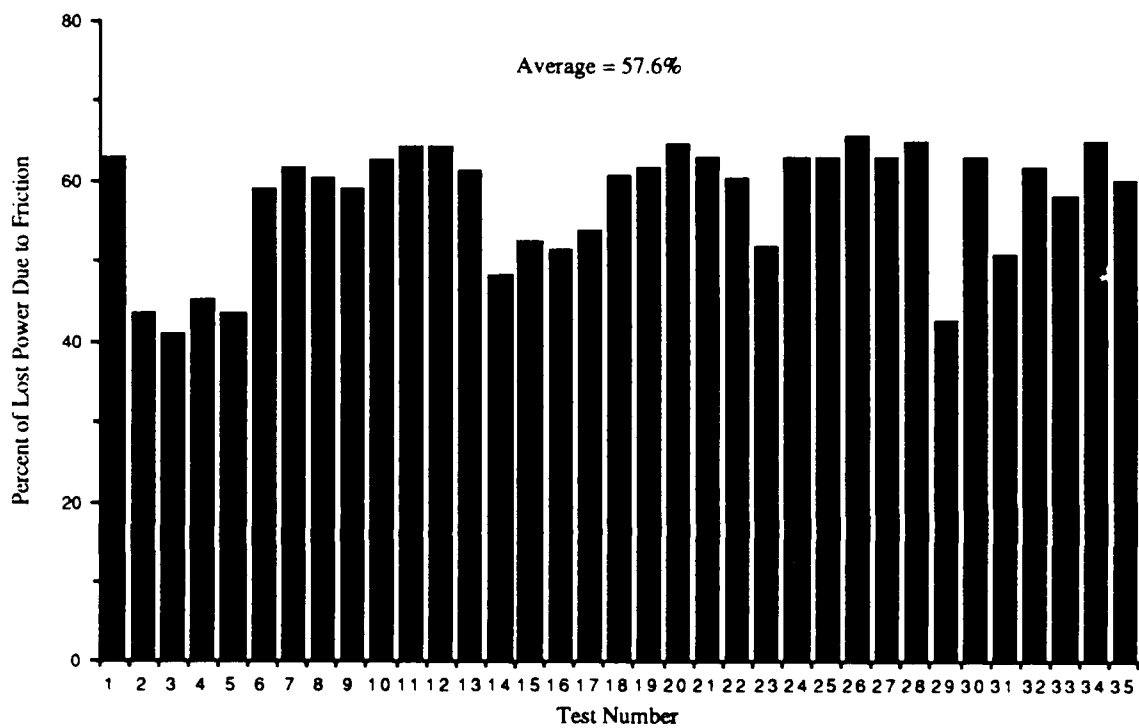


Figure 34: Percent of Total Power Loss Resulting from Friction

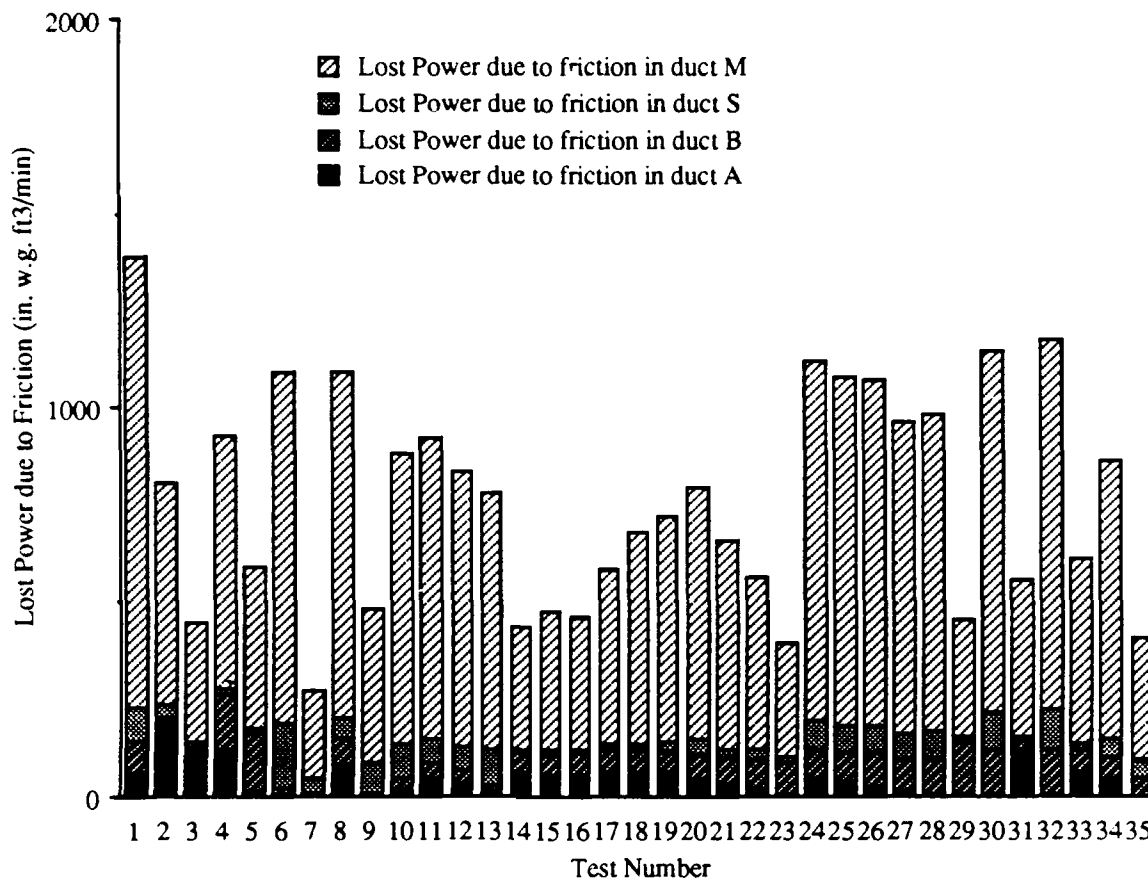


Figure 35: Contribution of Different Ducts to the Friction Power Losses

### Flow Estimation

The flows in the downstream main ( $Q_m$ ) were estimated from measured velocity pressures in the main ( $Q_{meas}$ ) and by summing the upstream airflows ( $Q_{mass}$ ). In twenty-six of 32 cases, the two estimates varied by less than 1%, but 8 varied by 1–2% and one varied by 3.1% (see Figure 36). Figure 37 shows that the percent error was normally distributed except for case number 2 which may represent a measurement error.

Since the dependent variable (lost power due to the junction) is a function of the *difference* in energy rates upstream and downstream of the junction,  $Q_{mass}$  was used for  $Q_m$

for power computations (see below). Otherwise a spurious power difference would exist attributable solely to differences between  $Q_{\text{mass}}$  and  $Q_{\text{meas}}$ .

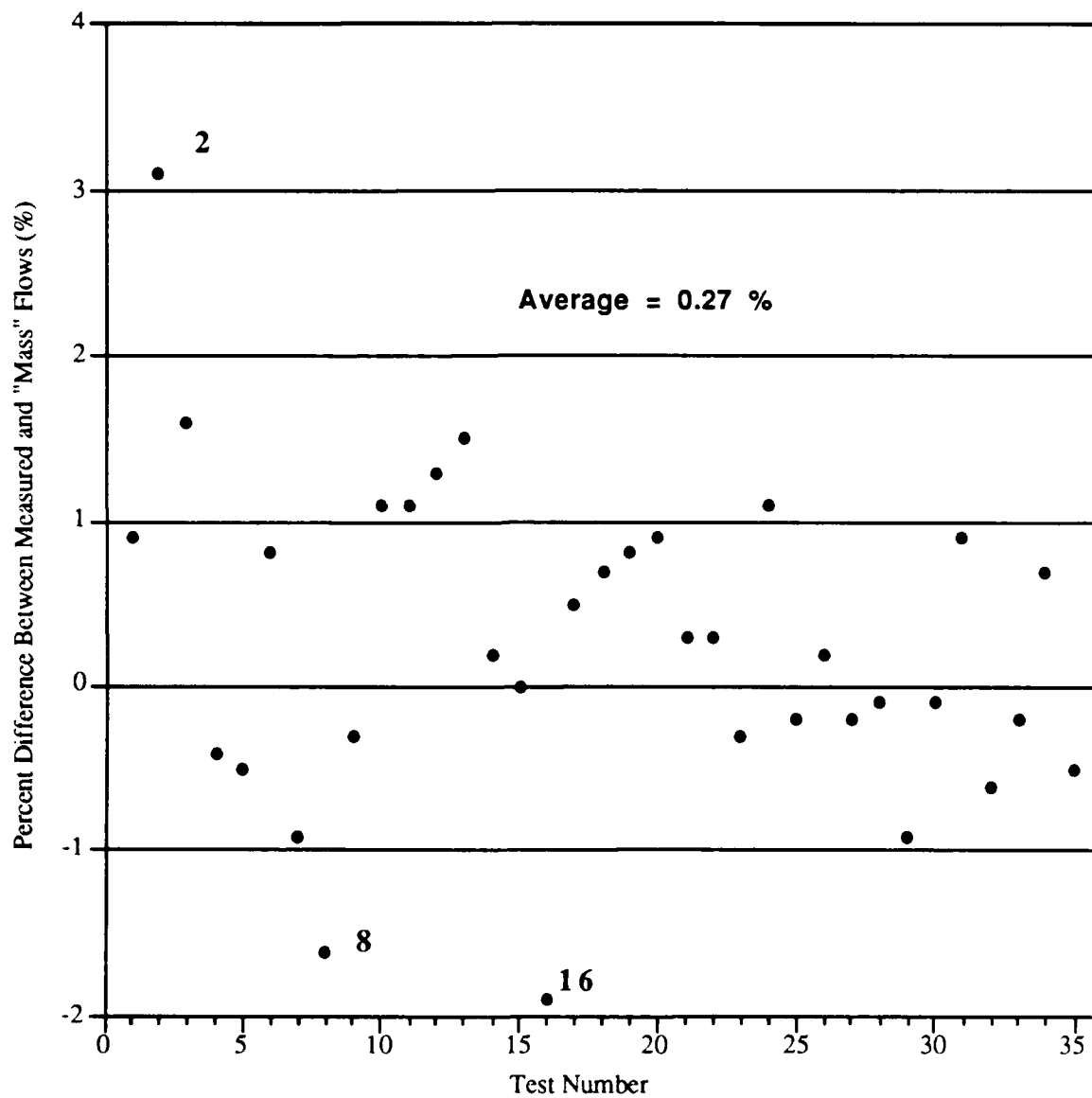


Figure 36: Percentagc of Error Between Measured and "Mass" Flows In Duct M

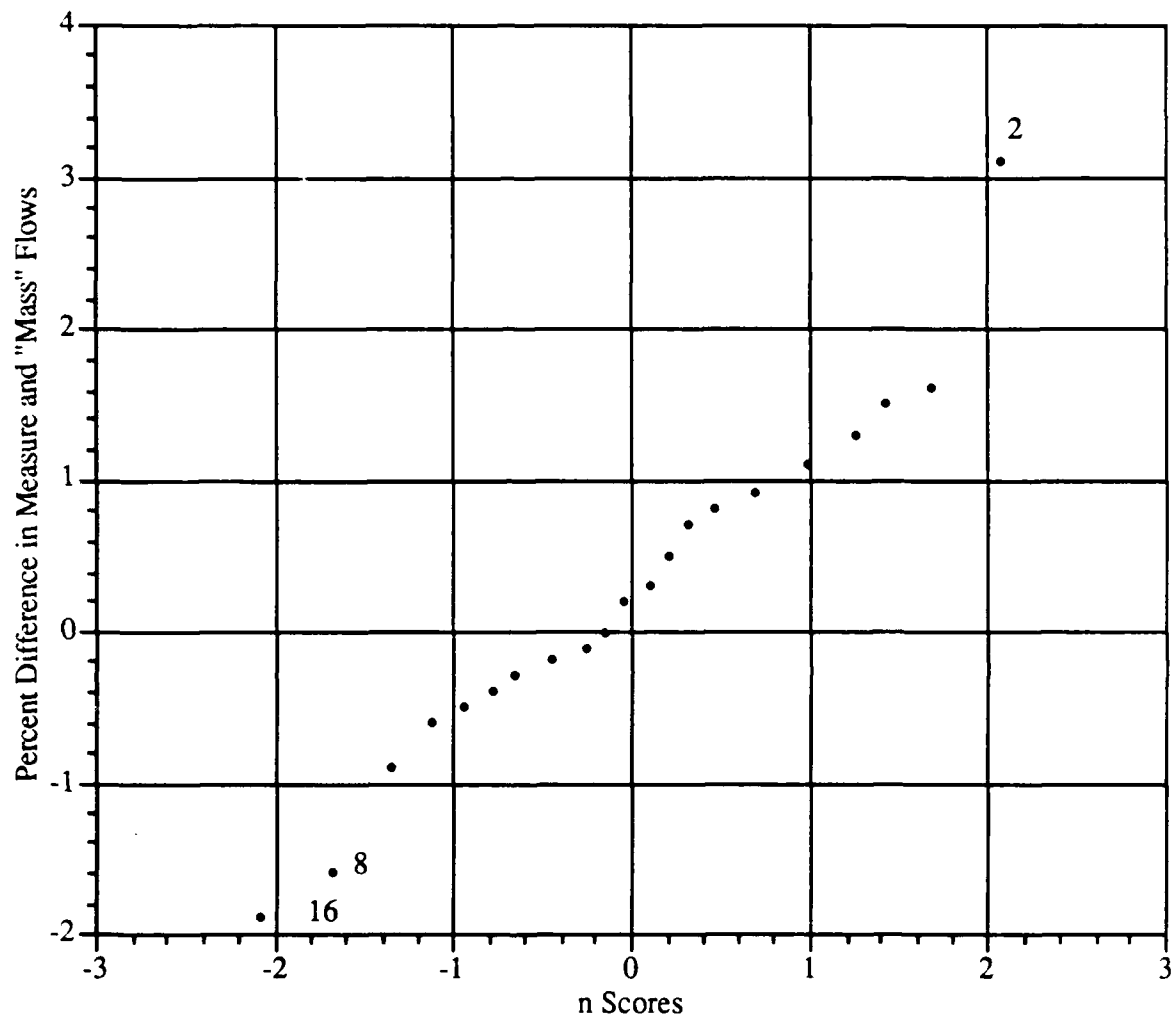


Figure 37: Normal Probability Plot for the Percent Error Between Measured and Mass Flows



## Junction Modelling

“Observed” values of lost power in the junction (LPJ) were fit to the linear kinetic power model, which was modified by the addition of a regression constant ( $C_0$ ) for purposes of statistical regression:

$$LPJ = Q_aVP_aK_a + Q_bVP_bK_b + Q_sVP_sK_s + C_0 \quad \dots(20)$$

Table 7 presents the results of several multiple regression runs. First the entire range of cases were analyzed, then various subgroups of the entire data set were selected based on velocity ratio ranges and were analyzed separately. To represent physical reality, the model should satisfy four criteria for each subset of data: 1) it should fit observed data well, 2) at zero flow, it should predict zero losses ( $C_0=0$ ), 3) the coefficient values  $K_a$  and  $K_b$  should be approximately equal, and, 4) it should satisfy diagnostic criteria for applicability of multiple regression analysis. To be useful, the model need not fit the entire range well as long as its fits the range of practical application well.

### Goodness of Fit

Although the model fit the full range of data moderately well ( $Adj R^2 = 0.896$ ), its fit improved dramatically ( $R^2=0.977$ ) when the data were narrowed to the velocity ratios that might be expected of high velocity ventilation systems ( $0.75 < V_{ratio} < 1.25$ ). The model fit all subsets of the data at least moderately well ( $R^2 > 0.86$ ). The values of  $R^2$  were determined with the regression constant included, but the values of  $K_a$ ,  $K_b$ , and  $K_s$  in Table 7 were determined with the regression constant excluded since the value of LPJ must be zero at zero flow.

### Predicted Value at Zero Flow

Since no losses are possible at zero flow, the model should predict a zero value of LPJ when flows are zero. In fact, the regression constant for the "all data" category was approximately 5% of the mean value of LPJ while that for the " $0.5 < V_{ratio} < 2.0$ " was less than 1% of the mean value of LPJ ; these were excellent findings. On the other hand, the

regression constant for the " $0.75 < V_{ratio} < 1.25$ " was approximately 24% of the mean value of LPJ; however, this finding is not surprising because of the reduced number of observations.

Table 7: Regression Results for Junction Modelling

Selector	N	$K_a^\ddagger$	$K_b^\ddagger$	$K_s^\ddagger$	Adj. $R^{2**}$	se
All Data	35	0.613	0.489	0.188	89.6%	63.7
$0.5 < V_{ratio} < 2.0$	19	0.604	0.374	0.216	90.9%	36.0
$0.75 < V_{ratio} < 1.25$	9	0.494	0.361	0.254	97.7%	23.0
$V_a = V_b$	16	X	1.10	0.215	95.7%	43.9
$V_a \neq V_b$	16	1.06	X	0.215	92.7%	57.5
$V_a \neq V_s$	19	0.642	0.579	0.119	94.1%	102.6
$V_b \neq V_s$	28	0.635	0.452	0.199	93.2%	56.8
$V_a \neq V_s \neq V_b$	26	0.597	0.512	0.197	89.9%	65.2
	9	0.646	0.569	0.133	86.4%	61.4

$V_{ratio}$  = Velocity ratios     $^\ddagger$ with no regression constant     $^{**}$ with regression constant included

Ideally, the value of  $K_a$  would be exactly equal to  $K_b$  since ducts A and B are physically identical. The difference between  $K_a$  and  $K_b$  may occur because the flows in the upstream branches were not set randomly. For much of the data, the velocity in two of the three upstream branches were set equal to each other while the flow in the third was varied. Thus,  $Q_a$  and  $VP_a$  were completely dependent of  $Q_b$  and  $VP_b$ ; the intercorrelation of independent variables is shown in Table 8. Intercorrelation of independent variables produces instability and distortion of the regression coefficients even when the coefficients accurately predict the losses<sup>(18,19)</sup>. To remove the intercorrelation, a subset of data ( $V_a \neq V_b$ ) was analyzed to produce values of coefficients for the kinetic power in duct A and duct B that were much closer (see Table 7). Another subset ( $V_a = V_b$ ) was analyzed by removing the kinetic power in duct A as a variable and then the kinetic power in duct B as a variable. When this was done the values of the coefficients were also much closer (see

Table 7). This further supports the likelihood that the differences in the coefficients for ducts A and B are an artifact of the multiple regression fitting.

Table 8: Summary Analyses for Collinearity Between Independent Variables

First Variable	Second Variable	R <sup>2</sup>
Kinetic Power in duct S	Kinetic Power in duct A	14.6%
Kinetic Power in duct B	Kinetic Power in duct A	27.1%
Kinetic Power in duct B	Kinetic Power in duct S	36.8%

### Regression Diagnostics

As will be shown next, except for the for the slight collinearity of the independent variables discussed above the basic multiple regression assumptions were met:

1. Independent variables are truly independent of each other. As discussed earlier, a check for collinearity indicated there was a slight relationship between the independent variables. See Table 8.
2. There is a linear relationship between each independent variable and the dependent variable.
3. No value of a independent or dependent variable exerts undue influence on the regression analysis.

The linear relationship between the lost power in the junction and the kinetic power in each branch was verified by creating partial regression plots which show the relationship between the dependent variable and an independent variable with the effects from the other independent variables removed. The partial regression plots showed that a linear relationship existed between the lost power in the junction and each of the kinetic powers in the branches

The influence of the particular values of independent and dependent variables was checked using leverage values and externally studentized residuals, respectively. A histogram of leverages indicated that case numbers 2, 4, and 6 contained extreme kinetic power values. A histogram and normal probability plot of externally studentized residuals indicated that case number 5 had an extreme junction power loss value as compared with the other case.

Histograms of Cook's distances and DFFITS were used as diagnostic tools to assess the overall influence of any one case on the regression results. These tests indicated that case numbers 5 and 6 may exert undue influence on the regression results.

The influence of these possible outliers was investigated by removing each case number identified from the regression analysis. Removing case numbers 5 and 6 from the regression improved the regression without having a substantial impact on the coefficients. Table 9 provides a summary of the results of all analyses.

The data for the cases identified as possible outliers were reviewed to see if removing these cases from the regression was justified. Histograms of the kinetic powers identified that case numbers 5 and 6 were the only cases that had a combination of both the highest and lowest kinetic powers of all the case numbers. Case number 5 had the highest kinetic power in duct B of all cases while also having extremely low kinetic powers in ducts A and S. Similarly, case number 6 had the highest kinetic power in duct S, while the kinetic powers in ducts A and B were among the lowest. Since case numbers 5 and 6 were extreme because of experimental design and not because of error, there was no justification for removing them when reporting the final results, especially since removing them had negligible effect on the values predicted by the model.

Table 9: Summary of Regression Results from After Removing Possible Outlying Data

Case Number(s) Removed	Regression Coefficients			Adj R <sup>2</sup>	se
	K <sub>a</sub>	K <sub>b</sub>	K <sub>s</sub>		
None	0.613	0.489	0.188	89.6	63.7
2	0.583	0.503	0.188	89.8	63.3
4	0.602	0.475	0.193	89.9	62.8
5	0.628	0.446	0.197	92.0	55.8
6	0.617	0.511	0.169	90.6	60.6
2,4,5,6	0.584	0.455	0.192	94.0	48.3
5,6	0.692	0.467	0.182	93.7	53.89

#### Influence of Branch Velocity Ratios on Junction Lost Powers

Figures 38–43 shows the relationship between the normalized lost power in the junction and the various velocity ratios. For graphical presentation, the lost power in the junction for each case number was normalized by the kinetic power in duct M, thus reducing each junction loss to an equivalent velocity pressure coefficient in the downstream duct. As expected, the normalized lost power due to the junction ( $LPJ/Q_m VP_m$ ) was lowest when the velocities of all three incoming branches were approximately equal (see Figure 38). Large velocity differences at the junction were expected to increase separation from the walls due to momentum or sudden expansions, thus increasing power losses.

#### Velocity in the Side Branches With Respect to the Center Branch

Figure 38 shows the relationship between the normalized lost power in the junction and velocity ratio,  $V_b/V_s$ . The apparent outliers in Figure 38 result from extreme values of the  $V_a$  compared to  $V_b$  and  $V_s$ . Figure 39 shows the normalized LPJ with the effects of the  $V_a/V_b$  and  $V_a/V_s$  ratios removed by plotting only the cases where the velocities in ducts A and B were equal.

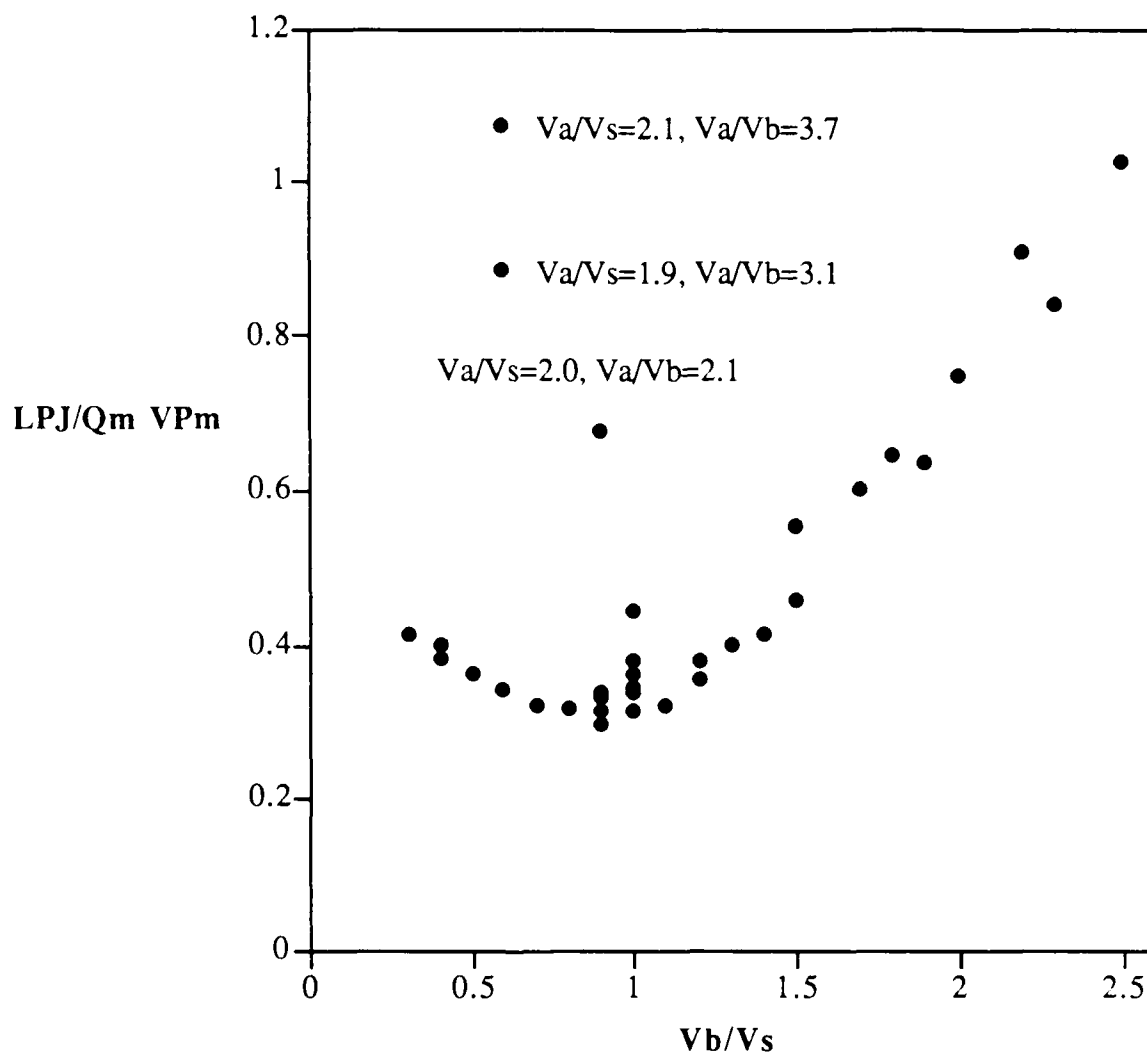


Figure 38: Influence of Velocity Ratio ( $V_b/V_s$ ) on Junction Lost Power

Figure 39 shows that power losses were smallest when the velocities in all three ducts entering the junction were approximately equal. Interestingly, this figure also shows that power losses increased slightly when the  $V_b$  decreased with respect to  $V_s$ , but increased rapidly as  $V_b$  exceeded  $V_s$ . This differential effect was expected since the momentum of flows in the lateral ducts would increase separation, while the momentum of flows in duct S would tend to reduce separation of flows A and B. The relationship between the power lost in the junction and the ratio  $V_a/V_s$  was similar (see Figures 40 and 41).

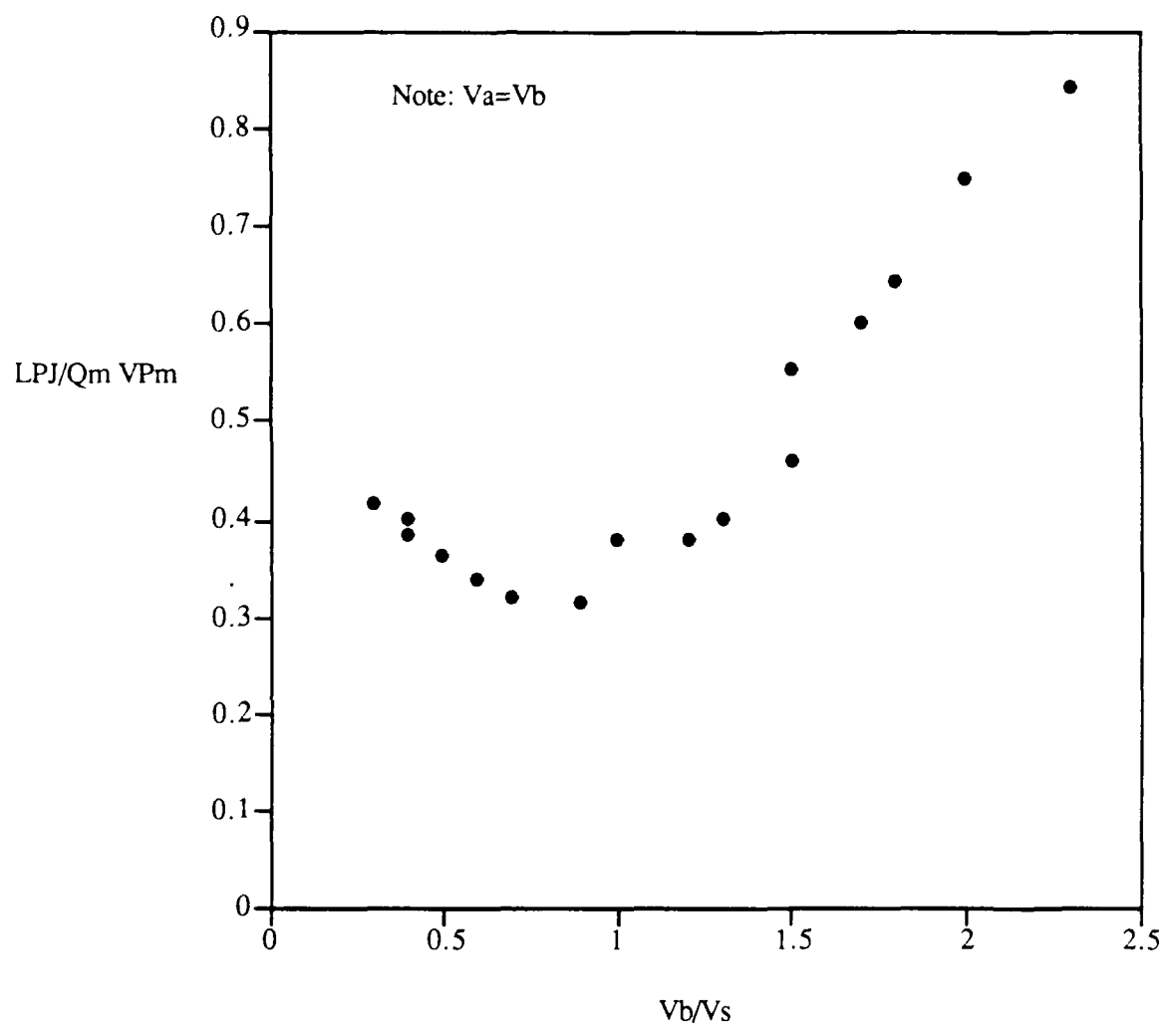


Figure 39: Influence of Lateral to Coaxial Duct Velocity Ratio ( $V_b/V_s$ ) on Junction Lost Power When  $V_a = V_b$

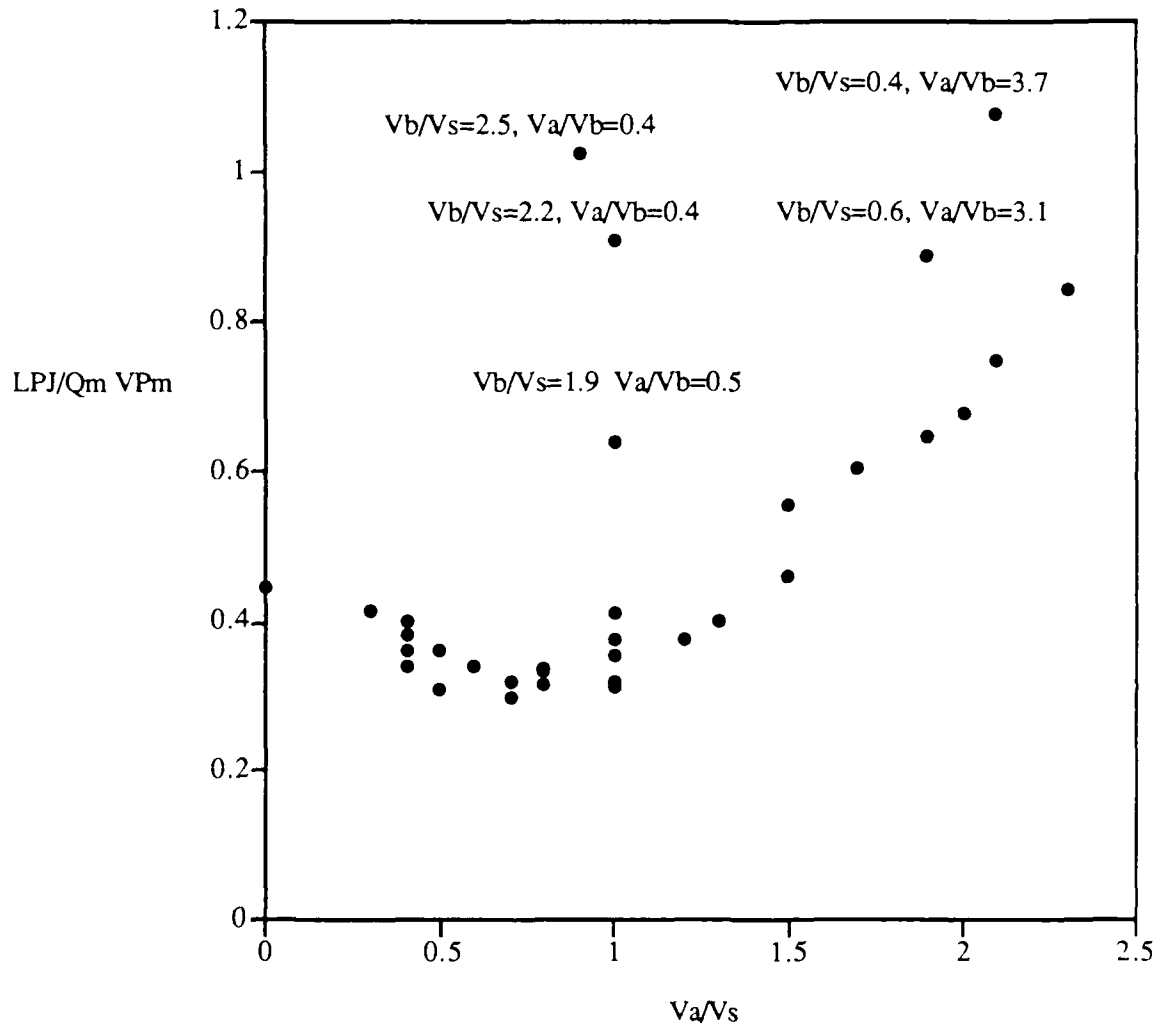


Figure 40: Influence of Velocity Ratio ( $V_a/V_s$ ) on Junction Lost Power



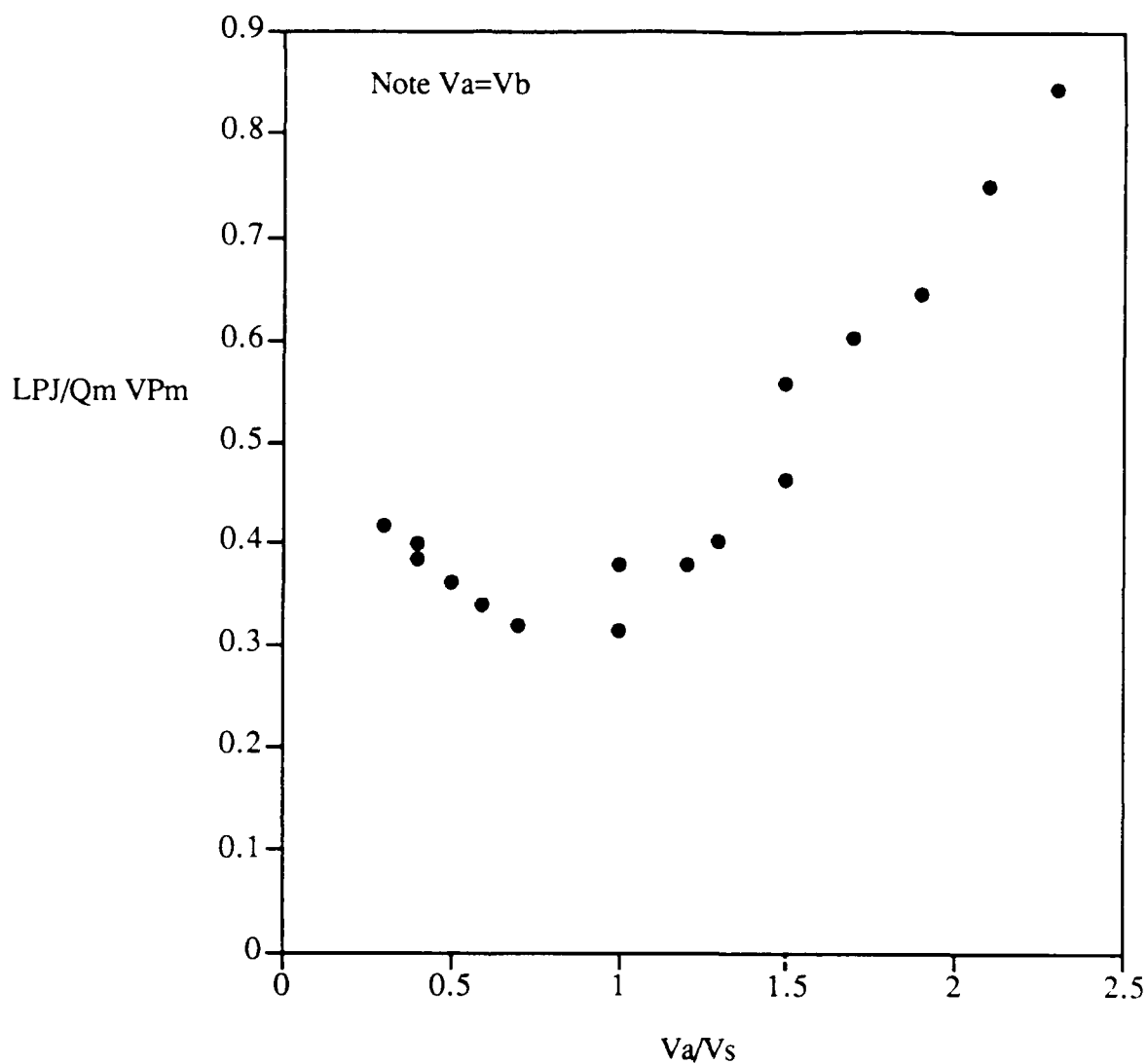


Figure 41: Influence of Velocity Ratio ( $V_a/V_s$ ) on Junction Lost Power When  $V_a = V_b$

#### Velocity of Side Branches With Respect to Each Other

Figure 42 shows that the lost power in the junction varies with respect to the velocity ratio of the laterals ( $V_a/V_b$ ). The independent effects of this ratio are not clear due to the confounding effects of the velocity ratios  $V_a/V_s$  and  $V_b/V_s$ . Figure 43 shows that the power losses rose rapidly when  $V_b$  increases with respect to  $V_a$  and  $V_s$ . The two points directly

above the  $V_b/V_a = 1.0$  in Figure 43 had nearly the same velocity ratios but different levels of total air flow. Ideally, these two points would have approximately the same normalized lost powers. The difference is likely due, in part, to a slight difference in velocity ratios. All velocity ratios were rounded to nearest 0.1; therefore, the true velocity ratios could differ by nearly 10% and still appear equal on the graphs. Some of the deviation also likely results from differing errors in estimating friction and other measurement errors.

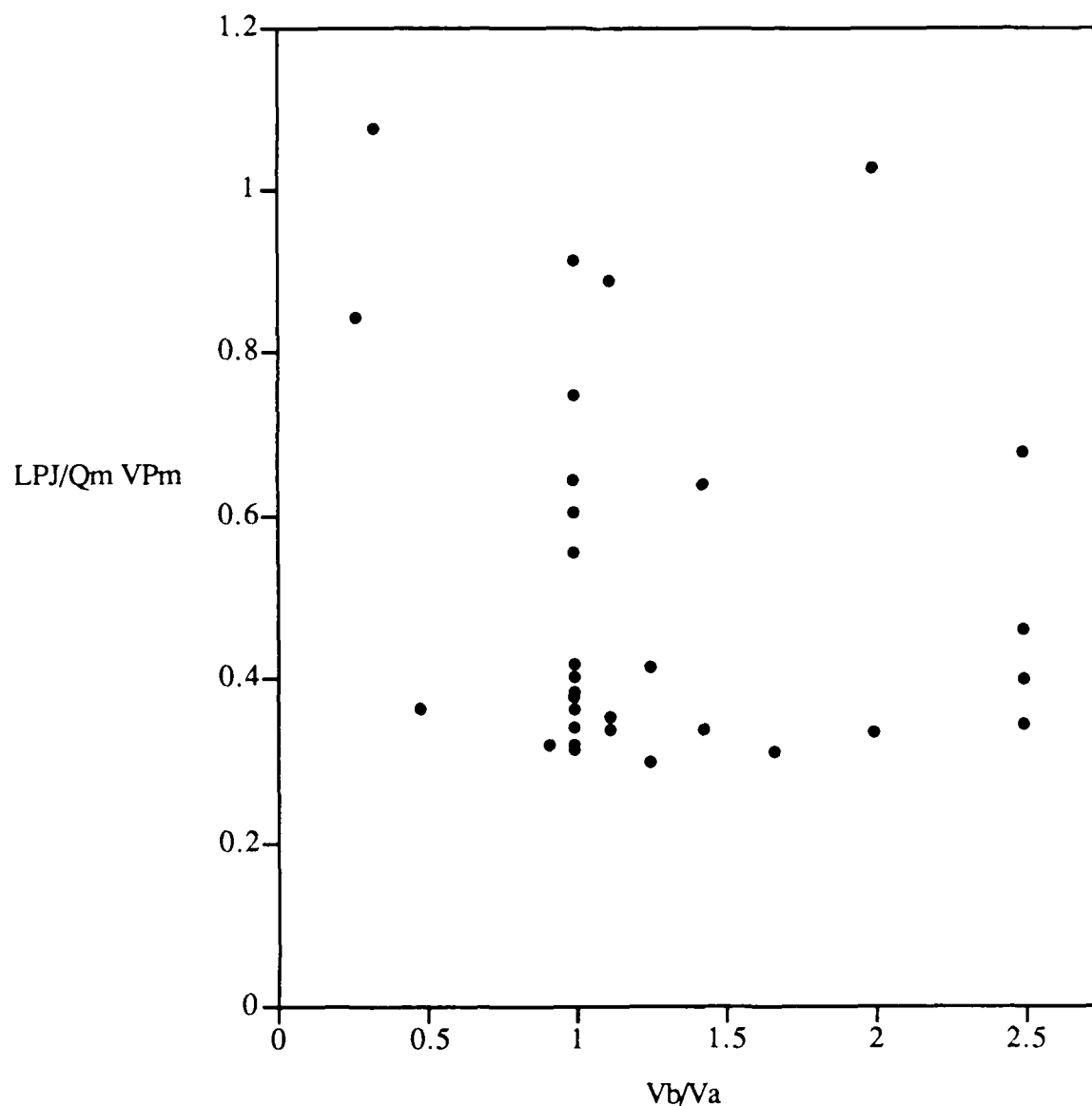


Figure 42: Influence of Velocity Ratio ( $V_b/V_a$ ) on Junction Lost Power

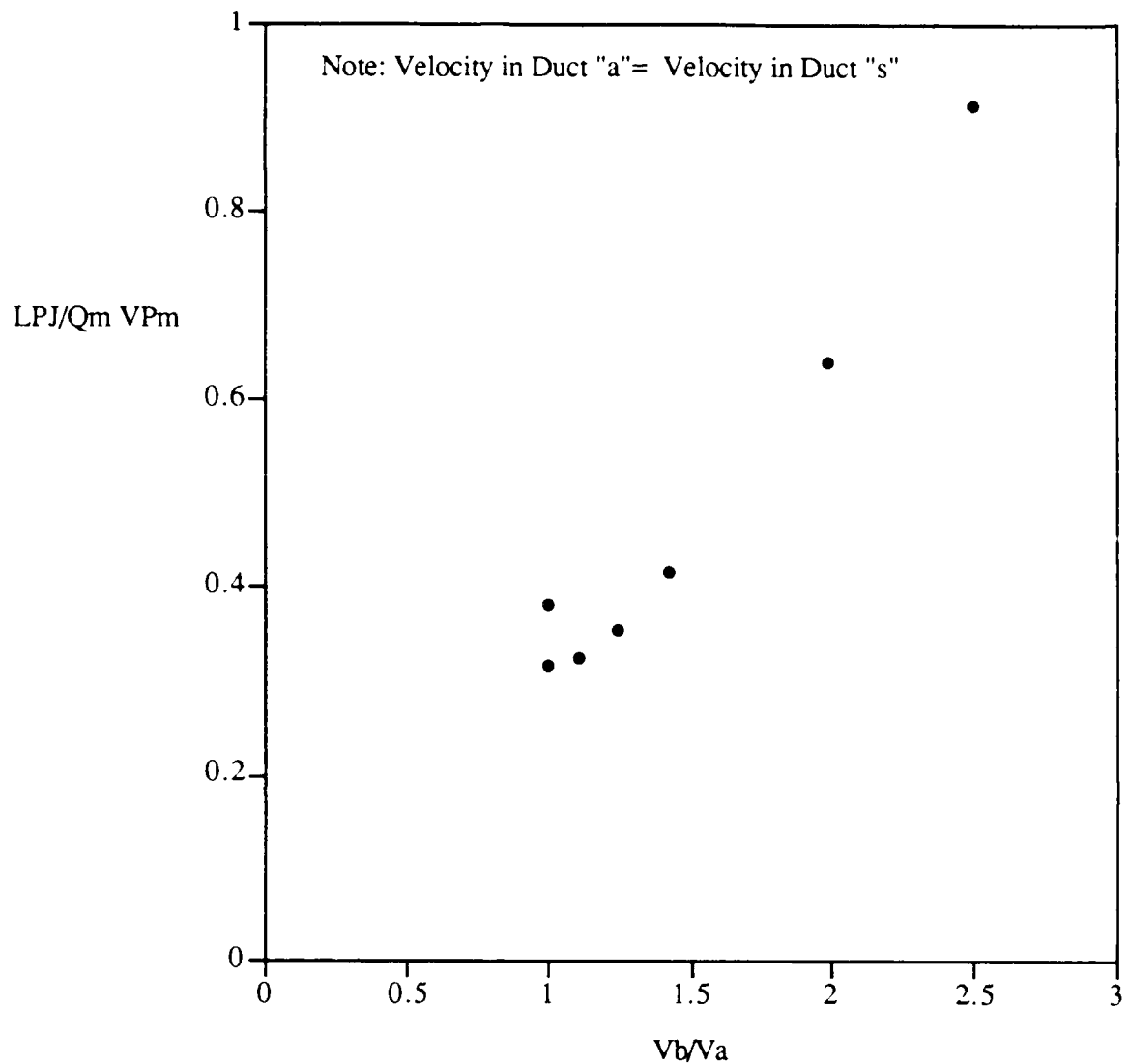


Figure 43: Influence of Velocity Ratio ( $V_b/V_a$ ) on Junction Lost Power  $V_a = V_b$

#### Estimation of "True" Coefficients for the Junction Tested

As discussed in the junction modelling and regression diagnostics sections, the experimental design produced a degree of collinearity of independent variables, which lead to non-equal values for the regression coefficients  $K_a$  and  $K_b$ . Since it is misleading to assign different values to two identical branches, the "true" (equal) values of  $K_a$  and  $K_b$  were each estimated by averaging  $K_a$  and  $K_b$ .

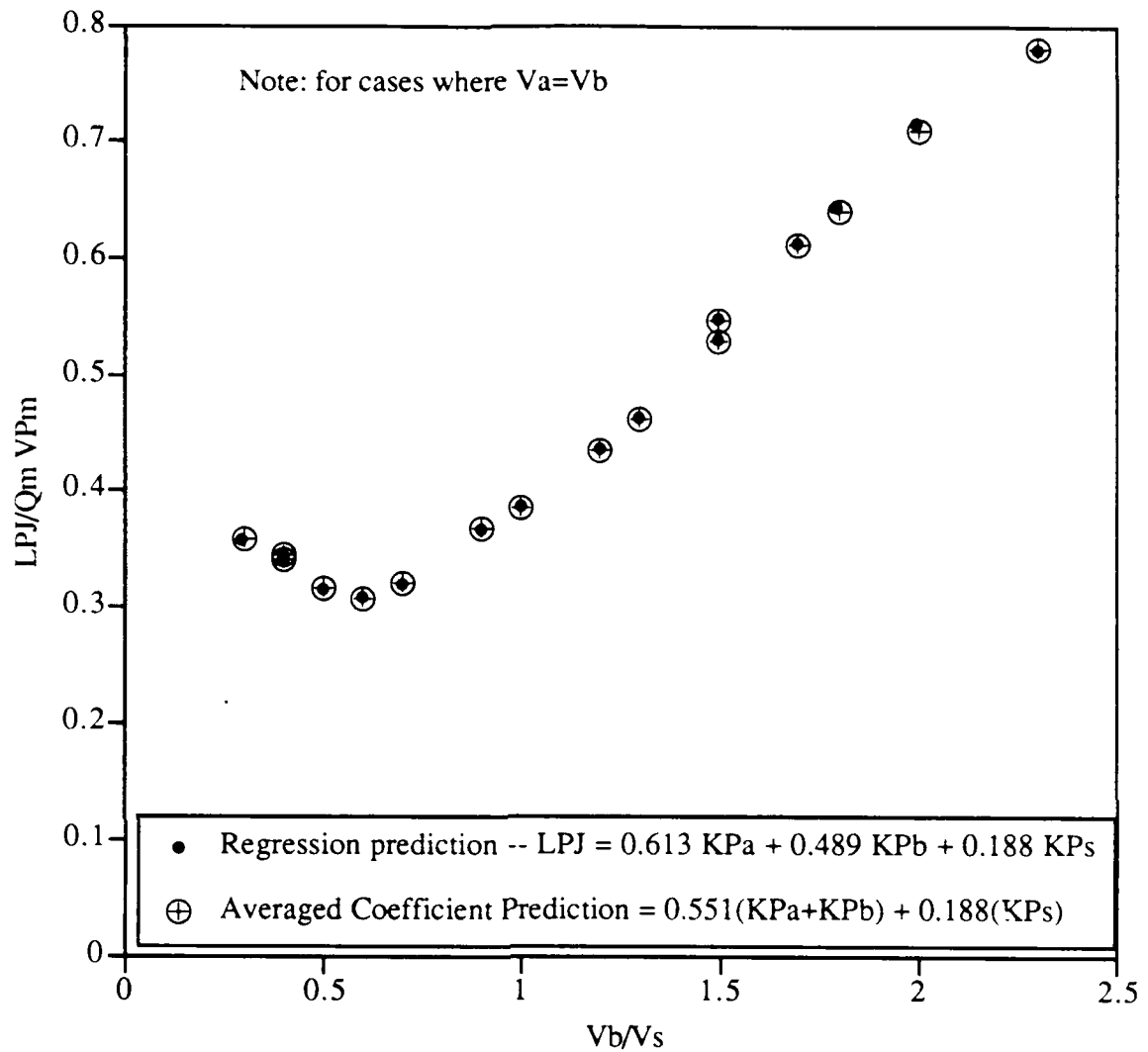


Figure 44: Comparison of Kinetic Power Coefficients Provided by Regression and an Average of  $K_a$  and  $K_b$

Figure 44 shows a close correspondence between the lost powers predicted by the regression coefficients and those predicted using the averaged values of  $K_a$  and  $K_b$ . However, Figure 45 shows there is some error when comparing either set of predicted values to the measured values. It should be reemphasized in Figure 45 that  $V_a$  was not exactly equal to  $V_b$  in any case, and that the ratio  $V_b/V_a$  varied somewhat from case to case due to the rounding of velocity ratios as discussed earlier. Since the predicted and observed values of  $LPJ$  are functions of  $V_b/V_a$ , even these slight variations prevent the values from following the smooth curve that might normally be expected.

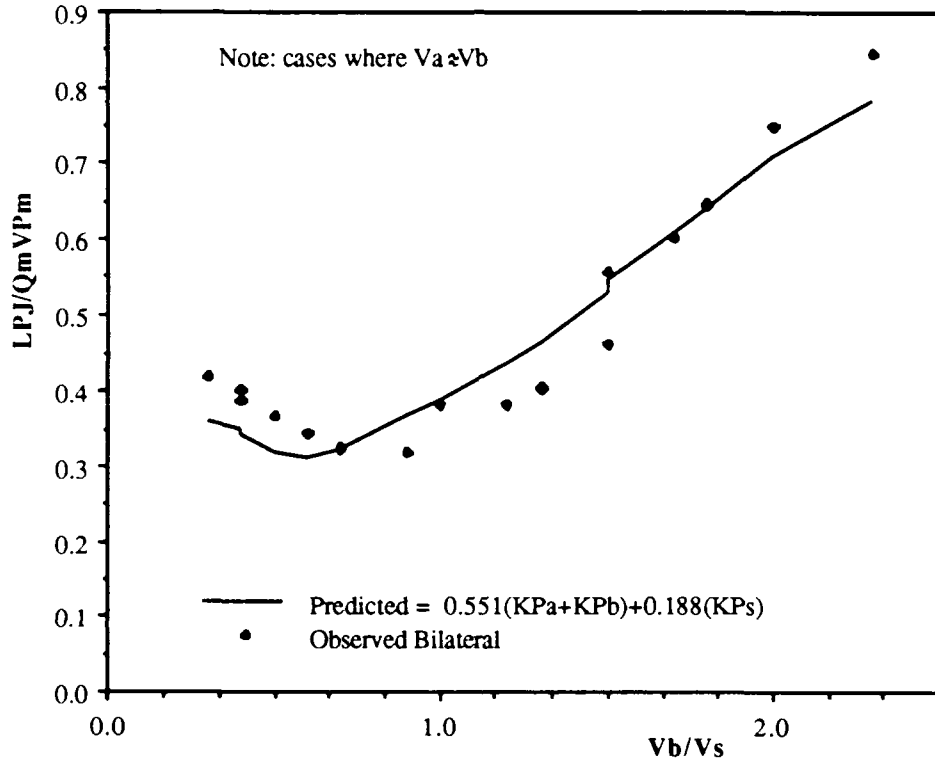


Figure 45: Comparison of Measured and Predicted Lost Junction Powers (normalized)

### Comparison of Power Losses From the Test Bilateral Junction to Losses from an Equivalent Double Single-Lateral Junction Setup

The second goal of this research was to determine if the power losses in the bilateral junction were significantly higher than the power losses predicted for an equivalent set of two single-lateral junctions. Figure 46 illustrates a hypothetical layout that is equivalent to the bilateral junction tested.

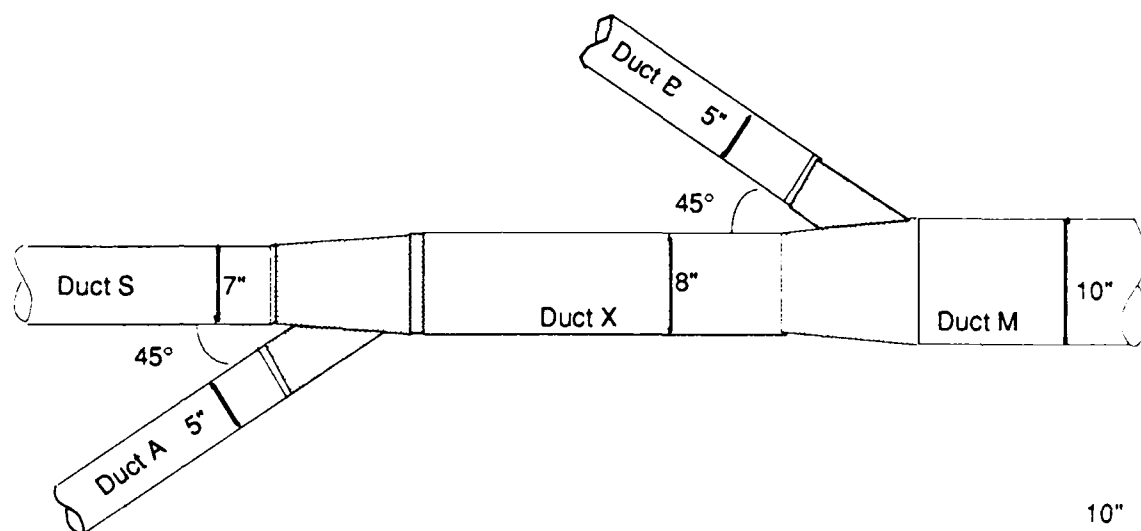


Figure 46: Hypothetical Setup with Two Single-Lateral Junctions Equivalent to the Bilateral Junction Tested

The power losses for two single-lateral junctions were predicted applying kinetic powers measured in the branches of the bilateral junction to equations developed by Guffey and Fraser<sup>(4)</sup> for single-lateral junctions. The following equation for the double single-lateral junction setup was derived by combining the predicted powers for two separate junctions into one expression:

$$LP_{J_{pred}} = 0.045 KP_s + 0.351 KP_a + 0.062 KP_x + 0.321 KP_b + 0.017 KP_m \quad \dots(21)$$

Use of Equation 20 assumes "ideal" conditions of no friction loss between the junctions, no interaction effects between the junctions, and no additional power losses due to longer laterals.

The measured power losses for bilateral junctions were an average 45% higher than the power losses predicted for the two single-lateral junctions. The range of the excess power losses for the bilateral junctions across all conditions was 14-92%. The excess power losses were at a minimum when the velocity ratios were nearly 1.0. The largest difference (92%) occurred when one branch of the bilateral junction was completely blocked so the junction was forced to behave as a single-lateral junction. Table 10 is a summary of analyses demonstrating that the excess power losses were highest for the extreme velocity ratios tested and that the excess power losses decreased as the velocity ratios approached 1.0. Figures 47 and 48 compare the normalized measured power losses in the bilateral junction with those predicted for two single-lateral junctions.

Table 10: Summary Statistics for the Percentage of Excess Power Losses in the Bilateral Junction as Compared with Predicted Power Losses for Two Single Lateral Junctions

<u>Selector</u>	<u>Average (%)</u>	<u>Range (%)</u>
All data	45.0	14-92
$0.5 < V_{ratio} < 2.0$	32.3	14-59
$0.75 < V_{ratio} < 1.25$	27.1	14-38

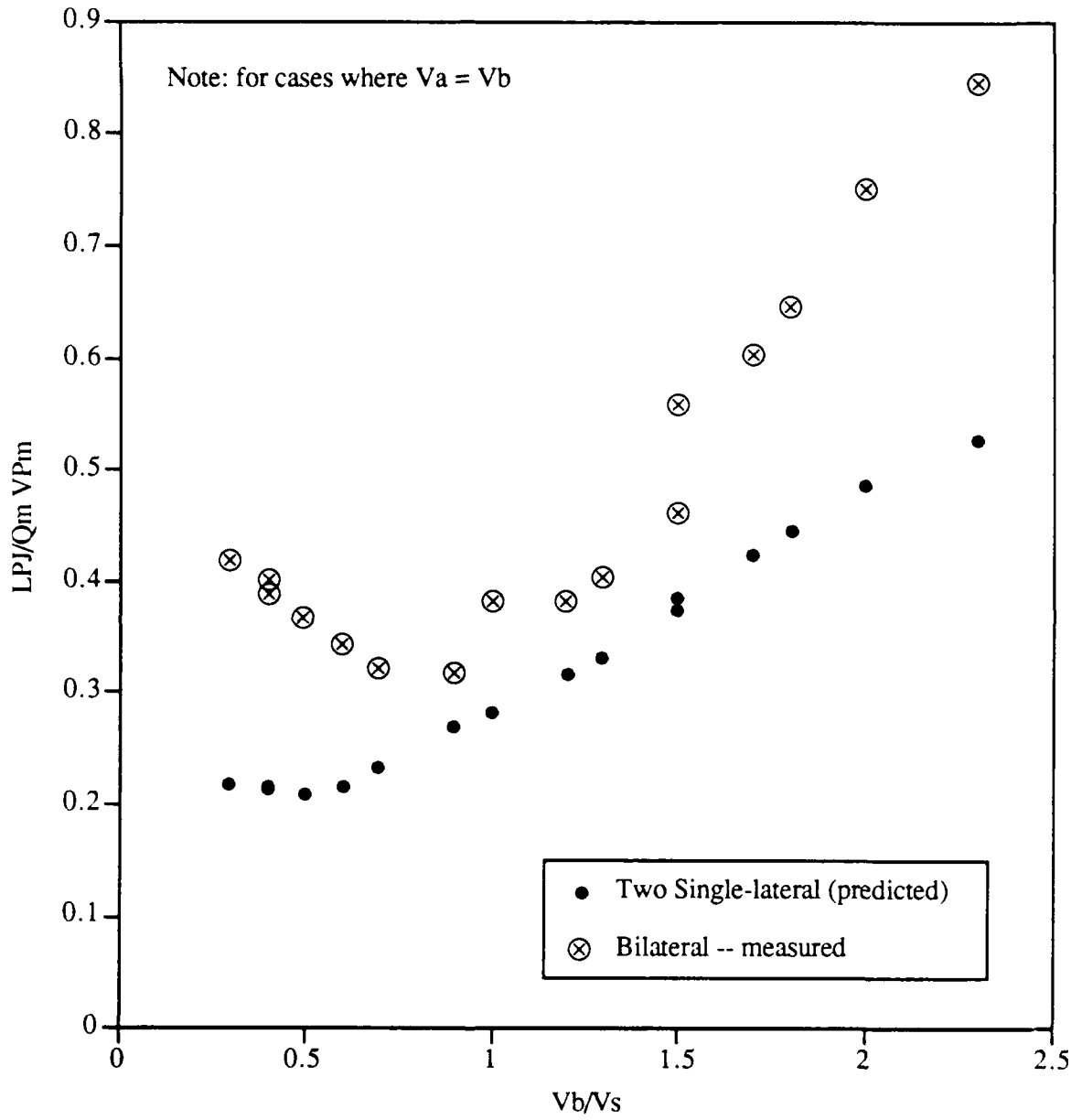


Figure 47: Comparison Measured Bilateral and Two Single-lateral Junction Power Losses for Velocity Ratio ( $V_b/V_s$ ) Where  $V_a = V_b$



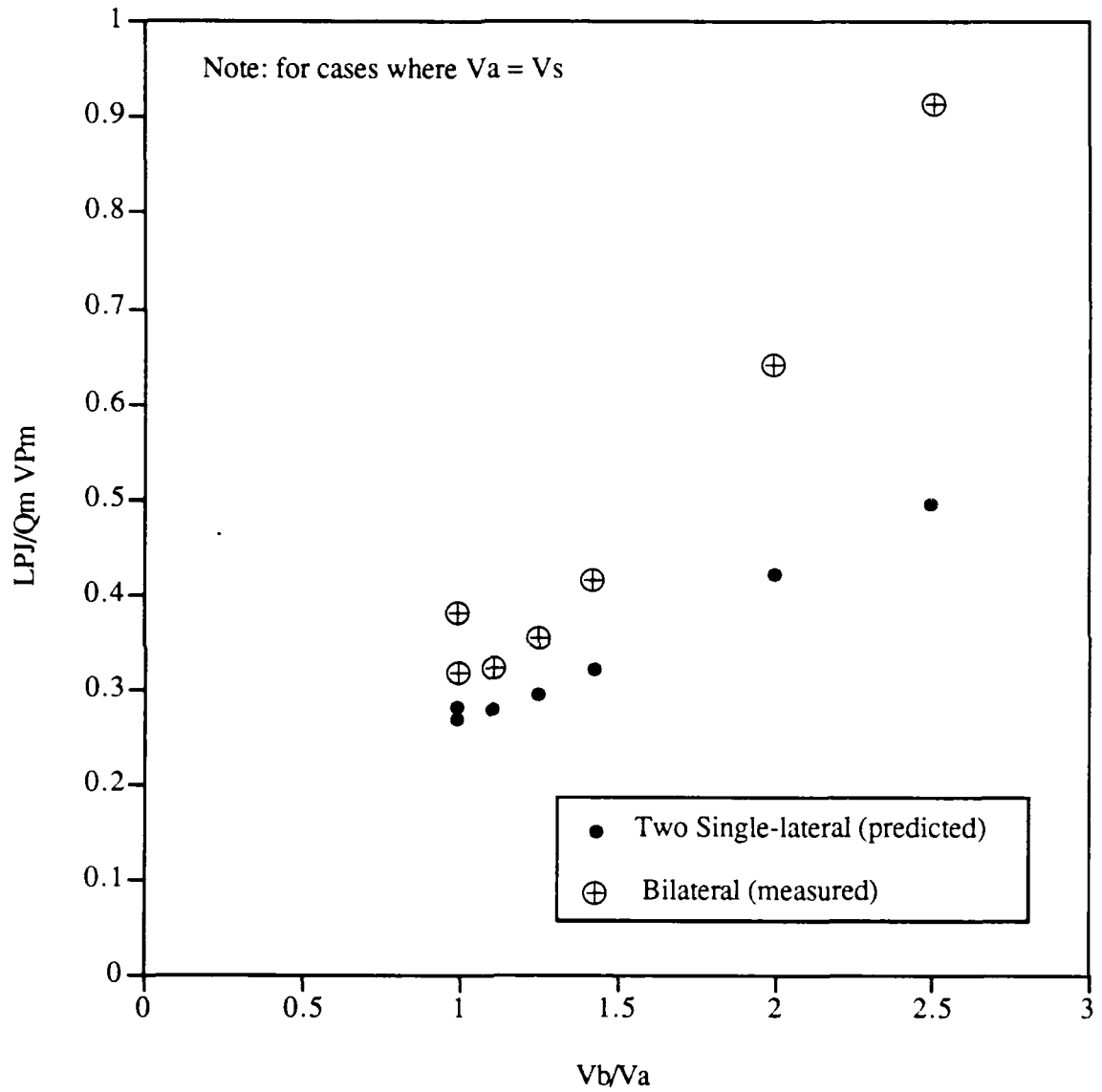


Figure 48: Comparison of Measured Bilateral and Predicted Two Single-lateral Junction Power Losses for Velocity Ratio ( $V_b/V_a$ ) Where  $V_a = V_s$

Significance of the Higher Power Losses For the Bilateral Junction Compared to the Single-lateral Junction Setup

Although the power losses appear substantially higher than those predicted for two single-lateral junctions, it is important to place these increases in the perspective of overall system pressure and power requirements. To provide a basis of comparison, an additional parameter will be developed. From Equation 5 (assuming no friction losses):

$$Q_m TP_m = Q_a TP_s + Q_b TP_b + Q_s TP_s - LPJ \quad \text{.....(22)}$$

Where: LPJ = lost power due to the junction

TP = total pressure in a duct

Q = flow in a duct

Subscripts a, b, s, and m represent reference cross-sections in ducts A, B, S and M

Rearranging equation 21 becomes:

$$TP_m = \left( \frac{Q_a}{Q_m} \right) TP_a + \left( \frac{Q_b}{Q_m} \right) TP_b + \left( \frac{Q_s}{Q_m} \right) TP_s - \left( \frac{LPJ}{Q_m} \right) \quad \text{.....(23)}$$

The units of  $LPJ/Q_m$  are pressure, so it is possible to define  $TPJ_{loss}$  as:

$$TPJ_{loss} = \frac{LPJ}{Q_m} \quad \text{.....(24)}$$

Where:  $TPJ_{loss}$  = total pressure lost due to the junction

If both sides of Equation 23 are divided by the downstream velocity pressure ( $VP_m$ ), then there exists an equivalent downstream velocity pressure coefficient such that:

$$F_J = \frac{TPJ_{loss}}{VP_m} \quad \text{.....(25)}$$

Where: VP = velocity pressure in a duct

FJ = equivalent downstream pressure coefficient for a junction

Subscripts a, b, s, and m represent reference cross-sections in ducts  
A, B, S and M

By normalizing lost power with downstream kinetic power to produce  $F_J$ , the power loss due to the mixing in the junction can be compared to loss coefficients for elbows and other components in the downstream duct.

As shown in Figure 47, the value of  $F_J$  for a bilateral junction ranges from approximately 0.30 to 0.85 as compared to a range of about 0.2 to 0.5 for two single-lateral junctions. The maximum difference of approximately 0.35 is less than that of two 90° elbows (see Figure 49). Also shown are equivalent lengths of 10 inch diameter ducts (size of main leaving the bilateral and second of the two single lateral junctions). Table 11 presents a comparison of  $F_J$  to other typical loss coefficients.

Table 11: Excess Bilateral Junction Losses as Equivalent Lengths of 10 inch Diameter Duct and 90° elbows for Velocities in the Range of 1000-4000 feet per minute

$\Delta F_J^*$	<u>Number of Diameters</u>	<u>Number of Elbows **</u>
0.30	16-18	1.6
0.20	11-12	1.1
0.15	7-8	0.79
0.10	4-5	0.52
0.05	2-4	0.26

$$*\Delta F_J = \frac{LPJ_{\text{observed bilateral}} - LPJ_{\text{predicted 2-laterals}}}{Q_m VP_m}$$

$\Delta F_J$  is the loss coefficient for the excess power losses in the bilateral junction as compared to two single-lateral junctions.

\*\* Elbows are 5-section with a radius of curvature equal to twice the diameter.

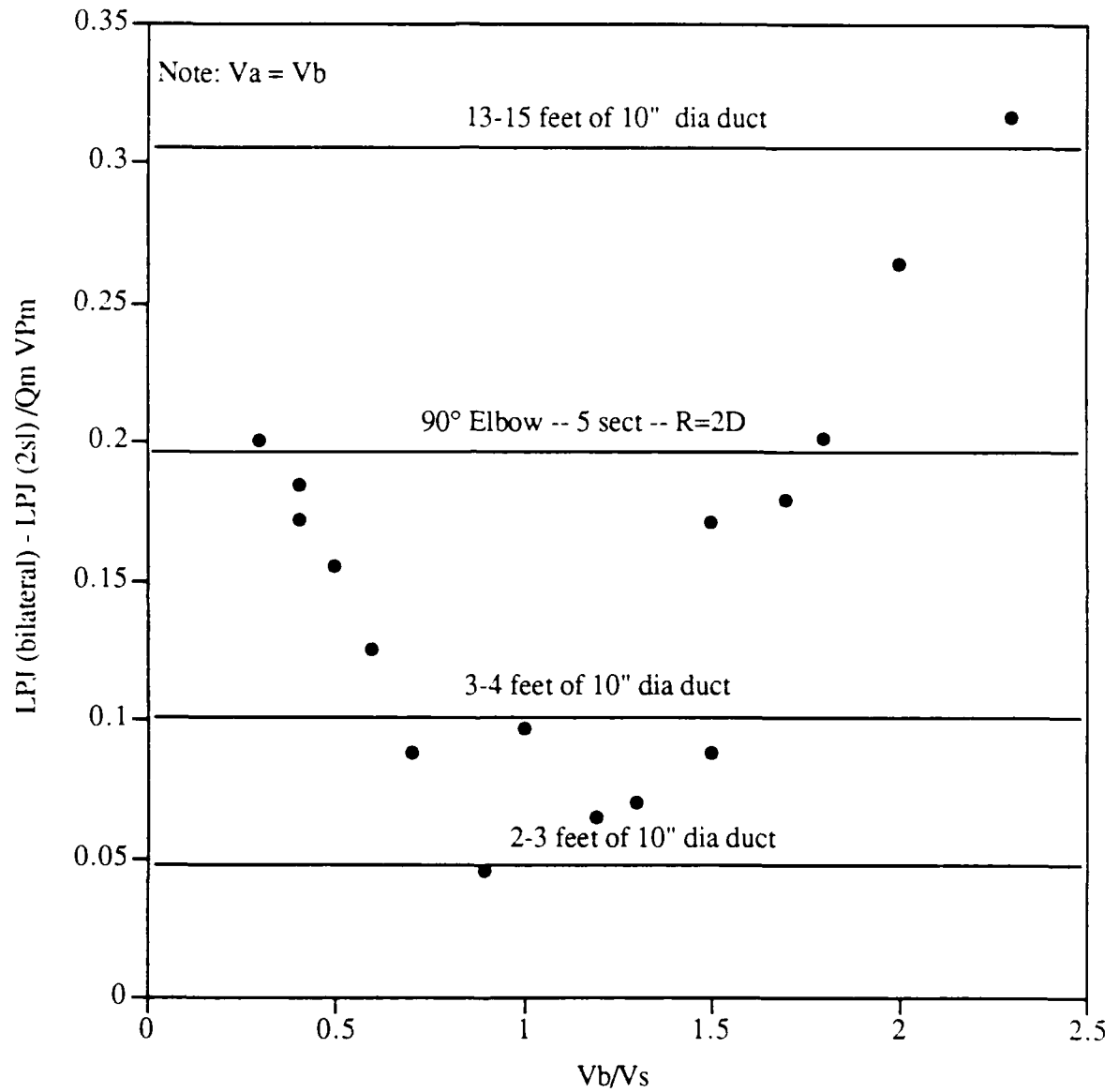


Figure 49: Comparison of Excess Bilateral Junction Losses to a 90° Elbow and Equivalent Lengths of 10" Diameter Duct for Velocity Ratio ( $V_b/V_s$ ) Where  $V_a = V_b$

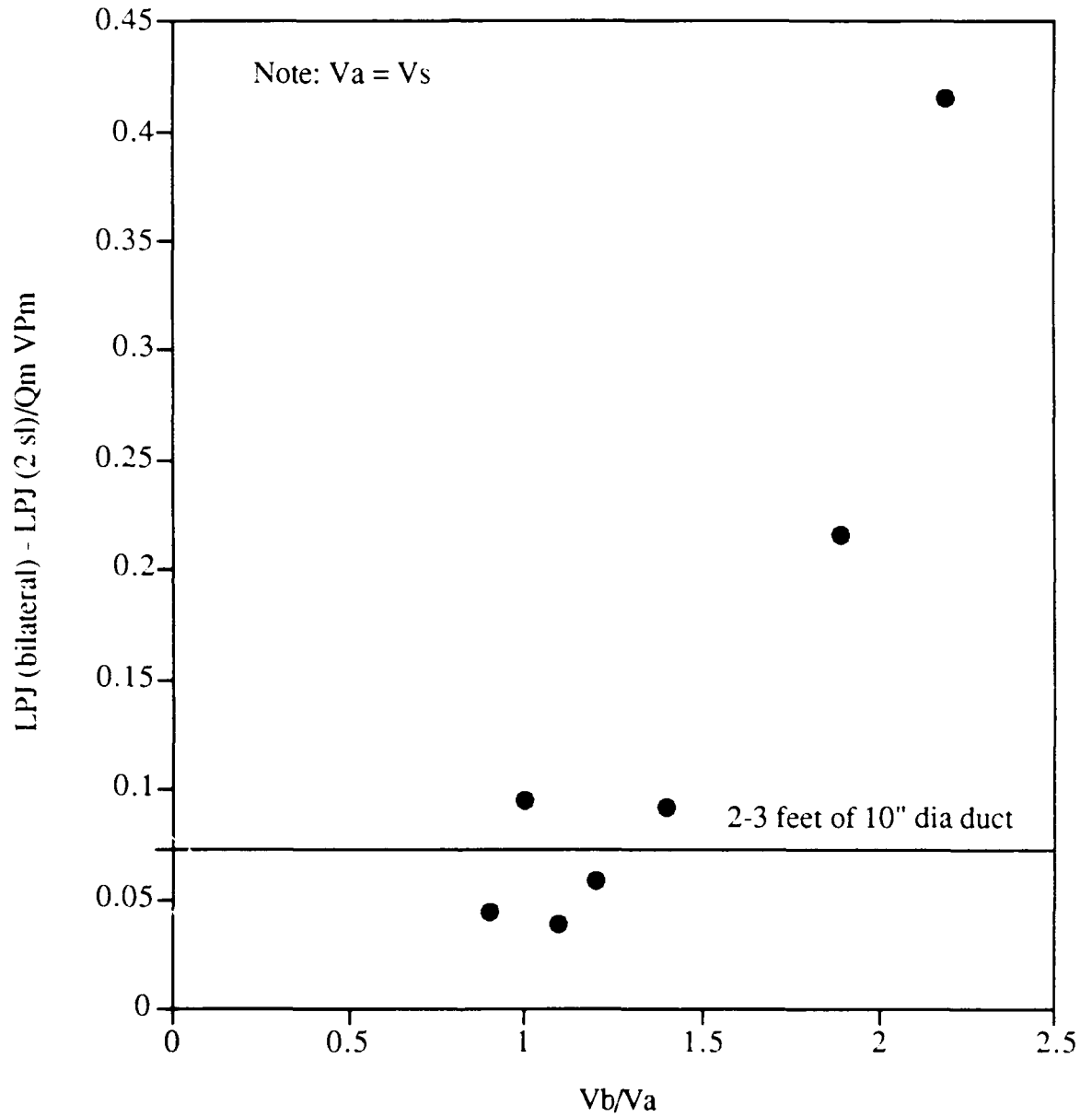


Figure 50: Comparison of Excess Bilateral Junction Losses to Equivalent Lengths of 10" Diameter Duct for Velocity Ratio ( $V_b/V_a$ ) Where  $V_a = V_s$

Finally, it should be noted that the predicted excess pressure losses due to using the bilateral junction instead of two single-lateral junctions would be very small in comparison to overall losses in typical ventilation systems. Even for the simple system constructed to test the bilateral junction, the greatest increase in total pressure was only 3.5% (Table 12), and that was for impractically extreme velocity ratios.

Table 12: Percentage of System \* Total Pressure Increase Resulting from the Bilateral Junction as Compared with the Predicted Total Pressure for a Two Single-lateral Setup

<u>Velocity Ratio</u>	<u>Percent Total Pressure Increase</u>	
	<u>Average</u>	<u>Maximum</u>
0.3 - 3.7	2.0	3.5
0.5 - 2.0	1.7	2.5
0.75 - 1.25	1.5	2.3

\* Pressure measured at the VP measuring station in duct "m".

When interpreting all of the results presented above it is important to remember that the predicted power losses for the two single-lateral junctions were estimated under "ideal" conditions and that any deviation from these conditions would increase the pressure requirement for the double single-lateral setup. In addition, the single-lateral junction model by Guffey and Fraser was fit to a more practical range of velocity ratios and then applied to very extreme velocity ratios in this research. Therefore, the junction power loss equation derived for the dual single-lateral setup may underestimate the true power losses at these extreme velocity ratios. This probably explains the divergence between the measured junction power losses for the bilateral junction and the predicted losses for the dual single-lateral set-up seen at extreme velocity ratios in Figure 47.

## CHAPTER IV CONCLUSIONS

The linear kinetic power model provided a good fit to the empirical data collected for a bilateral junction, and is likely to produce a similarly good fit for any other bilateral junction.

As was anticipated from momentum considerations, power losses were least when the velocities of the airstreams in the converging ducts were equal and were greatest when the lateral velocities exceeded the velocity of the center duct. Power losses increased rapidly when the lateral duct velocities exceeded the center duct velocity. Power losses increased to a lesser degree when the center duct velocity exceeded that of the laterals.

The dynamic power losses measured in the bilateral junction were 14-92% (average of 45%) greater than the power losses predicted for two single-lateral junctions in an equivalent setup. For most of the velocity ratios tested, the incremental increase in power lost for the bilateral junction was less than the power loss that would result from placing one 90° elbow (5 section,  $R=2D$ ) or an additional 10 feet of duct in the main. For some layouts, avoiding the use of bilateral junctions may require additional elbows and/or additional length in the branch ducts as shown in Figure 8. In these cases, a bilateral junction is likely to be more efficient than two single-lateral junctions in series; especially if the two single lateral junctions located are close together.

The ASHRAE table of coefficients is incorrect and should not be used to design systems containing bilateral junctions. Designers should refer to Idelchik <sup>(5)</sup> for coefficients for bilateral junction. Caution should also be used when using Idelchik's values since errors were also found in this table.

The linear kinetic power model was effective in predicting the losses in the bilateral junction studied. The fit to data was acceptable for the extreme range of velocity ratios tested (0-3.7) and very good for practical velocity ratios. The linear kinetic power model should be applied to empirical data from a diverse set of bilateral junctions so that loss coefficients can be modeled as functions of junction geometry as has been done for single-lateral junctions <sup>(4)</sup>. Research should be limited to a velocity ratio range of 0.5-2.0 since this range of velocity ratios should cover most design situations.

For many situations, a design incorporating bilateral junctions may have a lower power requirement than one which uses two single-lateral junctions in place of each bilateral junction. Even in cases where the single-lateral setup is more efficient, the advantages of the bilateral junction may outweigh the small potential energy savings of the single-lateral junctions.



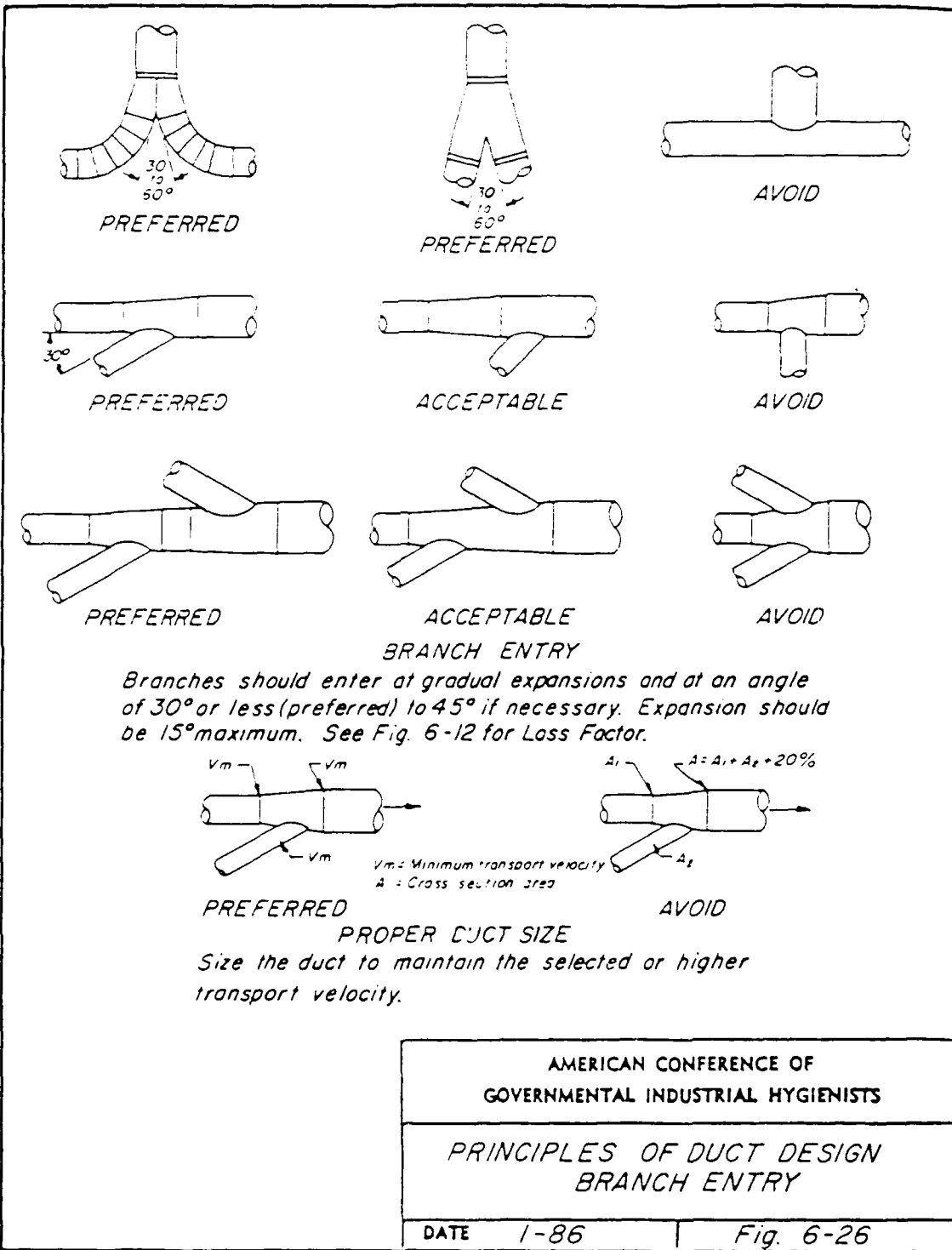
## REFERENCES

1. ACGIH, Industrial Ventilation - A Manual of Recommended Practice, 19th Edition, American Conference of Governmental Industrial Hygienists, Lansing, Michigan, 1986.
2. ASHRAE Handbook and Product Directory - 1989 Fundamentals Handbook, American Society of Heating, refrigerating and Air-Conditioning Engineers, Atlanta GA, 1989, pg 32.45.
3. Guffey, S.E., and Fraser, D.A., "A Power Balance Model for Converging and Diverging Flow Junctions," ASHRAE Transactions, Volume 95 Part 2 (in press).
4. Guffey, S.E., and Fraser, D.A., "Kinetic Power Model of Junction Losses," ASHRAE Transactions, Volume 95 Part 2 (in press).
5. Idelchik, I.E., Handbook of Hydraulic Resistance 2nd Edition, Hemisphere Publishing Corporation, Springer-Verlag, 1986, pp 373-379.
6. Ward-Smith, A.J., The Fluid Dynamics of Flow in Pipes and Ducts, Clarendon Press, Oxford, England, 1980, p 67.
7. Miller, D.S., Internal Flow Systems, Volume 5 in the British Hydromechanics Research Association Fluid Engineering Series, BHRA Fluid Engineering, 1978, p 198.
8. Miller, D.S., Internal Flow A Guide to Losses in Pipe and Duct Systems, The British Hydromechanics Research Association, Cranfield, Bedford England, 1971, pp 4.48.
9. ANSI/ASHRAE, Standard Methods for Laboratory Air Flow Measurement, 41.2-1987.
10. Guffey, S.E., "Simplifying Pitot Traverses," Applied and Occupational and Environmental Hygiene, 5(2), Feb 1990, pp 99-100.
11. Ower, E. and R. C. Pankhurst, The Measurement of Air Flow, Pergamon Press Ltd., London, 1966.
12. Winternitz, F. A. L. and C. F. Fischl, "A Simplified Integratin Technique for Pipe-flow Measurement." Water Power, Vol. 9, 1957, p 225.
13. Dwyer Instruments, Inc., Series 1425 Hook Gage Operating Instructions, Bulltein No. D-56, Michigan City, IN, 1985.
14. Meriam Instrument, General Installation, Operation & Maintenance Instructions for Meriam Manometers, File No. 022C-440-9, Cleveland, OH 1987.
15. Princo Instruments, Inc., Instruction Booklet for Use with Princo Fortin Type Mercurial Barometers, Southampton, PA 1983.
16. Guffey, S.E., "Impendance Method for Balancing Airflows in Ventilation Systems," unpublished manuscript.

17. Barbin, A.R. and Jones, J.B., "Turbulent Flow in the Inlet Region of a Smooth Pipe," Journal of Basic Engineering, March 1963.
18. Klienbaum, D.G., Kupper, L.L. and Muller, K.E., Applied Regression Analysis and Other Multivariable Methods, Second Edition, PWS-Kent Publishing Company, Boston MA, 1988.
19. Neeter, J., Wasserman, W. and Kutner, M.H., Applied Linear Statistical Models, Second Edition, Richard D. Irwin Inc., Homewood IL, 1985.

**Appendix A**

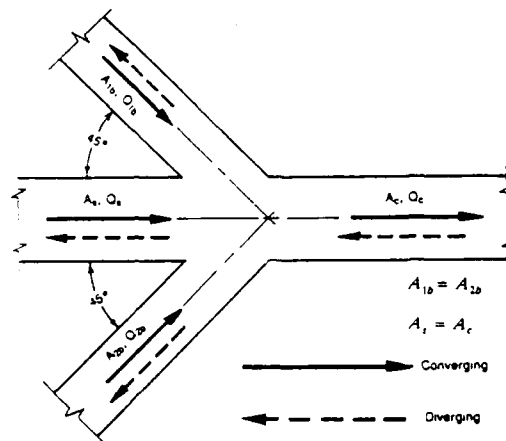
**ACGIH Bilateral Junction Recommendations**



**Appendix B**

**ASHRAE Coefficients for Bilateral Junctions**

5-34 Wye (Double), 45° Rectangular and Round (Idechik 1986, Diagram 7-27)



Converging Flow

		Branch, $C_{s,b}$						
$\frac{Q_{2b}}{Q_{1b}}$		$\frac{Q_{1b}}{Q_c}$						
$Q_{1b}$		0	0.1	0.2	0.3	0.4	0.5	0.6
$A_{1b}/A_c = 0.2$								
0.5	-1.0	-0.36	0.59	1.8	3.2	4.9	6.8	
1.0	-1.0	-0.24	0.63	1.7	2.6	3.7		
2.0	-1.0	-0.19	0.21	0.04				
$A_{1b}/A_c = 0.4$								
0.5	-1.0	-0.48	-0.02	0.58	0.92	1.3	16	
1.0	-1.0	-0.36	0.17	0.55	0.72	0.78		
2.0	-1.0	-0.18	0.16	-0.06				
$A_{1b}/A_c = 0.6$								
0.5	-1.0	-0.50	-0.07	0.31	0.60	0.82	0.92	
1.0	-1.0	-0.37	0.12	0.55	0.60	0.52		
2.0	-1.0	-0.18	0.26	0.16				
$A_{1b}/A_c = 1.0$								
0.5	-1.0	-0.51	-0.09	0.25	0.50	0.65	0.64	
1.0	-1.0	-0.37	0.13	0.46	0.61	0.54		
2.0	-1.0	-0.15	0.38	0.42				

		Main, $C_{s,t}$										
$\frac{A_{2b}}{A_{1b}}$		$\frac{Q_t}{Q_c}$										
$A_{1b}$		0	0.1	0.2	0.3	0.4	0.5	0.6	0.7	0.8	0.9	1.0
$A_{1b}/A_c = 0.2$												
0.5 &												
2.0	-2.9	-1.9	-1.3	-0.80	-0.56	-0.23	-0.01	0.16	0.22	0.15	0	
1.0	-2.5	-1.9	-1.3	-0.80	-0.42	-0.12	0.08	0.20	0.22	0.15	0	
$A_{1b}/A_c = 0.4$												
0.5 &												
2.0	-0.98	-0.61	-0.30	-0.05	0.14	0.26	0.33	0.34	0.28	0.17	0	
1.0	-0.77	-0.44	-0.16	0.05	0.21	0.31	0.36	0.35	0.29	0.17	0	
$A_{1b}/A_c = 0.6$												
0.5 &												
2.0	-0.32	0.08	0.11	0.27	0.37	0.43	0.44	0.40	0.31	0.18	0	
1.0	-0.18	-0.04	0.21	0.34	0.42	0.46	0.46	0.41	0.31	0.18	0	
$A_{1b}/A_c = 1.0$												
0.5 &												
2.0	0.11	0.36	0.46	0.53	0.57	0.56	0.52	0.44	0.33	0.18	0	
1.0	0.29	0.42	0.51	0.57	0.58	0.58	0.54	0.45	0.33	0.18	0	

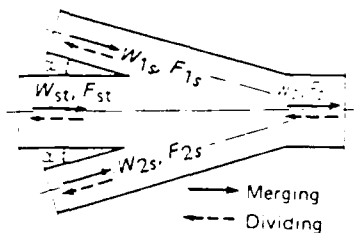
Diverging Flow: Use Fitting 5-23.

## **Appendix C**

### **Idelchik's Coefficients for Bilateral Junctions**

Four-way wye piece of the type  $F_{1s} = F_{2s} = F_s, F_{st} = F_c$   
 $\alpha = 15^\circ$  [11, 12]

Diagram  
7-25



1. Merging of streams (outlet four-way piece)

Side branch

$$\zeta_{i.c.s} = \frac{\Delta p_{i.s}}{\rho w_{i.s}^2 / 2} = 1 - \left( \frac{Q_{1s} F_c}{Q_c F_{1s}} \right)^2 - 3 \left( \frac{Q_{1s}}{Q_c} \right)^2$$

$$\times \frac{\{Q_c Q_{1s} - (1 - Q_{2s} Q_{1s})\}^2}{4 - (1 + Q_{2s} Q_{1s}) Q_{1s} Q_c} - 1.93 \left( \frac{Q_{1s}}{Q_c} \right)^2 \frac{F_c}{F_{1s}} \left[ 1 - \left( \frac{Q_{1s}}{Q_c} \right)^2 \right]$$

see the curves  $\zeta_{i.c.s} = f(Q_{st}/Q_c, Q_{2s}/Q_{1s})$  at different  $F_{1s}/F_c$ .

For the other side branch subscripts 1 and 2 change places.

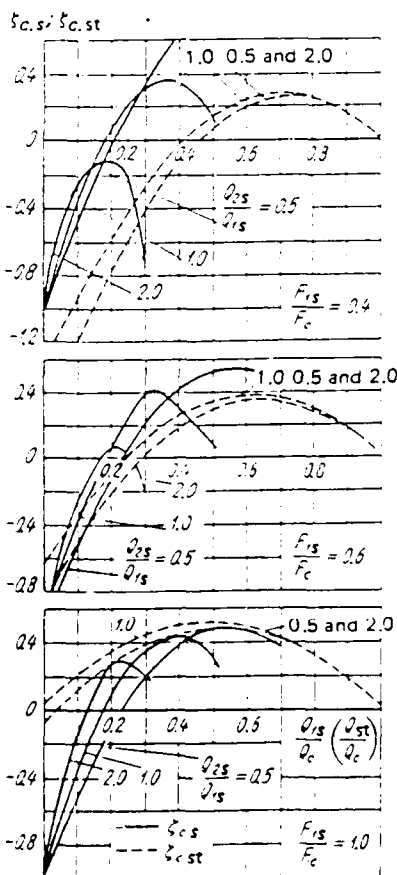
Main passage

$$\zeta_{c.st} = \frac{\Delta p_{st}}{\rho w_{st}^2 / 2} = 1 + \left( \frac{Q_{st}}{Q_c} \right)^2 - \left( \frac{Q_{st}}{Q_c} \right)^2 \frac{1 - Q_{st} Q_c}{(0.75 + 0.25 Q_{st} Q_c)^2}$$

$$- 1.93 \left( \frac{Q_{st}}{Q_c} \right)^2 \frac{F_c}{F_{1s}} \frac{(1 + Q_{2s} Q_{1s})^2}{(1 + Q_{2s} Q_{1s})^2} \left( \frac{Q_c}{Q_{st}} - 1 \right)^2$$

see the curves  $\zeta_{c.st} = f(Q_{st}/Q_c, Q_{2s}/Q_{1s})$  at different  $F_{1s}/F_c$ .

2. Division of flow (intake four-way piece).  $\zeta_{c.s}$  and  $\zeta_{c.st}$  are determined tentatively similar to diverging wyes from Diagrams 7-15 and 7-17 (curve 1)



Values of  $\zeta_{c.s}$

$\frac{Q_{2s}}{Q_{1s}}$	$Q_{1s}/Q_c$						
	0	0.1	0.2	0.3	0.4	0.5	0.6
$F_{1s}/F_c = 0.2$							
0.5	-1.0	-0.37	0.46	1.48	2.69	4.07	5.62
1.0	-1.0	-0.29	0.43	1.23	1.80	2.81	-
2.0	-1.0	-0.32	-0.31	-1.13	-	-	-
$F_{1s}/F_c = 0.4$							
0.5	-1.0	-0.50	-0.05	0.34	0.65	0.90	1.04
1.0	-1.0	-0.39	0.06	0.31	0.35	0.14	-
2.0	-1.0	-0.27	-0.10	-0.65	-	-	-
$F_{1s}/F_c = 0.6$							
0.5	-1.0	-0.51	-0.11	-0.21	0.42	0.55	0.53
1.0	-1.0	-0.39	0.05	0.40	0.31	0.09	-
2.0	-1.0	-0.22	+0.08	-0.18	-	-	-
$F_{1s}/F_c = 1.0$							
0.5	-1.0	-0.51	-0.12	0.20	0.39	0.49	0.37
1.0	-1.0	-0.38	0.09	0.36	0.44	0.28	-
2.0	-1.0	-0.18	0.27	0.19	-	-	-



Four-way wye piece of the type  $F_{1s} = F_{2s} = F_s; F_{st} = F_c$ ;  
 $\alpha = 15^\circ$  [11, 12]

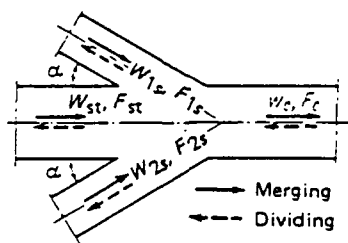
Diagram  
7-25

Values of  $\zeta_{c, st}$

$\frac{Q_{2s}}{Q_{1s}}$	$Q_{st}/Q_c$										
	0	0.1	0.2	0.3	0.4	0.5	0.6	0.7	0.8	0.9	1.0
$F_{1s}/F_c = 0.2$											
0.5-2.0	-4.37	-2.93	-2.04	-1.44	-1.08	-0.58	-0.22	0.03	0.16	0.14	0
1.0	-3.84	-2.93	-2.13	-1.44	-0.89	-0.45	-0.13	0.08	0.17	0.14	0
$F_{1s}/F_c = 0.4$											
0.5-2.0	-1.70	-1.19	-0.76	-0.40	-0.12	0.08	0.21	0.27	0.25	0.16	0
1.0	-1.42	-0.96	-0.58	-0.26	-0.02	0.15	0.26	0.29	0.26	0.16	0
$F_{1s}/F_c = 0.6$											
0.5-2.0	-0.81	-0.47	-0.19	0.04	0.20	0.30	0.36	0.35	0.29	0.17	0
1.0	-0.16	-0.31	-0.05	0.13	0.27	0.35	0.39	0.37	0.29	0.17	0
$F_{1s}/F_c = 1.0$											
0.5-2.0	-0.35	-0.11	0.10	0.26	0.36	0.42	0.43	0.39	0.31	0.18	0
1.0	-0.21	0.02	0.19	0.33	0.41	0.45	0.45	0.41	0.31	0.18	0

Four-way wye piece of the type  $F_{1s} = F_{2s} = F_s; F_{st} = F_c$ ;  
 $\alpha = 30^\circ$  [11, 12]

Diagram  
7-26



1) Merging of streams (outlet four-way piece).

Side branch

$$\zeta_{1c,s} = \frac{\Delta p_{1s}}{\rho w_c^2/2} = 1 + \left( \frac{Q_{1s} F_c}{Q_c F_{1s}} \right)^2 - 8 \left( \frac{Q_{1s}}{Q_c} \right)^2 \frac{[Q_c/Q_{1s} - (1 + Q_{2s}/Q_{1s})]^2}{4 - (1 + Q_{2s}/Q_{1s})Q_{1s}/Q_c} - 1.73 \left( \frac{Q_{1s}}{Q_c} \right)^2 \frac{F_c}{F_{1s}} \left[ 1 + \left( \frac{Q_{2s}}{Q_{1s}} \right)^2 \right]$$

see the curves  $\zeta_{1c,s} = f(Q_{1s}/Q_c, Q_{2s}/Q_{1s})$  at different  $F_{1s}/F_c$ .

For the other side branch subscripts 1 and 2 change places.

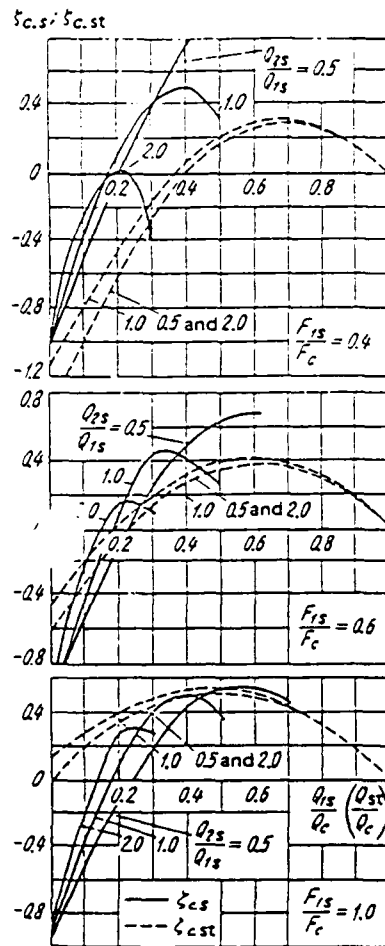
Main passage

$$\zeta_{c,st} = \frac{\Delta p_{st}}{\rho w_c^2/2} = 1 + \left( \frac{Q_{st}}{Q_c} \right)^2 - \left( \frac{Q_{st}}{Q_c} \right)^2 \frac{1 + Q_{st}/Q_c}{(0.75 + 0.25Q_{st}/Q_c)^2} - 1.73 \left( \frac{Q_{st}}{Q_c} \right)^2 \frac{F_c}{F_{1s}} \frac{1 + (Q_{2s}/Q_{1s})^2}{(1 + Q_{2s}/Q_{1s})^2} \left( \frac{Q_c}{Q_{st}} - 1 \right)^2$$

see the curves  $\zeta_{c,st} = f(Q_{st}/Q_c, Q_{2s}/Q_{1s})$  at different  $F_{1s}/F_c$ .

2) Division of flow (intake four-way piece):  $\zeta_{c,s}$  and  $\zeta_{c,st}$  are determined tentatively as for diverging wyes from Diagrams 7-15 and 7-17 (curve 1).

Diagram  
7-26



Values of  $\zeta_{cs}$

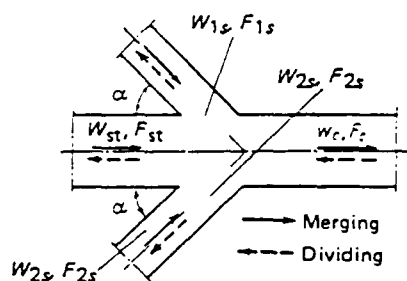
$\frac{Q_{2s}}{Q_{1s}}$	$\frac{Q_{1s}}{Q_c}$						
	0	0.1	0.2	0.3	0.4	0.5	0.6
$F_{1s}/F_c = 0.2$							
0.5	-1.0	-0.36	+0.51	1.59	2.89	4.38	6.10
1.0	-1.0	-0.27	0.51	1.41	2.12	2.91	-
2.0	-1.0	-0.27	0.11	-0.72	-	-	-
$F_{1s}/F_c = 0.4$							
0.5	-1.0	-0.49	-0.03	0.40	0.75	1.06	1.44
1.0	-1.0	-0.38	0.10	0.40	0.51	0.34	-
2.0	-1.0	-0.25	0.01	-0.42	-	-	-
$F_{1s}/F_c = 0.6$							
0.5	-1.0	-0.51	-0.10	0.25	0.50	0.65	0.68
1.0	-1.0	-0.38	0.08	0.45	0.42	0.25	-
2.0	-1.0	-0.21	0.15	0.08	-	-	-
$F_{1s}/F_c = 1.0$							
0.5	-1.0	-0.51	-0.11	0.22	0.43	0.55	0.55
1.0	-1.0	-0.37	0.10	0.40	0.51	0.38	-
2.0	-1.0	-0.17	0.31	0.28	-	-	-

Values of  $\zeta_{cst}$

$\frac{Q_{2s}}{Q_{1s}}$	$\frac{Q_{st}}{Q_c}$										
	0	0.1	0.2	0.3	0.4	0.5	0.6	0.7	0.8	0.9	1.0
$F_{1s}/F_c = 0.2$											
0.5-0.2	-3.81	-2.51	-1.81	-1.20	-0.86	-0.44	-0.13	0.08	0.18	0.14	0
1.0	-3.34	-2.53	-1.81	-1.20	-0.71	-0.32	-0.05	0.12	0.18	0.14	0
$F_{1s}/F_c = 0.4$											
0.5-0.2	-1.42	-0.97	-0.58	-0.26	0.02	0.15	0.26	0.30	0.26	0.17	0
1.0	-1.16	-0.76	-0.48	-0.14	0.07	0.21	0.30	0.31	0.27	0.17	0
$F_{1s}/F_c = 0.6$											
0.5-2.0	-0.52	-0.32	-0.07	0.13	0.27	0.35	0.39	0.37	0.29	0.17	0
1.0	-0.45	-0.18	0.04	0.21	0.33	0.39	0.41	0.39	0.30	0.18	0
$F_{1s}/F_c = 1.0$											
0.5-2.0	-0.03	0.21	0.34	0.45	0.50	0.52	0.49	0.43	0.32	0.18	0
1.0	0.13	0.29	0.41	0.49	0.54	0.54	0.51	0.44	0.32	0.18	0

Four-way wye piece of the type  $F_{1s} = F_{2s} = F_s$ ;  $F_{st} = F_c$ ;  
 $\alpha = 45^\circ$  [11, 12]

Diagram  
 7-27



1) Merging of streams (outflow four-way piece).

Side branch

$$\zeta_{1c,s} = \frac{\Delta p_{1s}}{\rho w_c^2 / 2} = 1 + \left( \frac{Q_{1s} F_c}{Q_c F_{1s}} \right)^2 - 8 \left( \frac{Q_{1s}}{Q_c} \right)^2 \frac{[Q_c / Q_{1s} - (1 + Q_{2s} / Q_{1s})]^2}{4 - (1 + Q_{2s} / Q_{1s}) Q_{1s} / Q_c} - 1.42 \left( \frac{Q_{1s}}{Q_c} \right)^2 \frac{F_c}{F_{1s}} \left[ 1 + \left( \frac{Q_{2s}}{Q_{1s}} \right)^2 \right]$$

see the curves  $\zeta_{1c,s} = f(Q_{1s}/Q_c, Q_{2s}/Q_{1s})$  at different  $F_{1s}/F_c$ .

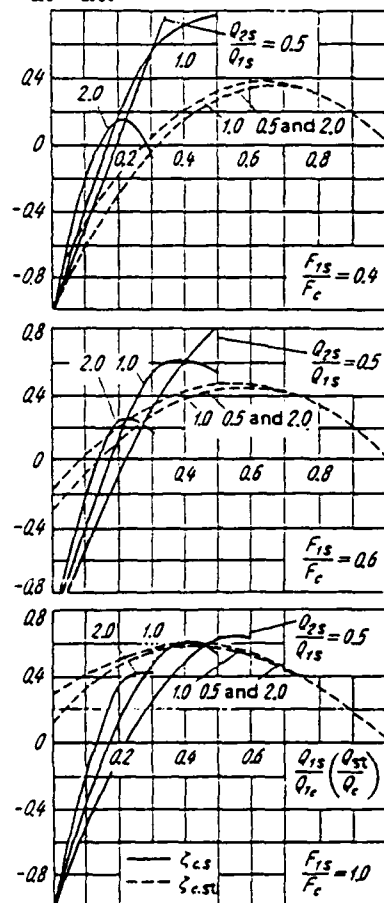
For the other side branch subscripts 1 and 2 change places.

Main passage

$$\zeta_{c,st} = \frac{\Delta p_{st}}{\rho w_c^2 / 2} = 1 + \left( \frac{Q_{st}}{Q_c} \right)^2 - \left( \frac{Q_{st}}{Q_c} \right)^2 \frac{1 + Q_{st}/Q_c}{(0.75 + 0.25 Q_{st}/Q_c)^2} - 1.42 \left( \frac{Q_{st}}{Q_c} \right)^2 \frac{F_c}{F_{1s}} \frac{1 + (Q_{2s}/Q_{1s})^2}{(1 + Q_{2s}/Q_{1s})^2} \left( \frac{Q_c}{Q_{st}} - 1 \right)^2$$

see the curves  $\zeta_{c,st} = f(Q_{st}/Q_c, Q_{2s}/Q_{1s})$  at different  $F_{1s}/F_c$ .

$\zeta_{c,s}$ ;  $\zeta_{c,st}$



2) Division of flow (diverging four-way piece);  $\zeta_{c,s}$  and

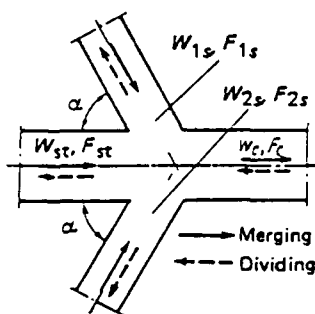
$\zeta_{c,st}$  are determined tentatively as for wyes from Diagrams 7-15 and 7-17 (curve 1).

Values of  $\zeta_{c,s}$

$\frac{Q_{2s}}{Q_{1s}}$	$\frac{Q_{1s}}{Q_c}$						
	0	0.1	0.2	0.3	0.4	0.5	0.6
$F_{1s}/F_c = 0.2$							
0.5	-1.0	-0.36	0.59	1.77	3.20	4.88	6.79
1.0	-1.0	-0.24	0.63	1.70	2.64	3.73	-
2.0	-1.0	-0.19	0.21	0.04	-	-	-
$F_{1s}/F_c = 0.4$							
0.5	-1.0	-0.48	-0.02	0.58	0.92	1.31	16.3
1.0	-1.0	-0.36	0.17	0.55	0.72	0.78	-
2.0	-1.0	-0.18	0.16	-0.06	-	-	-
$F_{1s}/F_c = 0.6$							
0.5	-1.0	-0.50	-0.07	0.31	0.60	0.82	0.92
1.0	-1.0	-0.37	0.12	0.55	0.60	0.52	-
2.0	-1.0	-0.18	0.26	0.16	-	-	-
$F_{1s}/F_c = 1.0$							
0.5	-1.0	-0.51	-0.09	0.25	0.50	0.65	0.64
1.0	-1.0	-0.37	0.13	0.46	0.61	0.54	-
2.0	-1.0	-0.15	0.38	0.42	-	-	-

Diagram  
7-27Values of  $\zeta_{c, st}$ 

$\frac{Q_{1s}}{Q_{1s}}$	$Q_{st}/Q_c$										
	0	0.1	0.2	0.3	0.4	0.5	0.6	0.7	0.8	0.9	1.0
	$F_{1s}/F_c = 0.2$										
0.5-2.0	-2.92	-1.87	-1.29	-0.80	-0.56	-0.23	-0.01	0.16	0.22	0.15	0
1.0	-2.54	-1.87	-1.30	-0.80	-0.42	-0.12	0.08	0.20	0.22	0.15	0
	$F_{1s}/F_c = 0.4$										
0.5-2.0	-0.98	-0.61	-0.30	-0.05	0.14	0.26	0.33	0.34	0.28	0.17	0
1.0	-0.77	-0.44	-0.16	0.05	0.21	0.31	0.36	0.35	0.29	0.17	0
	$F_{1s}/F_c = 0.6$										
0.5-2.0	-0.32	0.08	0.11	0.27	0.37	0.43	0.44	0.40	0.31	0.18	0
1.0	-0.18	-0.04	0.21	0.34	0.42	0.46	0.46	0.41	0.31	0.18	0
	$F_{1s}/F_c = 1.0$										
0.5-2.0	0.11	0.36	0.46	0.53	0.57	0.56	0.52	0.44	0.33	0.18	0
1.0	0.29	0.42	0.51	0.57	0.59	0.58	0.54	0.45	0.33	0.18	0

Four-way wye piece of the type  $F_{1s} = F_{2s} = F_s; F_{st} = F_c$ ;  
 $\alpha = 60^\circ$  [11, 12]Diagram  
7-28

1) Merging of streams (converging four-way piece).

Side branch

$$\zeta_{1c,s} = \frac{\Delta p_{1s}}{\rho w_c^2/2} = 1 + \left( \frac{Q_{1s} F_c}{Q_c F_{1s}} \right) - 8 \left( \frac{Q_{1s}}{Q_c} \right)^2 \frac{[Q_c/Q_{1s} - (1 + Q_{1s}/Q_{1s})]^2}{4 - (1 + Q_{1s}/Q_{1s}) Q_{1s}/Q_c} - \left( \frac{Q_{1s}}{Q_c} \right)^2 \frac{F_c}{F_{1s}} \left[ 1 + \left( \frac{Q_{1s}}{Q_{1s}} \right)^2 \right]$$

see the curves  $\zeta_{c,s} = f(Q_s/Q_c, Q_{1s}/Q_{1s})$  at different  $F_{1s}/F_c$ .

For the other side branch subscripts 1 and 2 change places.

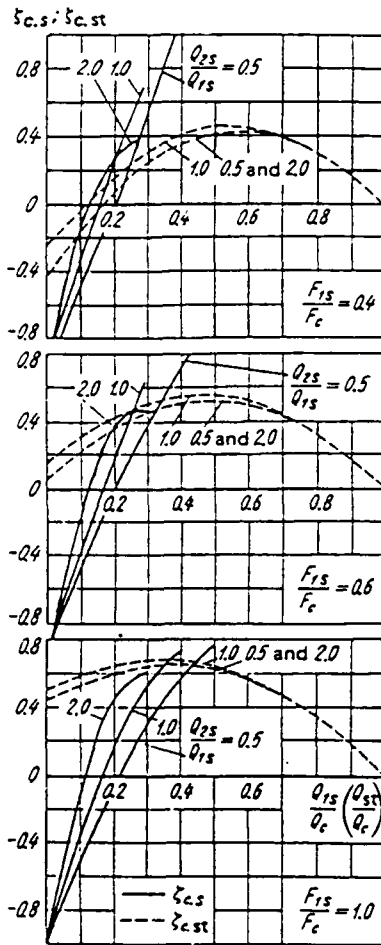
Main passage

$$\zeta_{c,st} = \frac{\Delta p_{st}}{\rho w_c^2/2} = 1 + \left( \frac{Q_{st}}{Q_c} \right)^2 - \left( \frac{Q_{st}}{Q_c} \right)^2 \frac{1 + Q_{st}/Q_c}{(0.75 + 0.25 Q_{st}/Q_c)} - \left( \frac{Q_{st}}{Q_c} \right)^2 \frac{F_c}{F_{st}} \times \frac{1 + (Q_{1s}/Q_{1s})^2}{[1 + (Q_{1s}/Q_{1s})]^2} \left( \frac{Q_c}{Q_{st}} - 1 \right)^2$$

see the curve  $\zeta_{c,st} = f(Q_{st}/Q_c, Q_{1s}/Q_{1s})$  at different  $F_{1s}/F_c$ .2) Division of flow (diverging four-way piece);  $\zeta_{c,s}$  and  $\zeta_{c,st}$  are determined tentatively as for diverging wyes from Diagram 7-17 (curve 1).

Four-way wye piece of the type  $F_{1s} = F_{2s} = F_s; F_{st} = F_c$ ;  
 $\alpha = 60^\circ$  [11, 12]

Diagram  
 7-28



Values of  $\zeta_{c,s}$

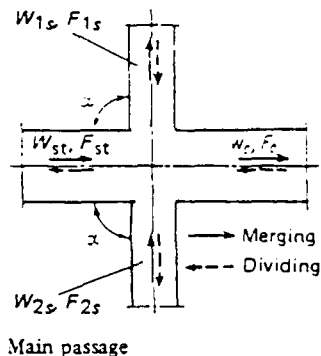
$\frac{Q_{1s}}{Q_{1s}}$	$\frac{Q_{1s}}{Q_c}$						
	0	0.1	0.2	0.3	0.4	0.5	0.6
$F_{1s}/F_c = 0.2$							
0.5	-1.0	-0.31	0.59	2.00	3.62	5.54	7.72
1.0	-1.0	-0.20	0.80	2.07	3.30	4.77	-
2.0	-1.0	-0.09	0.62	0.97	-	-	-
$F_{1s}/F_c = 0.4$							
0.5	-1.0	-0.47	-0.06	0.60	1.12	1.63	2.10
1.0	-1.0	-0.34	0.25	0.73	1.10	1.31	-
2.0	-1.0	-0.15	0.27	0.41	-	-	-
$F_{1s}/F_c = 0.6$							
0.5	-1.0	-0.50	0.04	0.38	0.74	1.03	1.23
1.0	-1.0	-0.36	0.18	0.67	0.82	0.87	-
2.0	-1.0	-0.15	0.40	0.47	-	-	-
$F_{1s}/F_c = 1.0$							
0.5	-1.0	-0.50	-0.07	0.30	0.58	0.79	0.88
1.0	-1.0	-0.36	0.16	0.53	0.74	0.75	-
2.0	-1.0	-0.13	0.46	0.61	-	-	-

Values of  $\zeta_{c,st}$

$\frac{Q_{1s}}{Q_{1s}}$	$\frac{Q_{st}}{Q_c}$										
	0	0.1	0.2	0.3	0.4	0.5	0.6	0.7	0.8	0.9	1.0
$F_{1s}/F_c = 0.2$											
0.5-2.0	-1.77	-1.02	-0.64	-0.30	-0.15	0.06	0.20	0.26	0.26	0.16	0
1.0	-1.50	-1.03	-0.64	-0.30	-0.05	0.13	0.24	0.29	0.26	0.16	0
$F_{1s}/F_c = 0.4$											
0.5-2.0	-0.40	-0.14	0.07	0.24	0.35	0.41	0.42	0.39	0.30	0.18	0
1.0	-0.25	-0.02	0.16	0.31	0.40	0.44	0.45	0.40	0.31	0.18	0
$F_{1s}/F_c = 0.6$											
0.5-2.0	0.06	0.23	0.36	0.46	0.51	0.52	0.50	0.43	0.32	0.18	0
1.0	0.16	0.32	0.43	0.51	0.55	0.55	0.51	0.44	0.33	0.18	0
$F_{1s}/F_c = 1.0$											
0.5-2.0	0.44	0.54	0.60	0.65	0.65	0.62	0.56	0.47	0.34	0.18	0
1.0	0.50	0.59	0.64	0.67	0.67	0.63	0.57	0.47	0.34	0.18	0

Cross of the type  $F_{1s} = F_{2s} = F_s; F_{st} = F_c; \alpha = 90^\circ$   
 [11, 12]

Diagram  
 7-29



1) Merging of streams (converging cross)

Side branch

$$\zeta_{1c.s} = \frac{\Delta p_{1s}}{\rho w_c^2 / 2} = 1 + \left( \frac{Q_{1s} F_c}{Q_c F_{1s}} \right)^2 - 8 \left( \frac{Q_{1s}}{Q_c} \right)^2 \frac{[Q_c' Q_{1s} - (1 + Q_{2s}' / Q_{1s})]^2}{4 - (1 + Q_{2s}' / Q_{1s}) Q_{1s}' Q_c}$$

see the curves  $\zeta_{1c.s} = f(Q_{1s}' / Q_c, Q_{2s}' / Q_{1s})$  at different  $F_{1s} / F_c$ .

For the other side branch subscripts 1 and 2 change places.

$$\zeta_{c.st} = \frac{\Delta p_{st}}{\rho w_c^2 / 2} = 1 + \left( \frac{Q_{st}}{Q_c} \right)^2 - \left( \frac{Q_{st}}{Q_c} \right)^2 \frac{1 + Q_{st} / Q_c}{(0.75 + 0.25 Q_{st} / Q_c)^2}$$

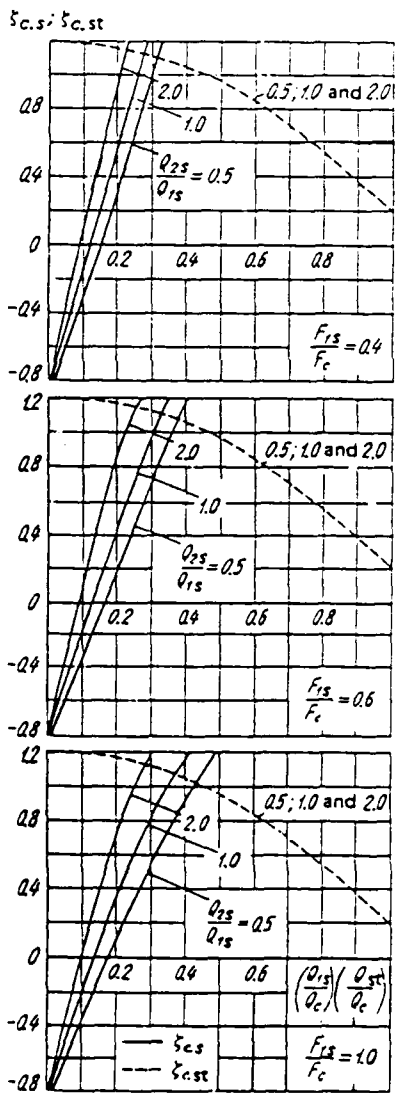
see the curves  $\zeta_{c.st} = f(Q_{st} / Q_c, Q_{2s} / Q_{1s})$  at different  $F_{1s} / F_c$ .

For standard crosses made of malleable iron at  $Q_{st} / Q_c > 0.7$

$$\zeta'_{c.st} = \frac{\Delta p_{st}}{\rho w_c^2 / 2} = \zeta_{c.st} + 2.5 \left( \frac{Q_{st}}{Q_c} - 0.7 \right)$$

2) Flow division (diverging cross);  $\zeta_{c.s}$  and  $\zeta_{c.st}$  are determined tentatively as for diverging wyes from Diagrams 7-15 and 7-17 (curve 1)

Values of  $\zeta_{c.s}$



$\frac{Q_{2s}}{Q_{1s}}$	$\frac{Q_{1s}}{Q_c}$										
	0	0.1	0.2	0.3	0.4	0.5	0.6				
$F_{1s} / F_c = 0.2$											
0.5	-0.85	-0.10	1.09	2.72	4.77	7.25	10.1				
1.0	-0.85	-0.05	1.35	3.12	5.05	7.40	-				
2.0	-0.85	-0.31	1.77	3.37	-	-	-				
$F_{1s} / F_c = 0.4$											
0.5	-0.85	-0.29	0.34	1.03	1.77	2.56	3.37				
1.0	-0.85	-0.14	0.60	1.33	2.05	2.71	-				
2.0	-0.85	0.12	1.02	1.68	-	-	-				
$F_{1s} / F_c = 0.6$											
0.5	-0.85	-0.32	0.20	0.72	1.22	1.70	2.13				
1.0	-0.85	-0.18	0.46	1.02	1.50	1.85	-				
2.0	-0.85	0.09	0.88	1.37	-	-	-				
$F_{1s} / F_c = 0.8$											
0.5	-0.85	-0.33	0.13	0.61	1.02	1.38	1.68				
1.0	-0.85	-0.18	0.41	0.91	1.30	1.54	-				
2.0	-0.85	0.08	0.83	1.26	-	-	-				
$F_{1s} / F_c = 1.0$											
0.5	-0.85	-0.34	0.13	0.56	0.93	1.25	1.48				
1.0	-0.85	-0.19	0.39	0.86	1.21	1.40	-				
2.0	-0.85	0.07	0.81	1.21	-	-	-				
$\frac{Q_{st}}{Q_c}$											
	0	0.1	0.2	0.3	0.4	0.5	0.6	0.7	0.8	0.9	1.0
$\zeta_{c.st}$ at all $F_{1s} / F_c$	1.20	1.19	1.17	1.12	1.05	0.96	0.85	0.72	0.56	0.39	0.20

**Appendix D**

**Corrected Coefficients for ASHRAE Table 5-34 based on Formulas  
Provided by Idelchik**

## Coefficients for Laterals

		<u>Qa/Qm</u>					
<u>Qb/Qa</u>	<u>Q</u>	<u>0.1</u>	<u>0.2</u>	<u>0.3</u>	<u>0.4</u>	<u>0.5</u>	<u>0.6</u>
<u>Aa/Am=0.2</u>							
0.5	?	-0.34	0.59	1.77	3.20	4.88	6.78
1	?	-0.24	0.63	1.60	2.63	3.70	4.77
2	?	-0.16	0.20	0.03	-0.79	-2.43	-5.11
<u>Aa/Am=0.4</u>							
0.5	?	-0.48	0.01	0.48	0.91	1.30	1.63
1	?	-0.36	0.17	0.55	0.76	0.79	0.58
2	?	-0.17	0.16	-0.06	-0.95	-2.68	-5.47
<u>Aa/Am=0.6</u>							
0.5	?	-0.50	-0.07	0.30	0.59	0.80	0.91
1	?	-0.37	0.12	0.45	0.59	0.51	0.18
2	?	-0.15	0.26	0.16	-0.56	-2.06	-4.59
<u>Aa/Am=0.1</u>							
0.5	?	-0.51	-0.09	0.25	0.50	0.65	0.70
1	?	-0.37	0.13	0.46	0.61	0.54	0.22
2	?	-0.12	0.38	0.43	-0.09	-1.33	-3.52

Notes: a = lateral  
 b = lateral  
 m = downstream main  
 ? = Equation has a zero in the denominator,  
 source of table values is unknown.



## Coefficients for the Collinear Duct

		<u>Qs/Qm</u>										
<u>Qb/Qa</u>	<u>0</u>	<u>0.1</u>	<u>0.2</u>	<u>0.3</u>	<u>0.4</u>	<u>0.5</u>	<u>0.6</u>	<u>0.7</u>	<u>0.8</u>	<u>0.9</u>	<u>1</u>	
<u>Aa/Am=0.2</u>												
0.5	?	-2.20	-1.56	-1.01	-0.57	-0.23	0.02	0.16	0.21	0.15	0	
1.0	?	-1.88	-1.31	-0.82	-0.43	-0.13	0.08	0.20	0.22	0.16	0	
2.0	?	-2.20	-1.56	-1.01	-0.57	-0.23	0.02	0.16	0.21	0.15	0	
<u>Aa/Am=0.4</u>												
0.5	?	-0.61	-0.30	-0.05	0.14	0.27	0.33	0.34	0.28	0.17	0	
1.0	?	-0.45	-0.17	0.05	0.21	0.32	0.36	0.36	0.29	0.17	0	
2.0	?	-0.61	-0.30	-0.05	0.14	0.27	0.33	0.34	0.28	0.17	0	
<u>Aa/Am=0.6</u>												
0.5	?	-0.07	0.12	0.27	0.38	0.43	0.44	0.40	0.31	0.18	0	
1.0	?	0.03	0.21	0.34	0.42	0.46	0.46	0.41	0.32	0.18	0	
2.0	?	-0.07	0.12	0.27	0.38	0.43	0.44	0.40	0.31	0.18	0	
<u>Aa/Am=0.1</u>												
0.5	?	0.35	0.46	0.53	0.57	0.56	0.52	0.45	0.33	0.18	0	
1.0	?	0.42	0.51	0.57	0.59	0.58	0.54	0.45	0.34	0.18	0	
2.0	?	0.35	0.46	0.53	0.57	0.56	0.52	0.45	0.33	0.18	0	

Notes: a = lateral  
 b = lateral  
 m = downstream main  
 s = collinear duct  
 ? = Equation has a zero in the denominator,  
 source of table values is unknown.

**Appendix E**

**Calibration Data Worksheet.**



**Appendix F**

**Equipment Calibration Curves**

## Calibration Curve Summary

98

### Inclined Manometer # 1

$$\text{Pressure} = 0.998487 (\text{Inc\#1 reading}) - 0.002390$$

### Inclined Manometer # 2

$$\text{Pressure} = 0.995042 (\text{Inc\#2 reading}) - 0.003129$$

### Merical

$$\text{Pressure} = 0.997269 (\text{Merical reading}) + 0.005857$$

### Transducer # 5

$$\begin{aligned} \text{Pressure} &= 1.89691 (\text{Transducer \#5 Volts}) \\ &+ 0.009559 (\text{Transducer \#5 Volts})^2 - 6.70500 \end{aligned}$$

### Transducer # 3

$$\begin{aligned} \text{Pressure} &= 7.81296 (\text{Transducer \#3 Volts}) \\ &- 0.033744 (\text{Transducer \#3 Volts})^2 - 0.769084 \end{aligned}$$

### Transducer # 4

$$\text{Pressure} = 1.98680 (\text{Transducer \#4 Volts}) - 7.00087$$

### Transducer # 8

$$\begin{aligned} \text{Pressure} &= 1.79956 (\text{Transducer \#8 Volts}) \\ &+ 0.020732 (\text{Transducer \#8 Volts})^2 - 6.63119 \end{aligned}$$

## Regression Results

99

### Inclined Manometer #1

Dependent variable is: Corrected Hook Gage

446 total cases of which 141 are missing

$R^2 = 100.0\%$   $R^2(\text{adjusted}) = 100.0\%$

$s = 0.0041$  with  $305 - 2 = 303$  degrees of freedom

Source	Sum of Squares	df	Mean Square	F-ratio
Regression	364.409	1	364	21303754
Residual	0.005183	303	0.000017	

Variable	Coefficient	s.e. of Coeff	t-ratio
Constant	<b>-0.002390</b>	0.0004	-6.25
Inc1	<b>0.998487</b>	0.0002	4616

**Pressure = 0.998487 (Inc#1 reading) - 0.002390**

### Inclined Manometer #2

Dependent variable is: Corrected Hook Gage

446 total cases of which 141 are missing

$R^2 = 100.0\%$   $R^2(\text{adjusted}) = 100.0\%$

$s = 0.0040$  with  $305 - 2 = 303$  degrees of freedom

Source	Sum of Squares	df	Mean Square	F-ratio
Regression	364.410	1	364	22921968
Residual	0.004817	303	0.000016	

Variable	Coefficient	s.e. of Coeff	t-ratio
Constant	<b>-0.003129</b>	0.0004	-8.48
Inc2	<b>0.995042</b>	0.0002	4788

**Pressure = 0.995042 (Inc#2 reading) - 0.003129**

**Mercial**

Dependent variable is: Corrected Hook Gage

446 total cases of which 309 are missing

$R^2 = 100.0\%$   $R^2(\text{adjusted}) = 100.0\%$

$s = 0.0069$  with  $137 - 2 = 135$  degrees of freedom

Source	Sum of Squares	df	Mean Square	F-ratio
Regression	1590.69	1	1591	33401107
Residual	0.006429	135	0.000048	

Variable	Coefficient	s.e. of Coeff	t-ratio
Constant	<b>0.005857</b>	0.0009	6.34
Mercial	<b>0.997269</b>	0.0002	5779

$$\text{Pressure} = 0.997269 (\text{Mercial reading}) + 0.005857$$

**Transducer #5**

Dependent variable is: Corrected Hook Gage

cases selected according To  $HK_{\text{corr}} > 0$

446 total cases of which 130 are missing

$R^2 = 100.0\%$   $R^2(\text{adjusted}) = 100.0\%$

$s = 0.0077$  with  $316 - 3 = 313$  degrees of freedom

Source	Sum of Squares	df	Mean Square	F-ratio
Regression	619.751	2	310	5249846
Residual	0.018475	13	0.000059	

Variable	Coefficient	s.e. of Coeff	t-ratio
Constant	<b>-6.70500</b>	0.0156	-430
Ch5	<b>1.89691</b>	0.0068	280
Ch5SQ	<b>0.009559</b>	0.0007	13.3

$$\text{Pressure} = 1.89691 (\text{Transducer \#5 Volts}) + 0.009559 (\text{Transducer \#5 Volts})^2 - 6.70500$$

### Transducer # 3

101

Dependent variable is: Corrected Hook Gage  
cases selected according To HKcorr>0  
446 total cases of which 194 are missing  
 $R^2 = 100.0\%$   $R^2(\text{adjusted}) = 100.0\%$   
 $s = 0.0055$  with  $252 - 3 = 249$  degrees of freedom

Source	Sum of Squares	df	Mean Square	F-ratio
Regression	316.568	2	158.284	5262728
Residual	0.007489	249	0.000030	

Variable	Coefficient	s.e. of Coeff	t-ratio
Constant	<b>-0.769084</b>	0.0017	-451
Ch3	<b>7.81296</b>	0.0118	664
Ch3SQ	<b>-0.033744</b>	0.0175	-1.93

$$\text{Pressure} = 7.81296 (\text{Transducer \#3 Volts}) - 0.033744(\text{Transducer \#3 Volts})^2 - 0.769084$$

### Transducer #4

Dependent variable is: Corrected Hook Gage  
cases selected according To HKcorr>0  
446 total cases of which 151 are missing  
 $R^2 = 100.0\%$   $R^2(\text{adjusted}) = 100.0\%$   
 $s = 0.0084$  with  $295 - 2 = 293$  degrees of freedom

Source	Sum of Squares	df	Mean Square	F-ratio
Regression	344.584	1	344.584	4908527
Residual	0.020569	293	0.000070	

Variable	Coefficient	s.e. of Coeff	t-ratio
Constant	<b>-7.00087</b>	0.0038	-1825
Ch4	<b>1.98680</b>	0.0009	2216

$$\text{Pressure} = 1.98680 (\text{Transducer \#4 Volts}) - 7.00087$$



**Transducer #8**

Dependent variable is: Corrected Hook Gage

cases selected according To HKcorr>0

446 total cases of which 156 are missing

R<sup>2</sup> = 100.0% R<sup>2</sup>(adjusted) = 100.0%

s = 0.0102 with 290 - 3 = 287 degrees of freedom

Source	Sum of Squares	df	Mean Square	F-ratio
Regression	337.586	2	1638047	
Residual	0.029574	287	0.000103	

Variable	Coefficient	s.e. of Coeff	t-ratio
Constant	<b>-6.63119</b>	0.0388	-171
Ch8	<b>1.79956</b>	0.0177	102
Ch8sq	<b>0.020732</b>	0.0020	10.4

**Pressure = 1.79956 (Transducer #8 Volts)**

**+ 0.020732(Transducer #8 Volts)<sup>2</sup> - 6.63119**

**Appendix G**

**Equipment List**

Duct - 20 and 24 gage spiral wound duct, connectors, expansions, and elbows purchased from United McGill Corporation, Stockton CA.

Junction - Bilateral junction with 5" diameter side laterals entering at a 45° angle from centerline; 7" diameter upstream coaxial duct; and 10" diameter downstream main. Expanded from 7" to 10" diameter over 7". Junction was purchased from United McGill Corporation, Stockton CA.

Fan - Buffalo Forge MW40 Centrifugal Fan, Buffalo NY.

Motor - Lincoln Motors, AC, 20 HP

Transmission - Infinitely Variable Mechanical Transmission Model 7-10A(E) 0:1-1 CCW by Speed Control Industries Inc, Richland WA.

Electronic Tachometer - DITAK 5 Model DT-5 by Red Lion Controls

Duct Tape

Pitot Tubes - Dwyer hemispherical probe Pitot tubes, 3/16"

Pitot Tube Holders - Guffey

Tygon® Tubing - American Scientific Products T6000-4, 3/16 ID x 1/16 wall thickness

High density polypropylene quick disconnect fittings

Inclined Manometer - Meriam Instrument, Model 40HE35WM

Hook Gage - Dwyer Instruments, Inc., Series 1425

Indicating Fluids:

Meriam 1000 Green Concentrate, No. 922WA

Dwyer Fluorescein Green Concentrate, 1.000 specific gravity

Hand Pump - Meriam Instruments, Model B34348

Pressure Transducers:

Omega Engineering, Inc., PX160 and PX 154 Series

Meri-cal<sup>®</sup> Model DP200I, Meriam Instruments

Transducer Power Supply - Omega<sup>®</sup> PST-4130 regulated power supply.

Barometer (Mercurial) - Princo Instruments, Inc., No. 453

Thermometers:

Glass Thermometer - Ever Ready Thermometer Company, Instrument No. 1446,  
ASTM Precision Specifications

Digital - Fluke 52 K/J Thermometer

Psychrometer - Cole-Parmer Instrument Co., Psychro-Dyne, No. 3312-40

Measuring Tapes:

Ace Hardware, No. 24988, 25 ft.

Empire Model 6550, 50 ft.

Stanley "Powerlock", No. 33-203, 3 m/10 ft.

Caliper (made in China -- manufacturer unknown)

Level - construction-type

Macintosh SE Computer

Thumb Wheel - Cherry Programmable Controller Peripheral, TH Series

Computer Programs:

Analog Connection Workbench™ 2.0 by Strawberry Tree Computers Inc.

Microsoft® Excel, Microsoft Corporation

Data Desk® 3.0, Odesta Corporation

**Appendix H**

**Friction Data Collection Procedure**

### Friction Data Collection Procedure

1. Calibrate equipment.
2. Clean duct.
3. Assemble and seal duct.
4. Drill holes in duct for differential static pressures.
5. Install Pitot tubes and Pitot tube holding devices.
6. Conduct leak test on duct and Tygon® tubing.
7. Check alignment of duct.
8. Start "Workbench" program and insure transducer is on for at least 30 minutes (for warm-up) before collecting data.
9. Turn on Fluke and allow to warm up for at least 15 minutes.
10. Check Fluke against mercury thermometer and adjust if necessary.
11. Zero barometer according to manufacturers instructions.
12. Turn fan on and set rpm to achieve the desired duct velocity.
13. Take the following measurements for the measurement station.
  - a. Record "Run" number on computer.
  - b. Record fan rpm on data collection worksheet (check reading periodically and note range).
  - c. Measure airstream temperature just upstream of the measuring station and record on data collection worksheet.
  - d. Conduct first 10 point Pitot traverse and collect centerline VP on transducer (BCD 1-10 and 31).
  - e. Conduct second 10 point Pitot traverse and collect centerline VP on transducer (BCD 11-10 and 32).
  - f. Conduct third 10 point Pitot traverse and collect centerline VP on transducer (BCD 21-30 and 33).
  - g. Record centerline static pressure of third traverse with transducer (BCD 34).
  - h. Check level and zero of inclined manometer.

- i. Measure centerline static pressure of third traverse with inclined manometer and record on data collection worksheet.
  - j. Measure centerline velocity pressure of third traverse with inclined manometer and record on data collection worksheet.
  - k. Measure wet and dry bulb temperatures and the barometric pressure and record on the data collection worksheet.
14. Record the transducer voltages for all static pressure differentials to a computer file.
  15. Recheck the level and zero on the inclined manometer.
  16. Measure all static pressure differentials with an inclined manometer and record the data on the data collection worksheet.
  17. Adjust the fan rpm to achieve a new duct velocity and return to step 13.
  18. Repeat until adequate data points are taken within the velocity range of interest.
  19. Change setup to a new duct diameter and repeat steps 2 through 18.



**Appendix I**

**Friction Data Collection Worksheet**

# Friction Data Collection Worksheet

Page \_\_\_\_\_ of \_\_\_\_\_

Date: \_\_\_\_\_ Computer File Name: \_\_\_\_\_

Description of work: \_\_\_\_\_

<i>Run Number</i>										
<i>Fan rpm</i>										
<i>BP (mm Hg)</i>										
<i>Dry Bulb Temp ( C)</i>										
<i>Wet Bulb Temp ( C)</i>										
<i>Air Temp in Duct ( C)</i>										
<i>SP at Meas STA</i>										
<i>Centerline VP</i>										
<i>del SP 1-2</i>										
<i>del SP 1-3</i>										
<i>del SP 1-4</i>										
<i>del SP 3-4</i>										
<i>del SP 5-6</i>										

**Appendix J**

**Junction Data Collection Procedure**

### Junction Data Collection Procedure

1. Calibrate equipment.
2. Clean duct.
3. Complete friction estimation for ducts.
4. Grind inside of junction to remove excess metal.
5. Connect ducts to junction and install velocity pressure measuring stations.
6. Drill holes to measure hood static pressures and airstream temperatures.
7. Check level of duct, straighten with stringline and seal with duct tape. Seal measuring station connections with duct tape and silicone sealant.
8. Install Pitot tubes and Pitot tube holders and zero.
9. Conduct leak test on system and Tygon® tubing.
10. Start "Workbench" program and insure transducer is on for at least 30 minutes (for warm-up) before collecting data.
11. Turn on Fluke and allow to warm up for at least 15 minutes.
12. Check Fluke against mercury thermometer and adjust if necessary.
13. Zero barometer according to manufacturers instructions.
14. Set desired branch velocity ratios by adjusting the blast gates in each branch using impedance method Adjust final velocities by using the variable drive transmission.
15. Check the level and zero of the inclined manometer and adjust as necessary.
16. Move control box to VP measuring station in the main.
17. Connect transducer and inclined manometer to the hand pump with Tygon® tubing and put under pressure.
18. Log calibration pressure on the computer. Record inclined manometer reading on data collection worksheet.
19. Take measurements for duct M.
  - a. Record "Run" number on computer.
  - b. Record fan rpm on data collection worksheet (check reading periodically and note range).
  - c. Measure airstream temperature just upstream of the measuring station and record on data collection worksheet.

- d. Conduct first 10 point Pitot traverse and collect centerline VP on transducer (BCD 1-10 and 31).
  - e. Conduct second 10 point Pitot traverse and collect centerline VP on transducer (BCD 11-10 and 32).
  - f. Conduct third 10 point Pitot traverse and collect centerline VP on transducer (BCD 21-30 and 33).
  - g. Record centerline static pressure of third traverse with transducer (BCD 34).
  - h. Measure static pressure differential between the centerline of M and the centerline of S with the transducer (BCD 35).
  - i. Check level and zero of inclined manometer.
  - j. Measure static pressure differential between the centerline of M and the centerline of S with inclined manometer and record on data collection worksheet.
  - k. Measure centerline static pressure of third traverse with inclined manometer and record on data collection worksheet.
  - l. Measure centerline velocity pressure of third traverse with inclined manometer and record on data collection worksheet.
  - m. Measure wet and dry bulb temperatures and the barometric pressure and record on the data collection worksheet.
- 20 Move the control box to the junction.
- 21 Check the level and zero of inclined manometer.
22. *Connect transducer and inclined manometer to the hand pump with Tygon® tubing and put under pressure.*
23. *Log calibration pressure with the control box at the junction. Record inclined manometer reading to data collection worksheet.*
24. Take measurements for duct S (repeat steps 19 a through 19 m above).
25. Take measurements for duct A (repeat steps 19 a through 19 m above except measure the static pressure differential between A and S).
26. Take measurements for duct B (repeat steps 19 a through 19 m above except measure the static pressure differential between B and S).
27. Return to step 14 above for new setup.
28. Return to step 10 at the start of a new day.

**Appendix K**

**Impedance Method**

### Impedance Method

The ratio of the airflows for each upstream branch was set using the impedance method (Guffey, unpublished manuscript) and the "Connect" and "Balance" programs developed by Dr. Guffey. To use the impedance method a baseline characterization of the system was first accomplished. The baseline was accomplished with all blast gates fully open and the fan at 1130 revolutions per minute (rpm). The static pressure just upstream of the junction and the hood static pressure (approximately 5 diameters upstream of the blastgate) were measured for each branch. The flow in each branch was estimated using the following equation:

$$\text{Average Velocity} = 4005 \sqrt{0.85 VP_{\text{centerline}}}$$

The physical layout of system components were entered into the "Connect" program. The resulting file was opened by the "Balance" program and the baseline system characteristics were entered. Once the baseline characteristics were entered, the target flow for each branch was entered. As output, the program gave the ratio of junction static pressure (SPJ) to hood static pressure (SPH) required for each branch to achieve the desired flow. Next, the blast gate in each branch was adjusted until the desired SPJ/SPH was achieved. The centerline velocity for each branch was checked to ensure the desired velocity ratios were attained. If required, the dampers were adjusted slightly to fine-tune the velocity ratios. The blast gates were fixed in position once the desired velocity ratios were achieved. The fan rotation rate was then adjusted to attain the desired velocities.

The Impedance Method of balancing the system worked very well considering the imprecision in the method of estimating the baseline air flows.

**Appendix L**

**Junction Data Collection Worksheet**



### Junction Data Collection Worksheet

Date: _____	Computer File Name: _____			
Description of work: Data collected using Channel _____	Main 'm'	Branch 'a'	Branch 'b'	Branch 'c'
Run Number				
Fan rpm				
BP (mm Hg)				
Dry Bulb Temp (°C)				
Wet Bulb Temp (°C)				
Air Temp in Duct (°C)				
SP at Mess STA (94)				
Centerline VP (91)				
* del SP s-x (BCD - 36)				
Pressure (BCD - 76)				
Pressure (BCD - 77)				
Pressure (BCD - 78)				
Pressure (BCD - 79)				

Inclined A  
 Merical  
 Inclined #1  
 Merical

**Appendix M**

**Friction Calculations**

## Summary of Empirical Equations For All Ducts for All Test Sections

### 4 inch diameter

$$\text{SPF4"} = 0.4081 \left( \frac{V_{\text{avg}}}{1000} \right)^{1.851} \left( \frac{L_{14}}{100'} \right) \text{ for N.T.P. in 4" spiral, fully developed flow}$$

$$\text{s.e.} = 0.02457, \text{ df} = 11$$

$$\text{SP12} = 1.0325 * \text{SP14}$$

$$\text{SP13} = 1.0015 * \text{SP14}$$

$$\text{SP23} = 0.984 * \text{SP14}$$

$$\text{SP56} = 40.5" = 1.85 * \text{SP14}$$

### 5 inch diameter

$$\text{SPF5"} = 0.3268 \left( \frac{V_{\text{avg}}}{1000} \right)^{1.85843} \left( \frac{L_{14}}{100'} \right) \text{ for N.T.P. in 5" spiral, fully developed flow}$$

$$\text{s.e.} = 0.0058, \text{ df} = 10$$

$$\text{SP12} = 1.0352 * \text{SP14}$$

$$\text{SP13} = 0.97205 * \text{SP14}$$

$$\text{SP23} = \text{n/a}$$

$$\text{SP34} = 1.083 * \text{SP14}$$

$$\text{SP56} = 1.6781 * \text{SP14}$$

### 6 inch diameter

$$\text{SPF6"} = 0.2854 \left( \frac{V_{\text{avg}}}{1000} \right)^{1.8342} \left( \frac{L_{14}}{100'} \right) \text{ for N.T.P. in 6" spiral, fully developed flow}$$

$$\text{s.e.} = 0.01106"$$

$$\text{SPF6"} = 0.2766 \left( \frac{V_{\text{avg}}}{1000} \right)^{1.7502} \left( \frac{L_{12}}{100'} \right) \text{ for N.T.P. in 6" spiral, fully developed flow}$$

$$\text{SPF6"} = 0.2468 \left( \frac{V_{\text{avg}}}{1000} \right)^{1.834} \left( \frac{L_{13}}{100'} \right) \text{ for N.T.P. in 6" spiral, fully developed flow}$$

$$\text{SPF6"} = 0.2774 \left( \frac{V_{\text{avg}}}{1000} \right)^{1.813} \left( \frac{L_{34}}{100'} \right) \text{ for N.T.P. in 6" spiral, fully developed flow}$$

$$\text{SPF6"} = 0.3615 \left( \frac{V_{\text{avg}}}{1000} \right)^{1.797} \left( \frac{L_{56}}{100'} \right) \text{ for N.T.P. in 6" spiral, fully developed flow}$$

$$\text{SP12} = 0.96285 * \text{SP14}$$

$$\text{SP13} = 0.99403 * \text{SP14}$$

$$\text{SP23} = \text{n/a}$$

$$\text{SP34} = 1.0603 * \text{SP14}$$

$$\text{SP56} = 1.375 * \text{SP14}$$

**7 inch diameter**

$$\text{SPF7"}L14 = 0.2156 \left( \frac{V_{avg}}{1000} \right)^{1.843} \left( \frac{L14}{100'} \right) \text{ for N.T.P. in 7" spiral, fully developed flow}$$

$$\text{SPL7"}12/100 = 0.224100 * (V/1000)^{1.8473}$$

$$\text{s.e.} = 0.01073 L14$$

$$\text{SP12} = 1.0433 * \text{SP14} \text{ -same exponent}$$

$$\text{SP13} = 0.9975 * \text{SP14}$$

$$\text{SP23} = 0.9502 * \text{SP14}$$

$$\text{SP56} = 1.2767 * \text{SP14}$$

**10 inch diameter**

$$\text{SPF10"} = 0.145 \left( \frac{V_{avg}}{1000} \right)^{1.889} \left( \frac{L14}{100'} \right) \text{ for N.T.P. in 10" spiral, fully developed flow}$$

$$\text{s.e.} = 0.01048"$$

$$\text{SP12} = 1.0118 * \text{SP14} : (\text{mSP151/L12})/(\text{uSP14/L14})$$

$$\text{SP23} = 1.0578 * \text{SP14} : (\text{mSP154/L23})/(\text{uSP14/L14})$$

## Regression Analyses for Friction

### SPF 6"

SPF 6"/100' =  $10^{-6.60445} * V^{1.85735} * 100/(447.6"/12")$  ' whole range  
 SPF 6"/100' =  $10^{-6.61150} * V^{1.8600} * 100/(447.6"/12")$  ' 1000<V3<5000  
 SPF 6"/100' =  $0.2551 * (V/1000)^{1.840}$

\*\*\*\*\* regression below \*\*\*\*\*

data collected 9-11 Jan90, re-analyzed 30 March 90

note: must do 9-10 WB file once for each CF file  
 comment: zero shift on tSP, especially tSP12

SP14/100' =  $0.2854 * (V/1000)^{1.83417}$   
 SP13/100' =  $0.246787 * (V/1000)^{1.8339}$   
 SP12/100' =  $0.276589 * (V/1000)^{1.75016}$   
 SPF34/100' =  $0.277487 * (V/1000)^{1.8127}$   
 SPF56/100 =  $0.361497 * (V/1000)^{1.79686}$

' \*\*\*\*\* show that transducer predicts VP well \*\*\*\*\*

Dependent variable is: mVPcl  
 24 total cases of which 1 are missing  
 $R^2 = 100.0\%$   $R^2(\text{adjusted}) = 100.0\%$   
 $s = 0.0093$  with  $23 - 2 = 21$  degrees of freedom

Source	Sum of Squares	df	Mean Square	F-ratio
Regression	23.5497	1	23.55	269696
Residual	0.001834	21	0.000087	

Variable	Coefficient	s.e. of Coeff	t-ratio
Constant	0.003403	0.0033	1.04
tVPclAvg	0.998343	0.0019	519

## SPF 6"(cont)

\*\*\*\*\* SP14 \*\*\*\*\*

Summary statistics for PrErr for cmSP14  
 cases selected according To selV 1500<V<6000  
 NumNumeric = 17  
 Mean = -0.00043  
 Standard Deviation = 0.01355

Dependent variable is: logcmSP14  
 cases selected according To selV 1500<V<6000  
 24 total cases of which 7 are missing  
 $R^2 = 100.0\%$   $R^2(\text{adjusted}) = 100.0\%$   
 $s = 0.0057$  with  $17 - 2 = 15$  degrees of freedom

Source	Sum of Squares	df	Mean Square	F-ratio
Regression	1.33947	1	1.3395	41604
Residual	0.000483	15	0.000032	

Variable	Coefficient	s.e. of Coeff	t-ratio
Constant	-1.01577	0.0053	-192
logVn	1.83417	0.0090	204

SP14 for 447.6" =  $10^{-1.01577} \cdot (V/1000)^{1.83417}$   
 0.096434

\*\*\*\*\* SP6" 12 \*\*\*\*\*

Dependent variable is: logcmSP12  
 cases selected according To selV 2000<V<6000  
 24 total cases of which 9 are missing  
 $R^2 = 99.8\%$   $R^2(\text{adjusted}) = 99.8\%$   
 $s = 0.0083$  with  $15 - 2 = 13$  degrees of freedom

Source	Sum of Squares	df	Mean Square	F-ratio
Regression	0.555646	1	0.555646	8126
Residual	0.000889	13	0.000068	

Variable	Coefficient	s.e. of Coeff	t-ratio
Constant	-1.64391	0.0120	-137
logVn	1.75016	0.0194	90.1

SP12 =  $10^{-1.64391} \cdot (V/1000)^{1.75016}$   
 $SP12 = 0.022703 \cdot (V/1000)^{1.75016}$   
 $SP12/100' = 10^{-1.64391} \cdot 100 / (98.5/12) \cdot (V/1000)^{1.75016}$   
 $SP12/100' = 0.276589 \cdot (V/1000)^{1.75016}$

## SPF 6"(cont)

\*\*\*\*\* SP13 \*\*\*\*\*

Summary statistics for PrErr  
 cases selected according To selV  
 NumNumeric = 22  
 Mean = -0.00195  
 Standard Deviation = 0.01055

Dependent variable is: logcmSP13  
 cases selected according To selV 2000<V<6000  
 24 total cases of which 2 are missing  
 $R^2 = 99.9\%$   $R^2(\text{adjusted}) = 99.9\%$   
 $s = 0.0110$  with  $22 - 2 = 20$  degrees of freedom

Source	Sum of Squares	df	Mean Square	F-ratio
Regression	3.87226	1	3.8723	31764
Residual	0.002438	20	0.000122	

Variable	Coefficient	s.e. of Coeff	t-ratio
Constant	-1.34419	0.0059	-228
logVn	1.83392	0.0103	178

SP13=0.045270\*(V/1000)^1.83392  
 SP13/100' = 0.045270\*100/(220.125/12)\*(V/1000)^1.83392  
 SP13/100' = 0.246787\*(V/1000)^1.8339

\*\*\*\*\* SP6" 34 \*\*\*\*\*

Summary statistics for PrErr  
 cases selected according To selV  
 NumNumeric = 16  
 Mean = 0.00015  
 Standard Deviation = 0.00690

Dependent variable is: logcmSP34  
 cases selected according To selV 1500<V<6000  
 24 total cases of which 8 are missing  
 $R^2 = 100.0\%$   $R^2(\text{adjusted}) = 100.0\%$   
 $s = 0.0063$  with  $16 - 2 = 14$  degrees of freedom

Source	Sum of Squares	df	Mean Square	F-ratio
Regression	1.30795	1	1.3079	32818
Residual	0.000558	14	0.000040	

Variable	Coefficient	s.e. of Coeff	t-ratio
Constan	1.81270	0.0100	181

SP6"=0.052607\*(V/1000)^1.8127  
 SPF6"/100' = 0.052607\*100/(227.5/12)\*(V/1000)^1.8127  
 SPF6"/100' = 0.277487\*(V/1000)^1.8127

## SPF 6"(cont)

\*\*\*\*\* SP56 \*\*\*\*\*

Dependent variable is: logcmSP56  
 cases selected according To selV  
 24 total cases of which 9 are missing  
 $R^2 = 99.7\%$   $R^2(\text{adjusted}) = 99.7\%$   
 $s = 0.0153$  with  $15 - 2 = 13$  degrees of freedom

Source	Sum of Squares	df	Mean Square	F-ratio
Regression	1.21144	1	1.2114	5162
Residual	0.003051	13	0.000235	

Variable	Coefficient	s.e. of Coeff	t-ratio
Constant	-1.81778	0.0145	-125
logVn	1.79686	0.0250	71.8

$SPF6" = 0.015213 * (V/1000)^{1.79686}$   
 $SPF56/100 = 0.361497 * (V/1000)^{1.79686}$

## SPF 7"

SPF 7" collected 18 Jan90 analyzed again 2 April 1990

$SP7"L14/100 = 0.215595 * (V/1000)^{1.84332}$   
 $SPL7"12/100 = 0.224100 * (V/1000)^{1.8473}$   
 $SPL7"23/100 = 0.214152 * (V/1000)^{1.80784}$

\*\*\*\*\* SP14 \*\*\*\*\*

Summary statistics for errPrSP14  
 cases selected according To selV  
 NumNumeric = 12  
 Mean = 0.00009  
 Standard Deviation = 0.01073

Dependent variable is: logcmSP14  
 cases selected according To selV  
 13 total cases of which 1 are missing  
 $R^2 = 100.0\%$   $R^2(\text{adjusted}) = 100.0\%$   
 $s = 0.0058$  with  $12 - 2 = 10$  degrees of freedom

Source	Sum of Squares	df	Mean Square	F-ratio
Regression	1.92434	1	1.9243	58046
Residual	0.000332	10	0.000033	

Variable	Coefficient	s.e. of Coeff	t-ratio
Constant	-1.04897	0.0041	-256
logVn	1.84332	0.0077	241



## SPF 7" cont

\*\*\*\*\* SPF 7" L12 \*\*\*\*\*  
 Summary statistics for errPrSP14  
 cases selected according To selV  
 NumNumeric = 12  
 Mean = -0.00042  
 Standard Deviation = 0.00657

Dependent variable is: logcmSP12  
 cases selected according To selV  
 13 total cases of which 1 are missing  
 $R^2 = 100.0\%$   $R^2(\text{adjusted}) = 100.0\%$   
 $s = 0.0062$  with  $12 - 2 = 10$  degrees of freedom

Source	Sum of Squares	df	Mean Square	F-ratio
Regression	1.93265	1	1.9326	49595
Residual	0.000390	10	0.000039	

Variable	Coefficient	s.e. of Coeff	t-ratio
Constant	-1.28100	0.0044	-289
logVn	1.84730	0.0083	223

SPF 7" L12 =  $0.05236 * (V/1000)^{1.8473}$   
 SPF 7" L12/100 =  $0.05236 * 100 / (280.375/12)$   
 SPF 7" L12/100 =  $0.224100 * (V/1000)^{1.8473}$

\*\*\*\*\* SP7 23 no couplers \*\*\*\*\*

Summary statistics for errPr23  
 cases selected according To selV  
 NumNumeric = 12  
 Mean = -0.00082  
 Standard Deviation = 0.00566

Dependent variable is: logcmSP23  
 cases selected according To selV  
 13 total cases of which 1 are missing  
 $R^2 = 99.9\%$   $R^2(\text{adjusted}) = 99.9\%$   
 $s = 0.0132$  with  $12 - 2 = 10$  degrees of freedom

Source	Sum of Squares	df	Mean Square	F-ratio
Regression	1.85097	1	1.8510	10678
Residual	0.001733	10	0.000173	

Variable	Coefficient	s.e. of Coeff	t-ratio
Constant	-1.74147	0.0094	-186
logVn	1.80784	0.0175	103

PrSP23 =  $0.018136 * (V/1000)^{1.80784}$   
 PrSP23per100 =  $0.018136 * 100 / (101.625/12) * (V/1000)^{1.80784}$   
 PrSP23per100 =  $0.214152 * (V/1000)^{1.80784}$

## SPF 7" cont

\*\*\*\*\* est SP coupler \*\*\*\*\*

Dependent variable is: estSPcoupler  
 cases selected according To selV>2000  
 13 total cases of which 5 are missing  
 $R^2 = 99.4\%$   $R^2(\text{adjusted}) = 99.3\%$   
 $s = 0.0009$  with  $8 - 2 = 6$  degrees of freedom

Source	Sum of Squares	df	Mean Square	F-ratio
Regression	0.000909	1	0.000909	1039
Residual	0.000005	6	0.000001	

Variable	Coefficient	s.e. of Coeff	t-ratio
Constant	-0.004680	0.0007	-6.61
uVP	0.019560	0.0006	32.2

Dependent variable is: estSPcoupler  
 cases selected according To selV>2000  
 13 total cases of which 5 are missing  
 $R^2 = 98.5\%$   $R^2(\text{adjusted}) = 98.3\%$   
 $s = 0.0025$  with  $8 - 1 = 7$  degrees of freedom

Source	Sum of Squares	df	Mean Square	F-ratio
Regression	0.002795	1	0.002795	450
Residual	0.000043	7	0.000006	

Variable	Coefficient	s.e. of Coeff	t-ratio
uVP	0.016015	0.0008	21.2

**SPF 10"** analyzed 4Feb90

note: SP12 here is the longest run upstream of the station, same as SP14 on other diameters  
 case 46: 2 Jan90 -- appears to be a typo. Replaced with transducer value  
 $SP12/100 = 0.144993*(V/1000)^{1.88942}$

\*\*\*\*\* L12 corresponds to SP13 for Jim and L14 for other ducts \*\*

Summary statistics for errPrcSP12  
 NumNumeric = 20  
 Mean = 0.00041  
 Standard Deviation = 0.01105

Dependent variable is: logSP12 doesn't include 12/01/89  
 35 total cases of which 15 are missing  
 $R^2 = 99.8\%$   $R^2(\text{adjusted}) = 99.8\%$   
 $s = 0.0159$  with  $20 - 2 = 18$  degrees of freedom

Source	Sum of Squares	df	Mean Square	F-ratio
Regression	1.97527	1	1.9753	7818
Residual	0.004548	18	0.000253	

Variable	Coefficient	s.e. of Coeff	t-ratio
Constant	-1.22126	0.0102	-120
log(V/1000)	1.88942	0.0214	88.4

$SP12/100 = 10^{-1.22126} * 100 / (497.25/12) * (V/1000)^{1.88942}$   
 $SP12/100 = 0.144993 * (V/1000)^{1.88942}$

about 86% of predicted by Colebrook for  $e=0.005$ "

## SPF 4"

SPF 4" data 16Jan90  
analyzed 14 Feb 90

1200<V<6000  
Summary statistics for Prerr  
NumNumeric = 13  
Mean = 0.00211  
Standard Deviation = 0.02457

Dependent variable is: LogSP14  
cases selected according To selV  
13 total cases of which 1 are missing  
 $R^2 = 100.0\%$   $R^2(\text{adjusted}) = 100.0\%$   
 $s = 0.0041$  with  $12 - 2 = 10$  degrees of freedom

Source	Sum of Squares	df	Mean Square	F-ratio
Regression	1.54516	1	1.5452	93958
Residual	0.000164	10	0.000016	

Variable	Coefficient	s.e. of Coeff	t-ratio
Constant	-0.732919	0.0032	-228
logV	1.85094	0.0060	307

$SPF4" = 10^{-0.732919} * (V/1000)^{1.85094}$   
 $SPF4" = 0.1850 * (V/1000)^{1.851}$

Dependent variable is: cSP14  
cases selected according To 1250<selV<5500  
13 total cases of which 2 are missing  
 $R^2 = 100.0\%$   $R^2(\text{adjusted}) = 100.0\%$   
 $s = 0.0237$  with  $11 - 2 = 9$  degrees of freedom

Source	Sum of Squares	df	Mean Square	F-ratio
Regression	15.4811	1	15.48	27638
Residual	0.005041	9	0.000560	

Variable	Coefficient	s.e. of Coeff	t-ratio
Constant	0.001316	0.0131	0.101
PrSP14	1.00074	0.0060	166

## SPF 5"

analyzed 13 Feb90  
 collected 12 Jan90  
 $SPF5'' = .3268 (V/1000)^{1.85843}$

Summary statistics for errPr14  
 NumNumeric = 12  
 Mean = -0.00179  
 Standard Deviation = 0.00791

No Ff value erred by more than 1%

Dependent variable is: logcSP14  
 75 total cases of which 63 are missing  
 $R^2 = 100.0\%$   $R^2(\text{adjusted}) = 100.0\%$   
 $s = 0.0038$  with  $12 - 2 = 10$  degrees of freedom

Source	Sum of Squares	df	Mean Square	F-ratio
Regression	2.10272	1	2.1027	142687
Residual	0.000147	10	0.000015	

Variable	Coefficient	s.e. of Coeff	t-ratio
Constant	-0.854544	0.0022	-384
LogV	1.85843	0.0049	378

$SPF5'' = 10^{-0.854544} (V/1000)^{1.85843} * 100/(513.25/12)$   
 $SPF5'' = .3268 (V/1000)^{1.85843}$

Dependent variable is: PredSPF  
 75 total cases of which 63 are missing  
 $R^2 = 100.0\%$   $R^2(\text{adjusted}) = 100.0\%$   
 $s = 0.0058$  with  $12 - 2 = 10$  degrees of freedom

Source	Sum of Squares	df	Mean Square	F-ratio
Regression	8.38512	1	8.3851	246134
Residual	0.000341	10	0.000034	

Variable	Coefficient	s.e. of Coeff	t-ratio
Constant	0.005201	0.0028	1.88
cSP14	0.993536	0.0020	496

**Appendix N**

**Selected Raw Data**

JUNCTION DATA					
Setup	Va/Vs	Vb/Vs	Va/Vb	LPmass	LPJmass
1	0.8	0.9	0.9	2220.8	829.5
2	1.9	0.6	3.1	1848.7	1044.2
3	2.1	0.6	3.7	1100.8	651.8
4	2.3	2.3	1	2063.6	1137.2
5	1	2.2	0.4	1364.2	769.3
6	0.4	0.4	1	1854.1	764.9
7	0.4	0.4	1	442.9	170.1
8	1	1	1	1810.8	717.3
9	0.3	0.3	1	819.3	335.1
10	0.6	0.6	1	1411.9	531.1
11	0.8	0.8	1.1	1442	517.3
12	0.7	0.7	1	1304.7	468.8
13	0.5	0.5	1	1277.6	495.7
14	2.1	2	1	901.6	466.6
15	1.7	1.7	1	908.4	430.7
16	1.9	1.8	1	904.7	441.2
17	1.5	1.5	1	1083.8	501.8
18	1.3	1.3	1	1120.1	442
19	1.2	1.2	1	1167.8	449.9
20	1	1.1	0.9	1224.2	431
21	1	1.2	0.8	1045.4	386.4
22	1	1.4	0.7	943.2	375.5
23	1	1.9	0.5	754	362.9
24	0.8	0.9	0.9	1778.9	659.4
25	0.8	0.9	0.8	1714.6	638.2
26	0.7	0.9	0.7	1635.2	561.4
27	0.6	1	0.6	1529.4	566.8
28	0.5	1	0.5	1515.8	531.8
29	0.9	2.5	0.4	1065.3	610.8
30	0.4	1	0.4	1821	676.7
31	2	0.9	2.1	1109.6	549.6
32	0.4	1	0.4	1895.1	727.8
33	1.5	1.5	1	1055.2	443.2
34	1	0.9	1	1322.7	464.2
35	0	1	0	680.8	273.6

DUCT A							
Setup#	VPpts	VPavg	Q	TP	SPF	Power	LPF
1	30	0.828	500.1	-3.445	0.124	-1722.8	61.8
2	30	1.878	760	-7.606	0.264	-5781	200.9
3	30	1.367	647.9	-4.833	0.197	-3131.1	127.5
4	30	1.381	651.6	-4.756	0.199	-3098.8	129.5
5	30	0.304	305.9	-6.491	0.049	-1986	14.9
6	30	0.268	287.6	-6.321	0.043	-1818	12.5
7	30	0.106	179.4	-2.443	0.018	-438.2	3.3
8	30	0.978	545	-3.317	0.144	-1807.5	78.6
9	30	0.13	198.9	-5.187	0.022	-1031.4	4.4
10	30	0.439	365.7	-3.89	0.069	-1422.3	25.1
11	30	0.698	459.9	-2.579	0.105	-1186	48.5
12	30	0.557	410.8	-2.103	0.085	-863.9	35.1
13	30	0.302	300.8	-4.09	0.049	-1230.2	14.6
14	30	0.822	496.1	-2.963	0.123	-1469.8	61
15	30	0.795	487.7	-2.896	0.119	-1412.5	58.1
16	30	0.81	492.3	-2.921	0.121	-1437.7	59.7
17	30	0.847	502.1	-3.124	0.126	-1568.4	63.5
18	30	0.827	497.7	-3.037	0.124	-1511.7	61.5
19	30	0.821	497.5	-2.94	0.123	-1462.7	61.1
20	30	0.711	463	-2.972	0.107	-1375.7	49.7
21	30	0.554	409.1	-3.381	0.085	-1383.3	34.8
22	30	0.447	365.5	-3.779	0.07	-1381	25.5
23	30	0.266	282.6	-4.305	0.043	-1216.5	12.2
24	30	0.746	478.6	-3.517	0.112	-1683.3	53.7
25	30	0.614	434.4	-3.752	0.094	-1630	40.7
26	30	0.496	385.4	-4.05	0.077	-1560.8	29.7
27	30	0.344	325.5	-4.253	0.055	-1384.3	17.8
28	30	0.289	293.5	-4.576	0.047	-1343.1	13.7
29	30	0.195	242.4	-6.409	0.032	-1553.3	7.8
30	30	0.174	228.4	-5.629	0.029	-1285.6	6.6
31	30	1.385	649.6	-4.983	0.199	-3236.9	129.5
32	30	0.177	232.5	-5.722	0.029	-1330.3	6.8
33	30	0.84	504.9	-3.108	0.125	-1569.3	63.3
34	30	0.752	477.5	-2.845	0.113	-1358.5	54
35 x		0	0	-3.701	0	0	0



DUCT B							
Setup#	VPpts	VPavg	Q	TP	SPF	Power	LPF
1	30	0.989	546.2	-3.151	0.146	-1721.2	79.7
2	30	0.194	244.8	-9.561	0.032	-2340.1	7.9
3	30	0.101	175.7	-6.312	0.017	-1109.2	3.1
4	30	1.44	665.3	-4.615	0.207	-3070.7	137.5
5	30	1.531	686.3	-4.976	0.219	-3415.4	150.1
6	30	0.272	289.6	-6.232	0.044	-1804.8	12.7
7	30	0.111	184	-2.404	0.019	-442.3	3.5
8	30	0.896	521.8	-3.364	0.133	-1755.6	69.5
9	30	0.14	207	-5.153	0.024	-1066.4	4.9
10	30	0.429	361.3	-3.878	0.067	-1401.4	24.2
11	30	0.618	433.2	-2.628	0.094	-1138.6	40.8
12	30	0.572	416.9	-2.049	0.088	-854	36.6
13	30	0.307	303.3	-4.04	0.049	-1225.3	14.9
14	30	0.76	476.9	-2.997	0.114	-1429.5	54.5
15	30	0.746	472.4	-2.925	0.112	-1381.8	53.1
16	30	0.748	472.5	-2.964	0.113	-1400.7	53.2
17	30	0.801	488.6	-3.159	0.12	-1543.3	58.7
18	30	0.782	484.5	-3.052	0.117	-1478.6	56.9
19	30	0.763	479.8	-2.979	0.115	-1429.5	55
20	30	0.812	495.1	-2.81	0.121	-1391.1	60.1
21	30	0.87	512.4	-2.95	0.129	-1511.7	66.3
22	30	0.941	530.7	-3.131	0.139	-1661.9	74
23	30	1.005	548.7	-3.357	0.148	-1841.6	81.3
24	30	0.941	537.8	-3.212	0.139	-1727.5	74.9
25	30	0.958	542.6	-3.277	0.141	-1778	76.7
26	30	1.019	551.9	-3.358	0.15	-1852.9	82.8
27	30	0.995	553.1	-3.391	0.147	-1875.8	81.1
28	30	1.053	560.8	-3.542	0.155	-1986	86.8
29	30	1.453	660.9	-4.804	0.209	-3174.7	137.9
30	30	1.268	616.6	-4.168	0.184	-2570.4	113.4
31	30	0.302	303.6	-6.286	0.048	-1908.5	14.7
32	30	1.293	628.1	-4.211	0.187	-2644.9	117.5
33	30	0.819	498.4	-3.104	0.122	-1546.9	61
34	30	0.736	472.4	-2.828	0.111	-1335.8	52.3
35	30	0.742	474.3	-2.683	0.112	-1272.4	52.9

DUCT S								
Setup#	VPpts	VPavg	Q	TP	SPF	Power	LPF	
1	30	1.331	1242	-3.112	0.074	-3865	91.6	
2	20	0.528	789.6	-9.25	0.031	-7304	24.8	
3	20	0.321	614.9	-6.126	0.02	-3767	12.2	
4	20	0.267	561.3	-6.09	0.017	-3419	9.4	
5	20	0.32	615.6	-6.505	0.02	-4005	12.2	
6	30	1.984	1532.6	-4.672	0.106	-7161	163	
7	30	0.734	926.7	-1.835	0.043	-1701	39.4	
8	30	0.903	1026.5	-3.549	0.052	-3643	52.9	
9	30	1.168	1169	-4.155	0.065	-4857	76.4	
10	30	1.306	1234.9	-3.105	0.072	-3834	89.4	
11	30	1.025	1091.8	-2.393	0.058	-2613	63.3	
12	30	1.026	1092.3	-1.762	0.058	-1925	63.4	
13	30	1.385	1261.2	-3.087	0.077	-3893	96.6	
14	20	0.188	465.7	-3.7	0.012	-1723	5.7	
15	20	0.26	546.7	-3.537	0.016	-1934	9	
16	20	0.235	519.9	-3.604	0.015	-1873	7.8	
17	20	0.353	635.3	-3.69	0.022	-2344	13.8	
18	20	0.498	757.4	-3.555	0.03	-2692	22.6	
19	20	0.566	809.3	-3.388	0.034	-2742	27.1	
20	20	0.706	905.1	-3.157	0.041	-2858	37.2	
21	20	0.574	816.1	-3.499	0.034	-2856	27.7	
22	20	0.469	734.4	-3.866	0.028	-2839	20.7	
23	20	0.277	564.7	-4.357	0.017	-2461	9.8	
24	30	1.048	1112.7	-3.413	0.059	-3798	65.8	
25	30	1.066	1122.2	-3.475	0.06	-3900	67.4	
26	20	1.131	1140.3	-3.574	0.064	-4075	72.4	
27	30	1.096	1137.6	-3.606	0.062	-4102	70	
28	20	1.16	1152.6	-3.801	0.065	-4381	75	
29	20	0.231	516.5	-6.415	0.015	-3313	7.6	
30	20	1.392	1267.4	-4.489	0.077	-5690	97.5	
31	30	0.336	628	-6.34	0.021	-3981	13	
32	30	1.393	1278.8	-4.58	0.077	-5856	98.2	
33	30	0.381	666.3	-3.752	0.023	-2500	15.5	
34	30	0.817	975.7	-2.968	0.047	-2896	45.9	
35	30	0.799	964.6	-2.932	0.046	-2828	44.4	

DUCT M								
Setup	#VPpts	Q	Qmass	VPavgmas	TPmass	SPFmass	Powermass	LPFmass
1	30	2308.7	2288.2	1.085	-4.165	0.506	-9530.3	1158.2
2	30	1852.4	1794.4	0.654	-9.626	0.318	-17273.4	570.9
3	30	1462.6	1438.6	0.421	-6.331	0.213	-9108.3	306.3
4	30	1871.3	1878.2	0.717	-6.204	0.346	-11651.7	650
5	30	1599.1	1607.9	0.524	-6.698	0.26	-10770.5	417.7
6	30	2126.8	2109.8	0.903	-5.99	0.427	-12637.7	901.1
7	30	1279.1	1290	0.341	-2.344	0.176	-3024.2	226.6
8	30	2061.2	2093.3	0.9	-4.308	0.426	-9017.4	892.5
9	30	1570.3	1574.9	0.509	-4.937	0.253	-7774.4	398.6
10	30	1984.2	1961.9	0.79	-4.113	0.378	-8069.9	742.1
11	30	2006.4	1985	0.814	-3.214	0.389	-6379.6	772.2
12	30	1945.2	1920	0.759	-2.577	0.365	-4947.7	700.9
13	30	1892.9	1865.3	0.728	-4.089	0.352	-7626.5	655.9
14	30	1441.8	1438.7	0.432	-3.839	0.218	-5523.7	313.9
15	30	1507.4	1506.8	0.473	-3.741	0.237	-5636.5	357.5
16	30	1457.6	1484.7	0.46	-3.783	0.231	-5616.4	342.8
17	30	1634.7	1626	0.554	-4.022	0.274	-6539.7	446
18	30	1751.1	1739.6	0.631	-3.91	0.309	-6802.5	537.1
19	30	1800.3	1786.6	0.661	-3.807	0.322	-6801.5	574.7
20	30	1879.2	1863.2	0.718	-3.676	0.347	-6848.8	646.2
21	30	1743.6	1737.5	0.624	-3.911	0.305	-6796	530.1
22	30	1635.3	1630.5	0.555	-4.186	0.274	-6825.4	447.5
23	30	1391.5	1396	0.406	-4.494	0.206	-6272.9	287.8
24	30	2152.2	2129.1	0.92	-4.221	0.435	-8987.8	925.2
25	30	2094.1	2099.2	0.897	-4.298	0.425	-9022.7	891.7
26	30	2081.2	2077.6	0.902	-4.392	0.428	-9123.9	888.9
27	30	2012.1	2016.2	0.826	-4.41	0.394	-8891.6	793.7
28	30	2004	2006.9	0.844	-4.597	0.403	-9225.5	808.5
29	30	1407.4	1419.7	0.419	-6.414	0.212	-9106.6	301.1
30	30	2109.6	2112.4	0.928	-5.381	0.439	-11366.7	926.9
31	30	1595	1581.2	0.512	-6.473	0.255	-10235.9	402.8
32	30	2126.3	2139.4	0.936	-5.481	0.442	-11726.5	944.8
33	30	1665.8	1669.6	0.574	-3.996	0.283	-6671.4	472.1
34	30	1939.2	1925.6	0.763	-3.59	0.367	-6912.6	706.3
35	30	1431.7	1438.9	0.426	-3.323	0.215	-4781	309.8

UNIVERSITY OF WASHINGTON  
SEATTLE, WASHINGTON 98195

13 June 1990

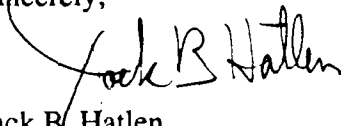
*Department of Environmental Health      SC-34*  
*School of Public Health and Community Medicine*

Captain William Edmonson  
Program Manager  
AFTT/CIMI  
Wright-Patterson Air Force Base, OH 45433-6588

Dear Captain Edmonson:

This is to inform you that James P. Curran has successfully completed the requirements for the Master of Science degree in the Department of Environmental Health, School of Public Health and Community Medicine, at the University of Washington. He will be awarded the degree in June 1990.

Sincerely,



Jack B. Hatlen  
Associate Professor and  
Graduate Program Coordinator

JBH:mlw